12-2020

Analysis for Hybrid Rocket Fuel Regression Using Stereolithographic Geometry

Michael P. King

ANALYSIS FOR HYBRID ROCKET FUEL REGRESSION USING STEREOLITHOGRAPHIC GEOMETRY

THESIS

Michael P. King

AFIT-ENY-MS-20-D-062

DEPARTMENT OF THE AIR FORCE
AIR UNIVERSITY

AIR FORCE INSTITUTE OF TECHNOLOGY

Wright-Patterson Air Force Base, Ohio

AFIT-ENY-MS-20-D-062

ANALYSIS FOR HYBRID ROCKET FUEL REGRESSION USING STEREOLITHOGRAPHIC GEOMETRY

THESIS

Presented to the Faculty

Department of Aeronautics and Astronautics

Graduate School of Engineering and Management

Air Force Institute of Technology

Air University

Air Education and Training Command

In Partial Fulfillment of the Requirements for the

Degree of Master of Science in Astronautical Engineering

Michael P. King, BS

November 2020

AFIT-ENY-MS-20-D-062

ANALYSIS FOR HYBRID ROCKET FUEL REGRESSION USING STEREOLITHOGRAPHIC GEOMETRY

Michael P. King, BS AAE

CIV, USAF

Committee Membership:

Dr. Carl Hartsfield
Chair

Dr. Frederick Schauer

Major Levi Thomas

Abstract

Hybrid Rocket Engines have characteristically low fuel regression that limits their performance. Additive manufacturing and rapid prototyping can possibly solve some of the problems with Hybrid propulsion regression by creating geometry not possible with conventional manufacturing. This work is attempting to make geometric regression simulation of Hybrid Rocket Engines easier by using STereoLithography (STL files) as the geometry. The STL file is generated by most CAD software. This analysis sets flow conditions, boundary conditions, propellant selection, and allows for fuel geometry to be altered to simulate geometry's effects on regression rate and propellant performance. This will allow for more complicated geometry to be analyzed. This work demonstrates a rudimentary analytical model that is can be refined to predict and compare regression rates of fuel and performance. This model can be used for more advanced geometric analysis to improve and predict performance of hybrid rocket engines.

Acknowledgments

I would like to express my sincere appreciation to my faculty advisor, Dr. Carl Hartsfield, for his guidance patience and support throughout the course of this thesis effort. The insight and experience I gained was certainly appreciated. I would, also, like to thank my boss Col. Steven Fisher for giving me the opportunity and the time off work to achieve my master's degree. I would also like to acknowledge my wife and daughter whom this thesis is in support of. They are my biggest distractions and greatest inspiration.

Michael P. King

Table of Contents

List of Figures

Page

List of Tables

Page

List of Symbols

A_p = Area of port [mm^2]
A_T = Throat area [m^2]
a = Empirically fit constant for burn rate [(mm/s)(g/cc)/(kg/ m^2 s)]
c = Mach velocity [m/s]
c^* = Characteristic exhaust velocity [m/s]
D_{Hyd} = Hydraulic Diameter [mm]
h_{fl} = enthalpy of flame [J/(kg K)]
h_w = enthalpy of fuel wall [J/(kg K)]
G_{ox} = Mass flux ($\dot{M}$/Ap) [kg/s-m^2]
$\dot{M}$ = Mass flow [kg/s]
$\dot{M}_f$ = Mass flow fuel [kg/s]
$\dot{M}_{ox}$ = Mass flow oxidizer [kg/s]
P_e = Pressure exit [Psi]
P_c = Pressure of chamber [psi]
T_c = Temperature of chamber [K]
T_{ad} = Adiabatic flame temperature [K]
R_{gas} = Specific gas const [J/(kg-mol-K)] Ru/Mw
R_{univ} = Universal gas constant 8314.3 [J/kg mol]
V_{ex} = Velocity exhaust [m/s]
V_w = Velocity at wall [m/s]
x = Location down the combustion port axis [mm]
n = Empirically fit exponent for burn rate [non-dimensional]

Latin
β = blowing coefficient [non-dimensional]
γ = ratio of specific heat [non-dimensional]
ΔH_v = Heat of vaporization/ Pyrolysis [MJ/kg]
μ = Combustion gas dynamic viscosity [mpoise]converted to [Pa-sec]
ρ_e = exhaust gas density [g/cc] often converted to kg/m^3
ρ_f = Fuel density [g/cc] often converted to kg/m^3

Subscripts
c chamber
e exhaust
f fuel
ox oxidizer
T throat
tot fuel + oxidizer
w wall

ANALYSIS FOR HYBRID ROCKET FUEL REGRESSION USING STEREOLITHOGRAPHIC GEOMETRY

I. Introduction

General Issue

Hybrid rocket engines (HRE) are rocket engines that have fuels and oxidizers that are in different phases of matter typically a solid inert fuel and a liquid or gas oxidizer. With features similar to both liquid rocket engines and solid rocket motors performance, HREs inherit characteristics of both solid and liquid rocket engines. Features unique to Hybrid rocket engines are higher safety during operation and performance parameters that are coupled with geometry. The performance of hybrids motors is frequently challenged by low fuel mass addition which is a function of fuel geometry and the flow rate of oxidizer. Often HRMs have varying performance conditions that shift over the run duration. The primary changes that effect performance is the oxidizer and fuel ratio. Despite the poor performance mechanics of simple hybrids over their flight time, hybrid rocket engines have been of commercial and military interest for their key advantages over solid rocket motors (SRM) and liquid rocket engine (LRE) systems.

- Hybrids have comparable to higher I_{sp} than solids and have comparable I_{sp} to most liquids.
- Hybrids have lower mechanical complexity than liquid rockets
- Decreased in inert mass compared to LRE from plumbing and pumps
- Simpler control mechanisms compared to liquids
- Less hazardous for manufacture/assembly/testing and launching than both SRM and LRE

- Inert fuel with safer operation, little to no explosive hazard for fuel
- Launch abort capable
- Typically, less toxic exhaust products than solid rocket motors (SRM)
- Fuel grains performance are crack and fracture tolerant
- HRE are active throttle capable and capable of non destructive shut off and restart. These features are not possible with SRM.
- Designable thrust curve

The ability to quickly iterate and analyze geometry would help in design iteration. Tracking how these coupled effects vary from classic regression equations can help to overcome several performance hurdles in testing and designing new hybrid rocket engines.

Problem Statement

Regression rates are the limiting factor for hybrid rocket performance. Recent trends in hybrid rocket research suggest that additive manufacturing and rapid prototyping may be a viable manufacturing method to solve some of these geometric coupled regression rates issues. Hybrids have proven that they can provide propulsion at a large scale with classical, simplified fuel-port geometry. The ability to simulate and predict the regression of more complex geometry will allow for better analysis of experimental results. Poor regression rates are a result of combinations of propellant composition, geometry, injector configuration, and scale. If some of these variables can be isolated, geometry can be better analyzed and optimized. A tool is needed that can

direct designers toward what sorts of unique geometry can provide positive results for HRE performance.

Research Objectives/Questions/Hypotheses

The intent of this thesis effort is to create a process to analyze the regression rate of a hybrid rocket fuel grain, using imported geometry from Stereolithography files (STL). This could couple the design and analysis process more directly to the geometric influences by looking at regression rates and how they relate to families of geometries.

Research Focus

The intent of this investigation is to look into the regression rate and how that changes with local geometries. Local geometries have an effect on the regression rate. This coupled nature is the major problem with hybrid rocket performance. The nature of this implies a Computational Fluid Dynamics (CFD) analysis that is not in the scope of this work. The explicit flame height and combustion phenomena are also outside the scope of this effort. We are focusing on a general case to prove the ability to import and analyze a stereolithography file (STL) as a solid fuel grain and see identifiable results that resemble performance of a hybrid rocket.

Investigative Questions

-Is it possible to regress accurate geometry that updates regression rates?

-Are there any limitations to using an STL file as a base for geometric regression?

-What are the inputs and definitions required to do regression analysis?

-What are the performance analysis characteristics to compare designs against?

-What parameters are sensitive to grid size analysis?

Methodology

Using a stereolithography geometry-based format for representing the burning/regressing surfaces, the regression can rate be tracked allowing for a more automated analysis of more complex geometry. The intent is to track the regression of a hybrid rocket motor using conventional experimentally derived relationships between the combustion participants and the local surface conditions. This involves using data from several studies and values from NASA CEA database.

Assumptions/Limitations

This exploration will look at using experimentally derived parameters for burn rates to match corresponding results when available. There are several oxidizer and fuel combinations, and this regression analysis would have to be tuned to each combination based on things such as; ablation/sloughing, adiabatic flame temperature, flame height, Injector techniques etc. For this analysis we will be using Hydroxyl Terminated Polybutadiene (HTPB) and liquid oxygen (LOX) and simple burn shapes to compare to literature. The regime of combustion for this analysis is limited to O/F (mass) ratios of 0.1-32 and Pressures from 100 psi to 2000 psi. The run conditions are not bounded by the capabilities of the core regression code but more by the code used for CEA analysis shorthand created to improve run time [further described in section III]. The regression regime is limited to the turbulent heat transfer regime seen in Figure 24. The radiative heat transfer is not accounted for in a significant way in the regression rate.

Implications

The work started here is designed to improve the analysis methods used to design and test additively manufactured hybrid rocket grains. Hybrid rocket grains have not enjoyed the same successes that liquid rocket engines and solid rocket motors in space faring ventures. Hybrid rockets have been seen to be far safer in manufacture, transport, testing, and operation. This is partly due to their inherent design but also their reduced operational complexity. This reduction in complexity can also reduce costs to manufacture, store and operate. With possible higher safety, lower costs and comparable large-scale thrust performance, hybrids could be an answer for reducing risk and costs to space missions. The next steps toward this possibility are refinement of analysis and investigating families of geometries that show positive performance results. This could also have implications that affect regression analysis of solids and of ablatives.

II. Literature Review

Chapter Overview

Hybrid rocket motors are rocket motors that have fuels and oxidizers in different phases of matter, for example a solid fuel that has a liquid oxidizer that flows through the fuel chamber. HREs are an attractive choice for a rocket but they have historically had performance issues. These performance issues are due to slow regression or fuel addition and an inability to achieve higher fuel regression rates that scale with thrust output.

Introduction to HRE

Traditional hybrid rocket engines have a liquid oxidizer that is flowed across a solid fuel grain. The heat of the flame and blowing conditions cause the solid fuel to transition to a vapor where it is then released from the fuel wall and contributes to further reactions. Fuel vaporizing or pyrolyzing at the face of the solid fuel grain causes the surface to regress. Hybrid rocket motors (HRM) have, from their start, been an attractive choice for many as an alternative to liquid rocket engines (LRE) and solid rocket motors (SRM). They are a combination of both ideas and bring advantages from both to the design.

Interest in Hybrid rockets started in the 1930's. Early researchers in rocket propellant were dismayed at the explosive hazard posed by SRMs and liquid rockets did not scale well until the invention of the turbopump due to plumbing and tank mass losses. The first hybrid rocket was launched August 17, 1933. It was called the Russian GIRD-09 , developed by Sergei Korolev and Mikhail Tikhonravov. They were using gelled gasoline/colophonium (solid resin/sap from pine trees) suspended on a metal mesh and

liquid oxygen (LOX) [5] [6]. The vehicle was 7 inches in diameter and 8 ft long and produced 500 N thrust for 15 seconds. This does not resemble what we consider a classical hybrid but is the first recorded attempt to combine the ideas of a solid fuel and a fluid oxidizer flowed over the fuel to propagate combustion and produce thrust.

From 1937-1939 Germany had several rocket scientists involved in hybrid experimentation. I.G Farben, Leonoid Andrussow, O. Lutz, and W. Noeggerath, were testing coal as a fuel and gaseous Nitrous Oxide as the oxidizer. These tests shared similar results with Hermann Oberth's experiment with Graphite and LOX wherein the heat of sublimation of the carbon was very high leading to very low regression rates [6]. Hermann Oberth experimented with more complex fuels like wood and Saltpeter (Potassium Nitrate, Sodium Nitrate or other Nitrogen containing compounds) bound together by tar as a fuel and liquid oxygen (LOX). These experiments represent something more familiar to the classical hybrids we see today.

The earliest flight-worthy hybrid engines came about in the 1940's from one of the first organizations set up in the US to engage in amateur rocketry, the Pacific Rocket Society. The society conducted test flights using Douglas fir (wood)-LOX, wax loaded with carbon black and LOX, and a rubber-LOX engine. The most successful of these tests achieved an altitude of 30,000 ft using liquid oxygen and rubber-based fuels. [6]

Hybrids have not gained popularity of use like SRMs or LREs since they also suffer from several disadvantages of both. However, there are many factors which make an HRE attractive when considering a HRE for a design: 1) Lower developmental and operational costs with little to no loss in thrust or I_{sp} performance, 2) Safer operation and manufacturing conditions, 3) They are capable of active throttling and abort [1].

Low cost of development comes from the reduced mechanical complexity. The handling and casting process costs should be significantly lower than those for solid propellants, as the fuel carries no oxidizer. HRE carry effectively half of the inert weight for things like plumbing, valves, regulators, and pumps that an LRE of the same thrust class might have. Having fewer components in the feed system leads to less possibility of failure and higher potential reliability. Hybrids can have higher values of specific impulse than solids and a density specific impulse comparable to many liquid bi-propellant rockets [1] . There are also potentially lower launch pad costs since there is only one liquid (oxidizer) used.

Solid fuels for an HRE are safer than SRM propellants in all stages of manufacture, transport, and operation. HRE solid fuels are less sensitive to defects like cracking debonding, meaning they are less sensitive to transport and environment [3]. Virtually all hybrid fuels are considered inert and can be transported using normal shipping techniques with no additional safety requirements. This is a benefit when compared to traditional solid propellants, where any processing is considered a hazardous operation.

A few examples of safety seen in HREs is highlighted in failures seen in 1984 and 1989. In 1984 a company called Starstruck with some expertise acquired from UTC, attempted to launch a vehicle called the Dolphin. Starstruck's Dolphin was powered by a Hybrid rocket booster that produced 35,000 lb_f of thrust. The unique thing about this vehicle was that it was water launched to reduce the launch costs. This also allowed for them to advertise a mobile launch capability and increase launch insertion possibilities. To launch, the Dolphin was slid off a boat and the rocket was erected in the water by a

weight attached to its aft end holding it upright. In early1984 there was a launch failure where during pre-launch repairs there was a fire that broke out while the vehicle was fueled and loaded. This was a great success in test safety for hybrid rockets where no secondary fires broke out or were possible due to the nature of the hybrid. Two additional attempts were made to launch the Dolphin later that year that both failed. The second launch failed from electronics exposure to saltwater. The third and final failure had a successful take off, but shortly after launch the large launch angle caused by exiting the water caused the thrust vector control system to fire to correct the attitude. After correcting the attitude thrust vectoring valve became stuck closed and the vehicle started tipping over and thrust was terminated remotely. This was an extremely valuable example of hybrids' ability to be remotely disabled and thrust terminated. Starstruck was primarily funded by private funds and was dissolved later that year [8].

In 1985, former members of Starstruck formed a new company American Rocket Co. (AMROC). AMROC was dedicated to making hybrid rocket for space launch. In 1987, AMROC developed a 75,000 lb_f engine called H-500 that was tested later that year and qualified for flight in 1989. The engine was developed for the SINGLE Engine Test-1 (SET-1) launch vehicle. In late 1989, AMROC attempted a launch of SET-1. The engine did not achieve sufficient thrust for lift-off due to a valve failure. The guidance for the vehicle was still operating and continued performing a pitch maneuver. Hydrogen peroxide (HTP), used for attitude control, was ejected and decomposed in the hot flame bucket beneath the vehicle. This produced oxygen sufficient enough to mix and reignite the fuel-rich flame from the main thrust and caused a fire beneath the rocket in the flame bucket. The fire engulfed the vehicle in flames. This consumed the aft skirt of the vehicle

and the rocket fell over. Only the bottom third of the vehicle suffered more than minor damage and the avionics were intact. The launch failure of SET-1 proved the safe and non-explosive nature of HRMs.

A quote from the Pacific rocket society captured the safety effects well; *"The Chamber pressure for a Solid-Liquid rocket engine is proportional to oxidizer flowrate and not the internal surface area exposed to the flame. Thus, there is no danger of explosions due to cracks and fissures in the charge as with solid propellant rockets commonly used for boosters"* ***Pacific Rocket Society 1947*** [3] . HREs radically improve safety in all phases of manufacture, vehicle stacking/assembly, ground testing, flight and reduce environmental concerns [3]. With inert fuels there is no explosive hazard.

Hybrids have been proven safer in failure conditions than other rocket designs. The failures seen on the Dolphin and AMROC's attempted a launch of the SET-1 and the many failures seen in Hybrid testing prove the operational safety of hybrids. An LRE or SRM in such conditions would probably have detonated and destroyed the entire vehicle, payload, launch pad, and surrounding area [1].

HREs are capable of throttling for a wide range of thrust, restart, and shutdown and restart. This is a feature not seen in SRMs. SRMs have extremely low mechanical complexity but can pose a hazard during operation since they are not throttleable and cannot be shut off and restarted. LREs do have the benefit of being throttleable but launch vehicles scale LREs have limited throttling due to combustion stability requirements.

Table 1 Comparing Propulsion Types [6]

	Liquid	Solid	Hybrid
Performance (I_{sp})	250-450 sec	200-280 sec	230-300 sec
Cost	High	Low	Moderate
Complexity	High	Low	Moderate
Throttle-ability	Yes	No	Yes
Restart	Yes	No	Yes
Explosive Hazard	Moderate	High	None
Handling & Transport Risk	Moderate	High	Very low
Storability	Low	High	Moderate to High
Operational Risk	High	High	Very Low
Environmental Impact	Low to High	Moderate to High	Very Low

While the hybrid enjoys many safety and environmental advantages over SRM and LRE systems, large scale hybrids have never been commercially viable. The principal reason is the inherent low burning rate of conventional fuels due to the nature of the combustion process.

Description

Hybrid Rocket Engines are classically a solid fuel with and a liquid oxidizer that is flowed over the fuel grain. The idea of a hybrid rocket engine is to store the oxidizer in a tank separate from the inert fuel. This renders them less susceptible to chemical explosion than conventional LRE or SRM designs [4]. Figure 1 depicts the classical configuration of a pressurized blow down HRE.

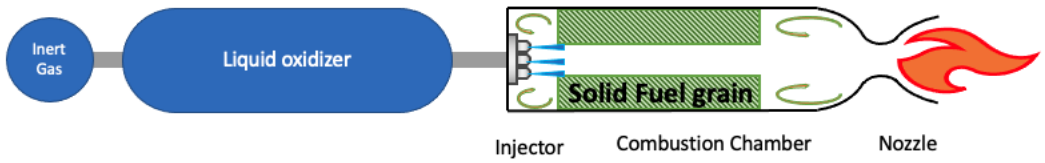

Figure 1. General Layout of Liquid Oxidizer Solid fuel Hybrid Rocket Engine

The basics of HRM establish the following parameters from the geometry seen in Figure 2. The area of the port is determined by the inner diameter in Eq. 1. The mass flow is initialized by the flow of oxidizer through the injector described in Eq. 2 . Fuel added to the mass flow is governed boundary layer combustion and the regression of the fuel wall. The surface area of the burn surface for a cylindrical port slice is described in Eq. 3.

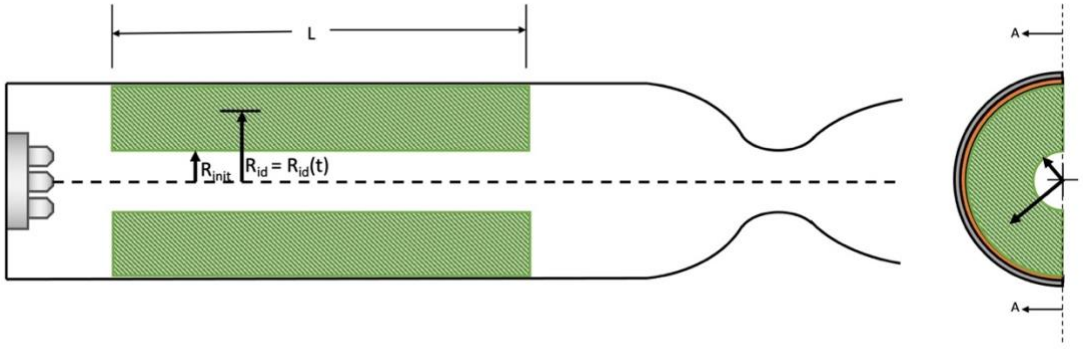

Figure 2 Geometry of a cylinrical Port HRE fuel grain

$$A_p = \pi {R_{id}}^2 \tag{1}$$

$$\dot{M} = \dot{M}_{ox} + A_b r \rho_f \tag{2}$$

$$A_b = 2\pi R_{id} L \tag{3}$$

Generic regression equation from classical texts takes the form of Eq. 4, where the coefficients a and n are experimentally determined and are specific to fuel and oxidizer combinations.

$$r = aG^n \tag{4}$$

$$G = \frac{\dot{M}}{A_p} \tag{5}$$

The mass flux described by the variable G in Eq. 5 rate of the hybrid rocket motor is the driving parameter for the rocket performance. The mass flux down the port drives the regression of the port section.

Classically the regression rate is measured in mm/sec or in/sec. Eq.4 is similar to the Saint/Robert law describing the regression rates of solid rocket motors. The difference is that this regression has a correlation to the mass flux instead of a relationship to pressure, as hybrids have a weak correlation to pressure. This dependency on mass flux makes HREs more difficult to analyze. By combining Eq. 1, Eq. 4, and Eq. 5 we get Eq. 6 .

$$r = a\left(\frac{\dot{M}}{\pi {R_{id}}^2}\right)^n \tag{6}$$

Typically, a ballistics analysis is done on meta-primitive shapes to get performance parameters and simulate a simple regression of a design. A good deal of geometric simplification is made to make this analysis easier. The regression rates for

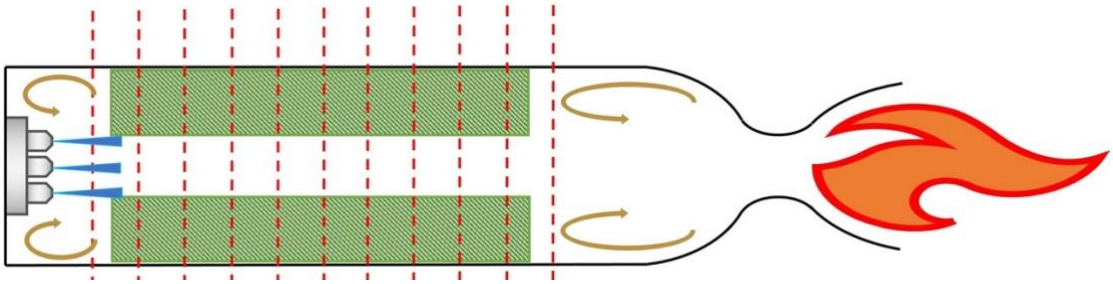

Figure 3 Ballistics slice shown with the flow of a Hyrbid Rocekt Engine

sections are tracked sometimes using profiles of cross sections of the slice. A general regression like the setup in Figure 3 does a sufficient job at regression simulation for conventional hybrid rocket engines. Simple geometries often result in poor performance. If the assumption is made that the mass flow rate is constant, then we see that the trend of

regression follows for a cylindrical port in Eq. 7. With this simple analysis it can be seen that a simple cylindrical surface producing the burning mass grows slowly over time in comparison to the cross-section area of the port. The cross-sectional area is inversely proportional to the mass flux, which is the major parameter for the regression equation. This means that the surface area producing mass increases as regression increases, but so does the cross section. The cross section increases at a much faster rate given a circular cross section.

$$r \propto {R_{id}}^{-2n} \tag{7}$$

This relationship means that for simple geometries, the regression rate will be inversely proportional to the radius of the port. Similar analysis can be done for other basic port geometries with similar results. This relationship in Eq. 8 describes two of the major problems with hybrids, their inconsistent burn rate with time, and their inability to easily scale for larger performance.

$$\underset{\text{Burn surface area}}{2\pi R_{id} h} \ll \underset{\text{Cross section area}}{\pi {R_{id}}^2} \tag{8}$$

Relevant Research in Fuel Regression

HREs rely on boundary layer combustion to generate hot gas. Figure 4 shows a typical example of the boundary layer. Classical HRE systems use polymer fuels that evaporate slowly, making it difficult to produce the high thrust needed for most applications. To compensate, the surface area or burning area must be increased. As the scale of a hybrid rocket increases, the number of required ports also increases, leading to a fuel grain designs such as the wagon wheel. Regression rates of HREs can be modified with design decisions like: propellant selection, injector technique, inclusion of additives, and fuel grain geometry like multi-port or wagon wheel designs.

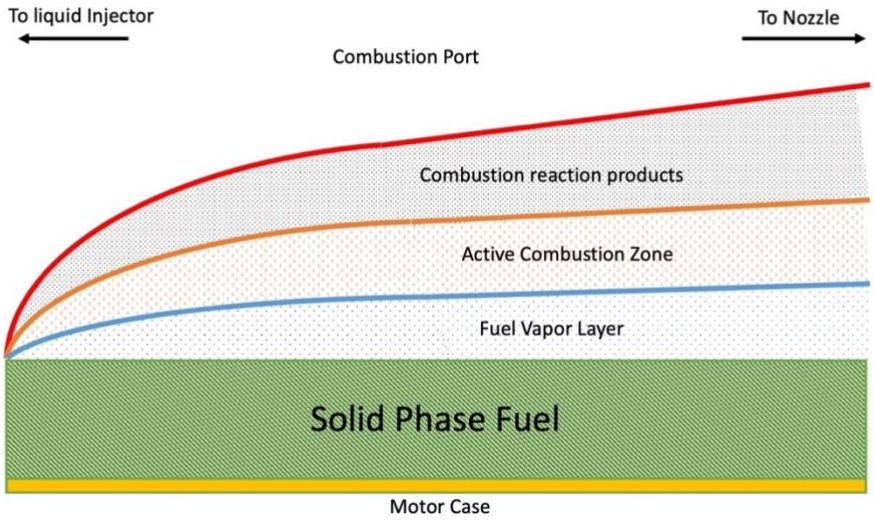

Figure 4 Example of Flame Boundary of a HRE

Propellant Selection

The starting point for most propulsion analysis is determining the fuel and oxidizer combinations. The fuels and oxidizers combination affect regression rate and what also what O/F ratios are needed to combust effectively. Some popular fuels are; hydroxyl-terminated polybutadiene (HTPB), acrylic/ plexiglas/ methyl methacrylate (MMA)/ poly methyl methacrylate (PMMA), paraffin wax, high density polyethylene (HDPE / PE), and rubbers (Synthetic or Natural).

Hydroxyl-terminated polybutadiene or HTPB is a common binder agent used for solid propellants. This fuel is one of the most commonly used fuels in hybrid rocket motors. The classical use of this fuel is paired with liquid oxygen (LOX). When run with LOX the Chemical Equilibrium Analysis (CEA) solutions are very close to the results for Rocket Propellant 1 (RP1) and LOX. A group called Hybrid Propulsion Demonstration Program (HPDP) developed a large-scale hybrid engine that was turbopump fed HTPB/LOX and represents the largest and most developed hybrid rocket system to have ever existed. In 1999 HPDP static fired this HRE 3 times with a gross thrust of 250k lbs. (1.1MN). This fuel is also commonly used with gaseous nitrous oxide (N_2O) and high-test peroxide H_2O_2 (HTP).

Paraffin wax is another commonly used fuel for smaller engines and test applications. Paraffin has shown regression rates up to 3-4 times higher than that of other polymer fuels [4]. It is an easy to manufacture and shape. This wax is not exactly the same as the wax used in candles, as it has a higher heat of vaporization (although still relatively low). This fuel has several problems when burning, mainly due to sloughing. Sloughing is when, instead of vaporizing in preparation for combustion, a significant

portion of the solid wall transitions to liquid droplets before forming a vapor. These fuel droplets are then entrained into the combustion mass flow. This can also produce some fuel grain disfiguration as fuel flows towards the nozzle outlet and can result in a lot of un-combusted fuel, fuel slivers/globs, and obstruction of the outlet. Regression rates of liquifying fuels behave differently than pyrolyzing/vaporizing fuels. Paraffin is classically used with high-test peroxide H_2O_2 (HTP), LOX, and N_2O. Figure 5 shows an example of entrained liquid fuel into the combustion region. [4]

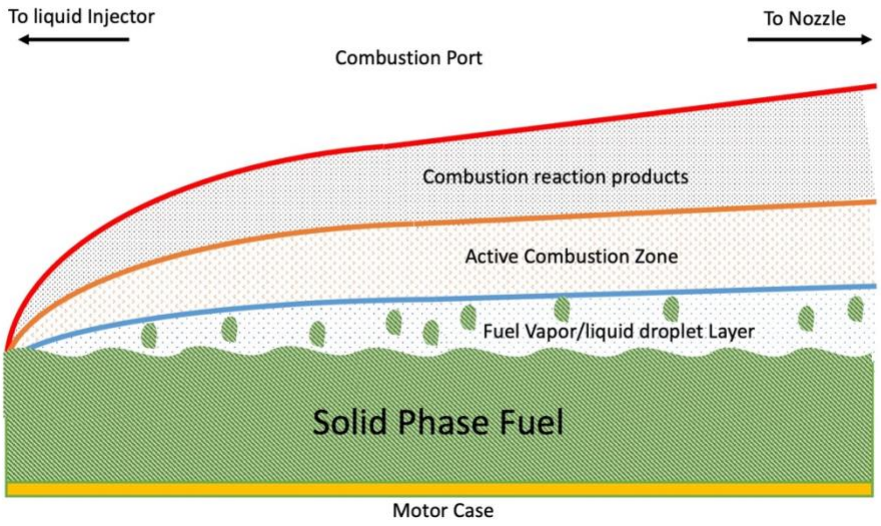

Figure 5 Example of flame boundary of a liquid entrained HRE

High-density polyethylene (HDPE) or polyethylene (PE) is a common fuel and is easy to shape form or manufacture into fuel grain and is often used for full scaled rocket applications. General Electric (GE) conducted the first United States commercial testing under the Army Ordinance Department in 1951-1956 [5] [7] using polyethylene and high-

concentration hydrogen peroxide (or high test peroxide, HTP). The GE work demonstrated easy throttling via a valve and stable combustion but a regression rate with limited capability to improve [3] [6]. The high-density variant is the more efficient when considering thrust efficiency and flight conditions. HDPE is commonly used with high-test peroxide H_2O_2 (HTP), gaseous nitrous oxide (N_2O), nitrogen tetroxide (NTO, N_2O_4), LOX and gaseous oxygen.

Another popular fuel adopted by American industry and military testing is the family of clear rigid plastics such as acrylic/ plexiglas/ methyl methacrylate (MMA)/ poly methyl methacrylate (PMMA). Rocketdyne started testing Plexiglas and oxygen motors in 1960. United Technology Center (UTC) & Beech aircraft began work on a target drone vehicle for the United States Air Force using Rocketdyne's research. Their system designs were using a combination of inhibited red fuming nitric Acid (IRFNA) and Plexiglas. Their target vehicle, originally called the Sandpiper, was followed by HAST (High Altitude Supersonic Target). Both vehicles were designed to be launched from aircraft and fly horizontally at various altitudes and speeds up to Mach 5 for about 100 miles. HAST's thrust time was 300 seconds and it could be throttled 8:1. In 1984, Teledyne Ryan reused the work proven by HAST to develop the Firebolt target missile. The Firebolt was capable of thrust levels from 0.53kN to 5.3kN. These materials are commonly used with nitrous oxide (N_2O), mixed oxides nitrogen of various concentrations MON-1, Nitrogen tetroxide (NTO, N_2O_4), red fuming nitric acid, or LOX.

The variation of performance parameters with firing duration is another problem that exist within hybrids. As seen in Figure 6 the solid line represents the conditions during a constant oxidizer flow. The dashed line represents an effective increase in regression rates and therefore fuel addition.

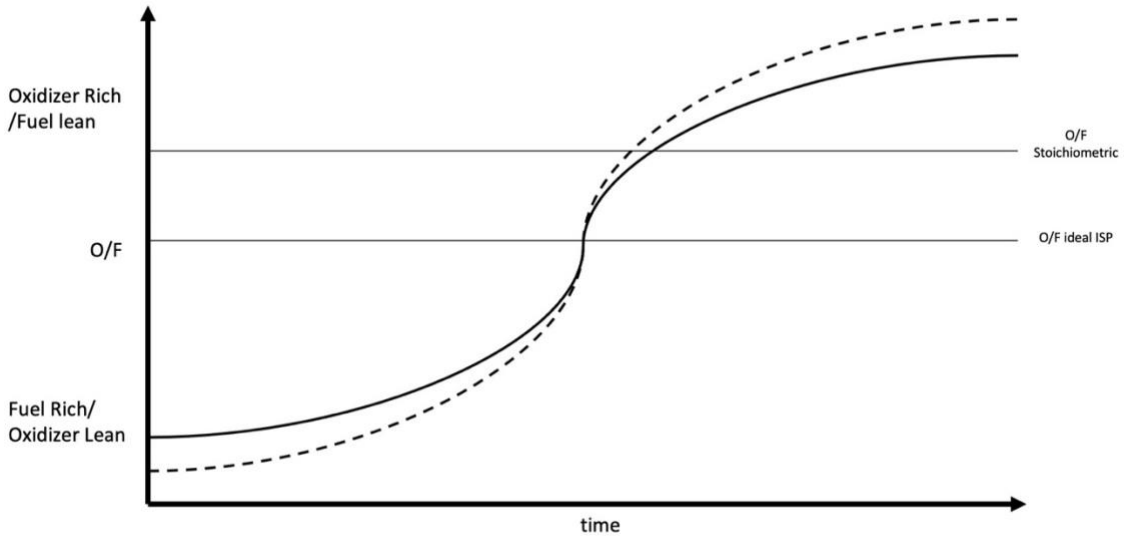

Figure 6 Example of shifiting oxidizer to fuel conditions over HRE burn duration [30]

The curves path these simulations follow is forced by effects of the geometry of the fuel grain. A simple increase in regression does effectively increase instantaneous mass flow therefore increasing thrust but this may not bring lasting benefits.

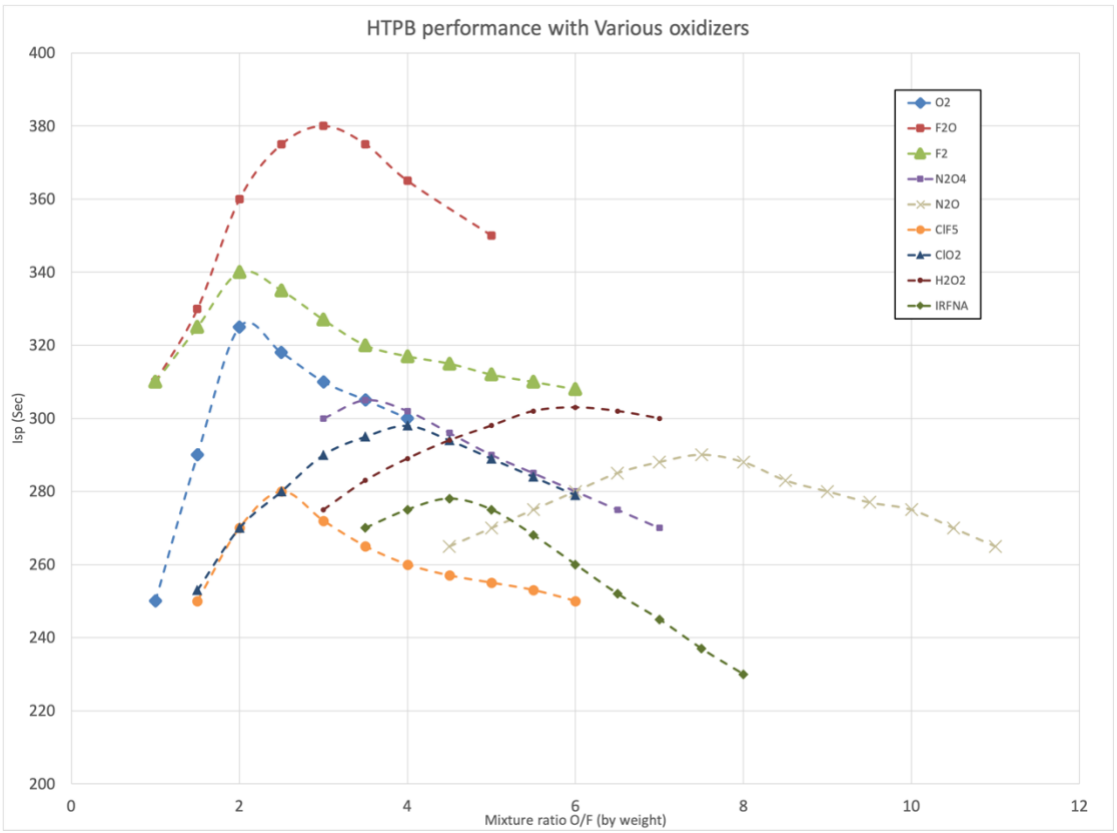

Figure 7 Specific Impulse (I_{sp}) of HTPB with Various Concentrations of Oxixizers

There are two critical O/F ratios to keep in mind when running these combustion analyses. The stoichiometric O/F, which is optimal for a balanced and stable reaction. The other is the O/F for ideal I_{sp}, which is more concerned with the properties of the resulting species to optimize thrust. The effective thrust performance parameter I_{sp} is shown for HTPB with various oxidizers over a range of mixture ratios. Maintaining a more optimal O/F for I_{sp} is critical for ideal thrust performance. Figure 7 [7] [8] shows some I_{sp} vs O/F ratio for several oxidizers with HTPB.

Additives

In the 1950's aluminum particles, when included in solid fuel, demonstrated a significant increase in performance, and since has become common for SRMs. The presence of metals has shown to increased regression rates by altering the heats of combustion and increasing the flame temperature. They also increase solid-fuel density and the net mass flux through the nozzle and can increase the total impulse of the system. These can also increase the heat transfer through the solid fuel and often do. There are three main metalized fuel additives that are studied: aluminum, lithium, and boron. Aluminum has a high heat of combustion and is easy to ignite, producing a characteristic white smoke when fired. Lithium is highly reactive additive but possesses a relatively low heat of combustion. Boron has a high heat of combustion but is difficult to ignite. Carbon black/coal can increase the radiative effects of heat flux on the top layers of the fuel and is more effective in translucent fuel grains. Most of these pose some health hazard and are often considered when trying to increase performance of existing fuels. It has been demonstrated that inclusion of additives in nano- or micro-sized particles can improve the mass burning rate of solid fuels[9].

Injector techniques

Hybrid rocket motors have an inherent flame instability if there is not stability in the flame boundary layer. A flame-holder or recirculation zone can be used to eliminate the non-acoustic instabilities in their combustion [3].

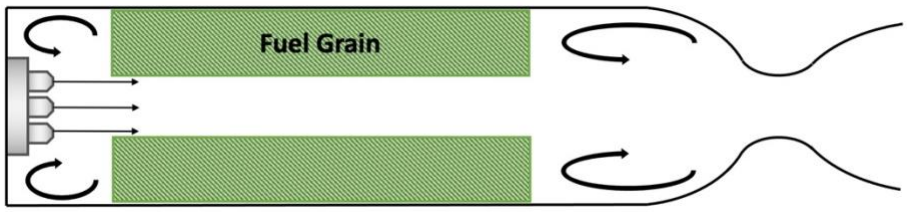

Figure 8 simple injector with good recircualtion and conditions

For better performance and flame holding and strong recirculation a small injector orifice is suggested as in Figure 8 [7] [3]. Good mixing and stable combustion is harder to attain when the injector head is a shower head or divergent spray configuration as seen in Figure 9 [3]. The vortex seen at the head and aft of the combustion chamber are main drivers for regression rates at the end faces of the fuel grain.

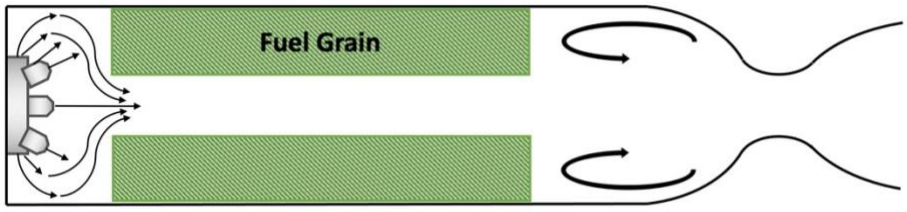

Figure 9 diffusion injector with poor recirculation conditions

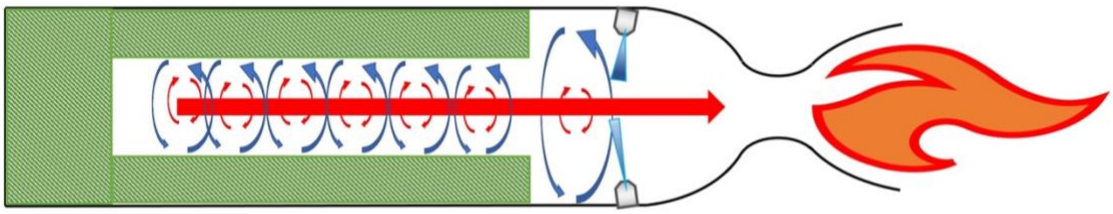

Figure 10 Example of a vortex injected HRE

A novel oxidizer injection technique represented in Figure 10, is a vortex injection hybrid, came about during the 1990s in research for higher regression rates from ORBITEC. Laboratory scale vortex injection with a swirl mechanic at the aft end of the chamber showed that the vortex created coaxial-bidirectional-vortexes that propagated first up the chamber along the fuel walls and then spiraled downward toward the nozzle. Regression rates were seen as high as 6 times faster than classical hybrids with same mass flux [4] [5]. The empirical fit to the regression rate displayed in these vortex injected HRE is in Eq. 9.

$$r = 0.193G^{0.54} \tag{9}$$

Where r is mm/s, and G is in kg/ s-m^2. Additional relations showed that the vortex injection was more directly correlated to the velocity of injection and fuel port geometry than correlated to the mass flux.

$$\frac{\rho_f r}{G} = 0.082{R_{e_D}}^{-0.03}(St_{sw}/St_o)(St_v/St_{sw})\beta \tag{10}$$

This is a dimensionless regression rate. Reynolds number is based on the average port diameter two Stanton number ratios, and a blowing parameter described in Eq. 11.

$$\beta = \Delta H_r + (h_{bulk} - h_w)/(\Delta H_v)_{eff} \quad (11)$$

In this relation, the Reynolds correlation describes the boundary layer process in the vortex hybrid differently from conventional pipe flow. The reaction zone of a hybrid will cause the boundary layer to differ from conventional turbulent flow. The first of the two stanton ratios describes the enhanced local heat transfer due to tangential injection. The other stanton ratio was included by the researchers as an enhanced wall blowing term to describe combustion effects from the inner vortex. The vortex hybrid was shown to produce high regression rates at relatively low mass fluxes because of the nature of the bidirectional vortex. The vortex was capable of compressing the injected oxidizer into a thin layer close to the fuel surface relative to the port diameter. With this effect, the fuel experiences an effectively higher mass flux compared to the port size. It is yet to be seen if this can scale to much higher mass fluxes of interest to classical hybrids on the order of 500 kg/(m^2s) or greater. The effects seen from this injection method may help explain some of the differences seen in other injection profiles. The regression of the vortex injection is more a function of injection velocity and the geometry. The work included in this thesis effort will allow for geometric effects like these to be propagated on this model.

Geometry Derived

Several studies identify that the challenge to overcoming HRE adoption is the optimizing of the fuel grain design. Most studies focus on multiport designs and optimization. Studies of multi-port hybrids comparing performance of a fixed oxidizer flow and similar injector and aft chamber set up showed that as the number of port increased, the grains shift toward their optimum O/F condition. The multiport effect showed an increased effective regression rate for 3-5 ports with respect to single port solutions [10]. In the early 1990's Purdue used a genetic algorithm called HYROCS to optimize total mass against inert mass to run series of performance studies to determine the optimal number of fuel ports for a hybrid system. This was effective at determining that HTP was better for optimizing the inert mass where LOX/HTPB was better for optimizing gross liftoff weight [12]. A related study optimizing fuel grain design with wagon wheel design assumed, showed that a HTP/HTPB design optimizes at around 10 port wagon wheel solution where a LOX/HTPB combination optimizes around a 15-20 port solution. AMROC designed several large-scale engines in 1993 and test fired an HRE called the H-1800 four times at 250k lbs. thrust (1.1MN). These tests were effective at demonstrating scalability using 15 or more wagon wheel ports with an HTPB/LOX configuration. Fuel mass slivers and chamber pressure when ports merge still remains a problem with multiport solutions. Paraffin was shown to be effective with a single port due to the faster regression rates [11] [4].

Additive manufacturing has, in recent years, spurred the interest in unique fuel grain geometry to help with the mass addition blowing coefficient and regression

problems seen by HRE designs. Rapid prototyping has been identified by many to be a technique to produce geometrically complex grain shapes that may improve the performance characteristics of HREs. Many new concepts have been tested by Aerospace Corporation like: helix ports, coaxial ports, swirls, spiral-star patterns with central ports and the "port injected liquid" engine. Many studies of additively manufactured grains focus on experiments and are often inconclusive when trying to compare results, since average regression rates are difficult to determine with classical assumptions and most classical propellants are not printable with the same properties. These tests were done using an acrylic printed fuel grain.

Helical path fuel ports showed regression rate increases up to 50%. Star swirl experiments, results indicate that the star grain significantly increases the burn surface area at the start of burn to about 3 times that of a tube grain. Most of the regression rates of the profile are higher than that of the tube grain. The combustion efficiency is also better than that of a tube grain since the spiral induces a swirl in the aft mixing chamber. The results reported suggest an increase in the exponential power relating mass flux to the regression rate. Star-swirl shaped ports for fuel grains tested in these studies between 1/8-1/2 turn-per-inch showed a positive correlation between the pitch and regression rates [15]. In comparison to simple port geometry the swirl or helix shapes all showed improvements in regression rate. The star-swirl shape is a geometry that could be analyzed by this work [16]. A "coaxial" port design was designed by Aerospace to test a passive flow management scheme. The coaxial ports are arranged to change flow path as the burn progresses. With this regression scheme new burning surface are continually being added to the grain [17]. This idea of changing burn geometry is key to the purpose

of this analysis. The tests performed by all these studies were all on fairly small grains (they could fit in your hand the smallest was about 4 inches in length and less than 1.25 inches in diameter) and results were shown comparing several materials. It is unclear what regression regime these motors fall in due to their scale. Regression rates fall in three distinct regimes based on the mass flux as shown in Figure 24 in section 3. Usually, the regression regime that we look to see the effects of additives and geometry is the turbulent heat transfer. The turbulent heat transfer regime is correlated directly to the mass flux with the ability to offset the rate by changing geometry or fuel content. For low mass flux rates the regression is dominated by radiation effects and is no longer a strong function of the mass flux. If the mass flux is too high the regression could be dominated by pressure and heat of reaction. In addition, at small scale the differences seen in port area versus surface area are not proportionate to similarly scaled geometry. It is unclear if these results would scale-up well into larger more practical motors

The last system of interest with a unique geometrical design to overcome performance issues is the “Port Injected Liquid” Fuller/McVey engine from Aerospace demonstrated in 2018. Aerospace had been experimenting with a liquid fuel grain hybrid. Instead of a classical rocket grain they printed a hollow fuel grain of ABS (based off a Stereolithography file) and filled it with kerosene. This grain burned much of the vaporized layer of kerosene and slowly burned the ABS exposing more and more surface area of the kerosene liquid layer. This design allows the combustion chamber to be more compact due to the high fuel mass addition rate of the kerosene. This design lowered the bulkhead position, allowing more oxidizer storage as well. A few successful flights were performed and the design outperformed the HTPB/nitrous oxide system it was based on

[18]. This design seems to the set the bar for analytical complexity. Features such as complex geometry regression, and multi-fuel-multiphase regression are a few of the many problems this thesis effort can help to solve for this type of engine. Tests have been done on this unique and effective system, but the experiment cannot be compared to an analytic model. Without a strong idea of how this design performs, optimization is simply guessing and checking.

Summary

High regression rates and performance increases can be achieved by unique configurations and clever mechanisms. These increases in regression and performance are not attractive if they come with low combustion efficiency. There are several studies that publish misleading results for enhanced regression rates that are not applicable with respect to scaling or have enhanced regression rates on material whose performance is poor for propulsion. The most misleading aspect when researching hybrids is that an advance in a single performance direction can lead to solving the problem of scaling hybrids.

There are few standards for testing hybrids, making comparison of results challenging. Scalability is a difficult problem to approach because there are so many combinations of fuel and oxidizers and some do not scale well but others do. A key focus not seen, is the design of a hybrid that can scale based on the ability to manufacture for the intended performance at scale. HRE's are a viable contender to replace SRM and LRE. If HRE can gain in popularity and overcome performance hurdles, their incredible safety, simplicity and low cost will allow for hybrids to be the answer for safe manned and unmanned space launch.

III. Methodology

Chapter Overview

This work is attempting to make geometric regression simulation easier by having the geometry generated in a native format that most CAD software packages produce. A good deal of effort in HRM analysis is generating geometry data within an existing simulation software. With flow conditions set, starting geometry can vary and it may be able to de-couple, simplify, or reduce the number of free variables when it comes to analyzing regression equations. This will allow for more complicated geometry to be analyzed.

The regression rate of the solid fuel of a hybrid has been of key interest for most studies and is the primary focus of this analysis of HREs. Analysis for performance of hybrid rockets starts with a ballistics element approach for a basic cylindrical-single-port.

The regression Eq. 5 is a general regression equation that is adequate at describing the regression characteristics of a wide variety of operating regression regimes, materials and configurations. To accurately describe the turbulent heat transfer regime where we have an ablating fuel with minimal radiation heating effects, we use the Eq. 12 described by Marxman [7] [11].

$$\dot{r} = 0.036 \frac{G^{0.8}}{\rho f} \left[\frac{\mu}{x}\right]^{.2} \beta^{.23} \tag{12}$$

Substituting in Reynolds number represented in Eq. 13 using the breakdown in Eq.14 the regression equation becomes more unit agnostic and we get Eq. 15. Which is also attributed to Marxman through the Chiarverini text. The blowing coefficient term is described by Marxman as well in Eq. 16.

$$Re_x = \frac{\rho_e \, v_e \, x}{\mu} = \frac{\dot{G}x}{\mu} = \frac{\dot{M}x}{\pi\left(\frac{D_h}{2}\right)^2 \mu} \tag{13}$$

$$Re_x{}^{-0.2} = \left[\frac{\mu}{\rho_e \, v_e x}\right]^{0.2} = \left[\frac{\pi \, D_h \mu}{4\dot{M}}\right]^{0.2} = \left[\frac{\pi\left(\frac{D_h}{2}\right)^2}{\dot{M}}\right]^{0.2} \left[\frac{\mu}{x}\right]^{0.2} = G^{-.2} \left[\frac{\mu}{x}\right]^{0.2} \tag{14}$$

$$\dot{r} = 0.036 \frac{G}{\rho f} Re_x{}^{-0.2} \beta^{0.23} \tag{15}$$

$$\beta = \frac{Ve}{V_{fl}} * \left[\frac{(h_{fl} - h_w)}{\triangle H_{v,eff}}\right] \tag{16}$$

Test Subjects

The simplest case for regression is a cylindrical grain with a cylindrical port down the middle. HTPB has a robust history of being used as a basic propellant for hybrids and HTPB and LOX are classical combinations for testing HRM's. The abundance of data for HTPB/LOX its and its simple chemical analysis makes it an ideal candidate for baseline comparisons [7]. The reaction that the combustion is being modeled as is represented by Eq. 16.

$$C_4H_6 + \frac{11}{2} O_2 \rightarrow 3H_2O + 4CO_2 \tag{17}$$

The flame of this reaction can reach temperatures in excess of 3,500K at stoichiometric ratios. For mass fluxes up to 150 kg/s-m^2 radiation can account for up to 30% of the total heat flux. The applications in this work are likely to cross the threshold where heat flux due to radiation may ultimately need to be considered. The ranges of

mass flux we are anticipating range from 35 - 350 kg/s-m^2. With HTPB as our material selection we avoid a fuel that has the complexities of liquid entrainment and simplify our regression and CEA calculations. This fuel choice also eliminates geometric distortion due to sloughing. This simulation is taking geometry and flow conditions from a study done by Sapienza University of Rome and the University of Naples titled *Numerical Modeling of GOX/HTPB Hybrid Rocket Flowfields and Comparison with Experiments* [19]. This paper has detailed information with respect to flow conditions of a simplified cylindrical port engine. The work contained experimental data and contributed to two separate analysis one ultrasonic acoustic analysis and one CFD analysis to predict regression rates. There were several mass flow conditions tested at the average diameter of 42 mm. The regression rates at several internal diameters 25mm 30 mm 35 mm 42 mm 49mm 60mm were tested as well at the flow rate of 133 g/s. For the analysis we intend it will be more important to explore the problem space with fixed oxidizer flow. Figure 11 show some of the regression results as a function of the port length.

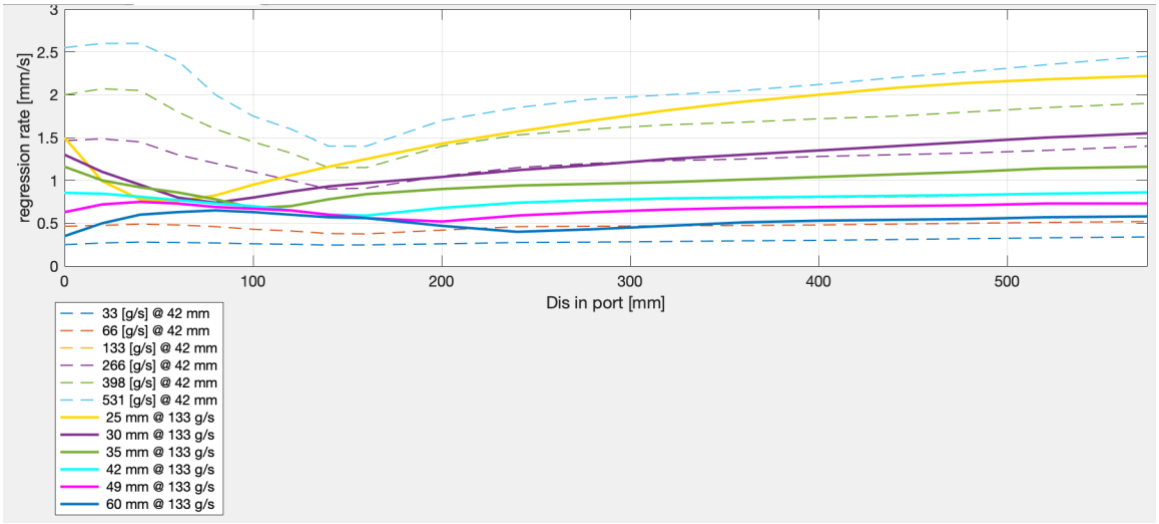

Figure 11 Regression vs. port length comparing to various mass flow rates

Process

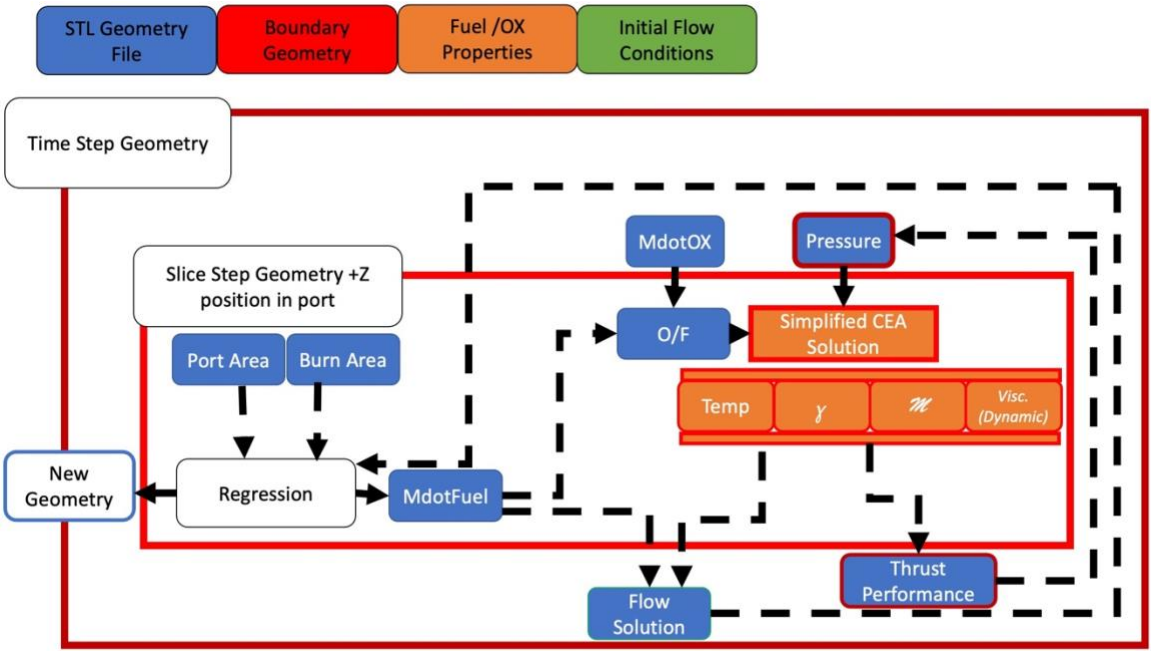

Figure 12 Hybrid Regression Code process flow Diagram

The analytic process this work is using to describe performance expected from running a HRE rocket engine cycle is displayed in Figure 11 and covered in detail in the following section.

1. STL file
    a. STL definition
    b. STL creation
    c. STL import & vertex reduction\face vertex consolidation
2. Boundary condition definition
3. CEA to for combustion properties

4. Potential flow solution to set blowing condition
    a. Least min square solution to solve for matrix of source strengths separated into vector components
5. Ballistics analysis
    a. Solve for O/F at each slice
    b. Regression and fuel added at slices and overall performance.
    c. Track facet neighbors to detect large changes in orientation to one another and to track sheet bodies for geometric family analysis.
6. Produce new geometry based off regression rate
7. Calculate starting conditions for next time step
8. Calculate performance parameters

Stereolithography Files (Tessellated Geometry)

The STL (STereo Lithography) format was developed primarily by Albert Consulting Group and is supported and a format distributed and encouraged for use by 3D systems starting in 1988. STL is a standard for rapid prototyping systems, representing and simplifying point cloud data. The format is available in an ASCII format as well as a binary [20] [21].

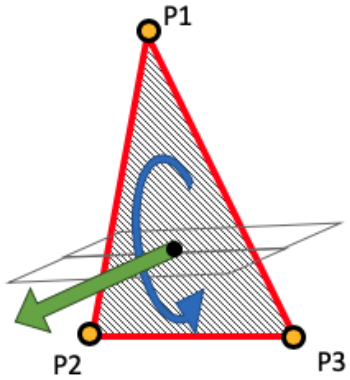

Figure 13 facet defined by 3 points and normal vector using right-hand rule

A core concept to this work is the implementation of an STL file or Stereolithographic file to accurately represent geometry in three-dimensional space [22]. Stereolithographic files are a collection of faces that approximate the shape of the outer surface of a solid object using many small interlocking triangles Figure 12 shows a representation of one of these triangular facets. Typical assumptions with an STL file are that your object is singular, watertight and is solid inside the outer boundary defined by

all facets in the file. The definition is composed of 3 primary data pieces: facets, normal direction for facets, and vertices defining the bounds of each facet [21].

Facets are the largest class of definition in an STL. The definition of a facet starts by declaring a facet normal vector. The normal vector is a unit normal direction of the facet to define direction of the outer surface of the object. The surface normal is not always required depending on the STL reader/writer. The outward surface normal can be determined by the right-hand rule. The vertices are defined next as three points that are used to define a facet. These are defined in cartesian coordinates and are [x, y, z]. The points are assigned in a specific order so that the flow from point 1 →2→3 acts as the right-hand rule with the surface normal vector pointing in the outward direction from the object. In yellow as P1 P2 P3 in Figure 13. The order of the vertices with the cross-product of the vectors formed by going from one vertex to another in the specified order will achieve the direction of the outward surface normal [23]. An example of the facet is depicted in Figure 13.

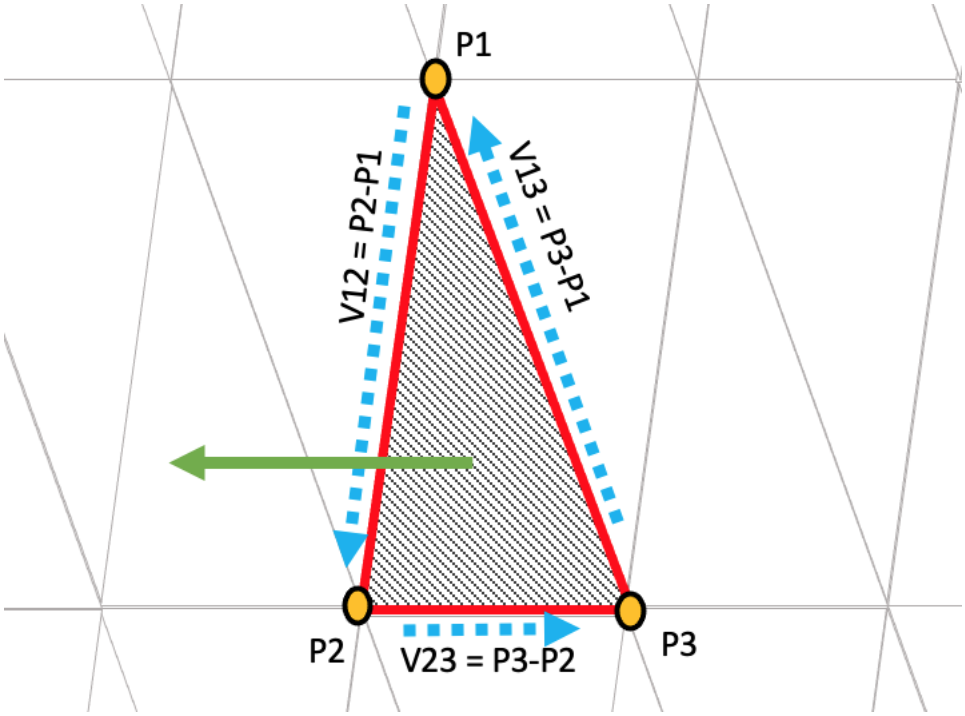

Figure 14 facet defined by 3 points and the vectors created by connections

$$\overrightarrow{V_{\perp}} = \overrightarrow{V_{12}} \times \overrightarrow{V_{23}} = \overrightarrow{V_{23}} \times \overrightarrow{V_{31}} = \overrightarrow{V_{31}} \times \overrightarrow{V_{12}} \tag{18}$$

$$\widehat{V_n} = \frac{\overrightarrow{V_{12}} \times \overrightarrow{V_{23}}}{\left\|\overrightarrow{V_{12}} \times \overrightarrow{V_{23}}\right\|} = \frac{\overrightarrow{V_{23}} \times \overrightarrow{V_{31}}}{\left\|\overrightarrow{V_{23}} \times \overrightarrow{V_{31}}\right\|} = \frac{\overrightarrow{V_{31}} \times \overrightarrow{V_{12}}}{\left\|\overrightarrow{V_{31}} \times \overrightarrow{V_{12}}\right\|} \tag{19}$$

$$A_{face} = ½\left\|\overrightarrow{V_{12}} \times \overrightarrow{V_{23}}\right\| = ½\left\|\overrightarrow{V_{23}} \times \overrightarrow{V_{31}}\right\| = ½\left\|\overrightarrow{V_{31}} \times \overrightarrow{V_{12}}\right\| \tag{20}$$

In the course of this work it will be necessary to recalculate the surface normal of each vector Eq 18 describes finding a normal vector then to normalize the surface normal

vector Eq.19 is used. For getting the burn area of the facets and the port area swept by facets we will be using variations of the surface area equation seen in Eq. 20.

Creating Geometry

The geometry can be created using most computer aided design (CAD) software. The geometry for this effort was created using the software Autodesk Fusion 360. The CAD software you use may or may not give control over the resolution of the stereolithography files output. Several factors you might wish to control are facet size and angular resolution. Autodesk Fusion 360 give the user some control of these features. Other software you might use for post processing and analysis for geometry would be CloudCompare or Meshlab. Figure 15 depicts an extremely simple test geometry used to develop and refine the geometric shape regression mechanism of this code.

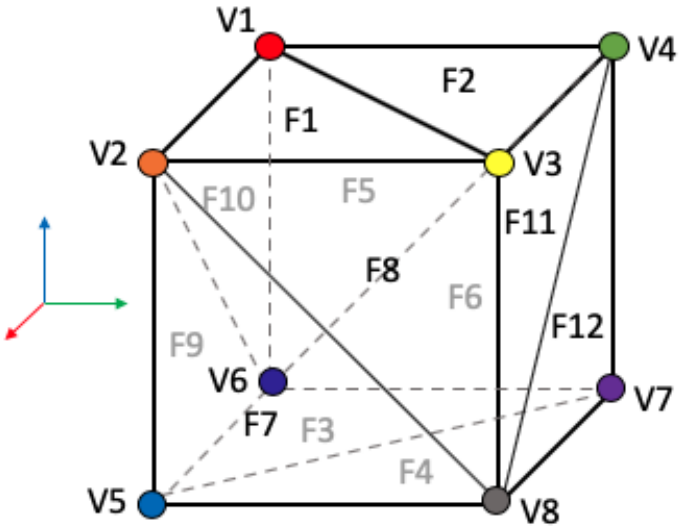

Figure 15 Cube defined in STL format

Geometric Definition limits

The geometry needs to be defined so that the shape is clearly visible otherwise the analysis is useless. When considering the quality of STL, the more uniform the facet size the better. Large or long facets make for uneven regression when they are crossed by more than a few slices in the analysis. Regression on large or long facet can cause jagged

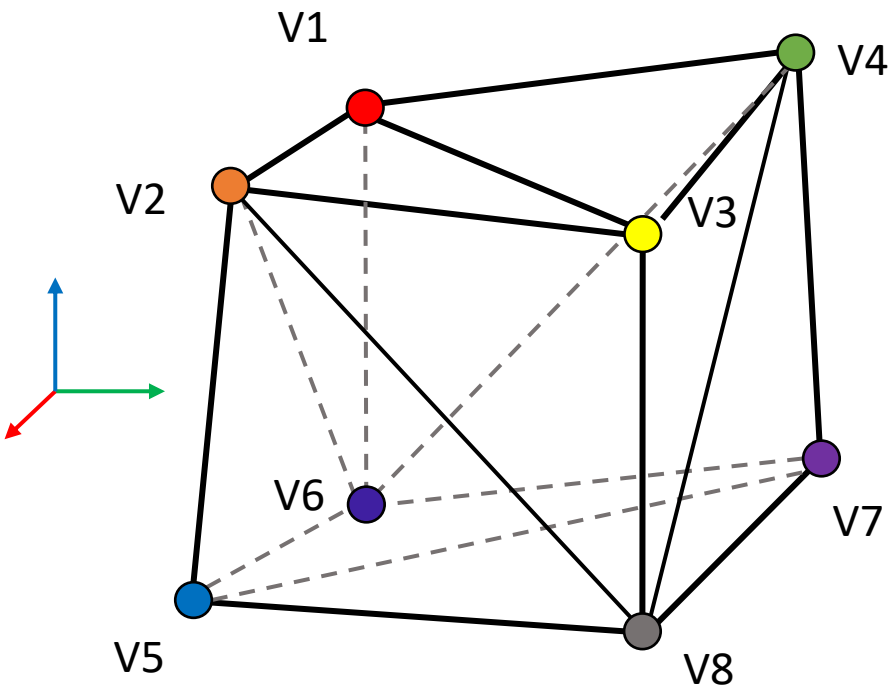

Figure 16 Basic Cube regressed shows large facet Jagged regression

or misshapen geometry as seen in the Figure 16 where we see the cube from Figure 15 regressed uniformly based on facet normal direction summed at the connecting vertices. There are too large and too few facets to accurately preserve the cube shape accounting for uniform regression of all vertices associated to facets. Reducing model resolution for the fuel grain geometry will give the same result with too few facets and will make an

object coarse and tessellated looking and will cause random spikes in performance due to geometric edges appearing and disappearing. These larger facets will not give the desired results due to the resolution. Also, if the model is too coarse the simulation will not accurately represent the intended geometry.

Having too many facets is not usually a problem in terms of representing geometric accuracy. However, this will increase run time of the simulation and there has been a resolution study recorded in Appendix C looking at how many facets are reasonable for this work.

Geometry intended to be used in this analytic code should be manifold. This means that all facets are connected on all sides to other facets and that the model is "Water-tight." On top of being manifold, the model should have one centrally located port. This means that there is a single path going through the object and there is one entrance and one exit.

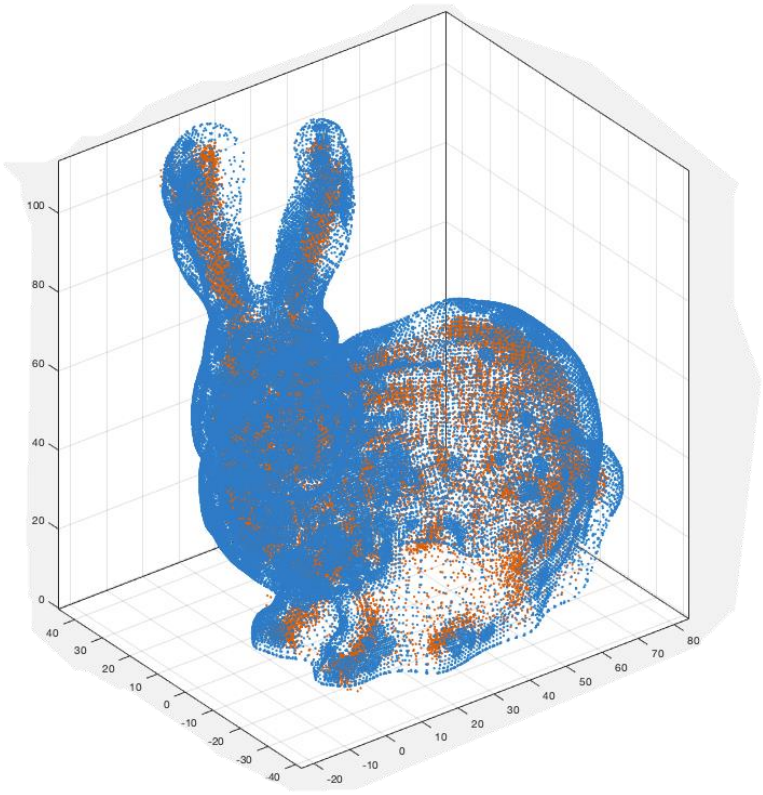

Figure 17 Stanford bunny test article for regression on organic shapes

Shown in Figure 17 is a common test file called the Stanford bunny has been regressed by this analysis. The Stanford bunny has many facets and a good amount of detail. As a test article of this analysis the STL file was regressed to troubleshoot the regression mechanic.

The regression on the bunny is uniform over the surface. The original bunny is in blue and the regressed geometry in orange. This result appears to look similar to a scaling change in the shape, due to the small regression distance. The key difference is that the

regression will ultimately reduce the geometry to a point (in theory). With this model we can see several problems that might arise. The ears are one such problem because they are long and narrow, they will regress away first leaving nothing of the ears' facets. If those facets disappear, how do we solve for a manifold body? Maybe the ears' connection to the rest of the geometry will disappear first, leaving 3 bodies instead of one, a sliver condition if it occurred in an SRM or HRE. In the current way the regression is configured, as the facets approach the geometry's opposing surfaces, the regression will turn those facets inside out relative to the rest of the model. If left to regress after the volume reaches its minimum volume the geometry will invert and continue to get larger and larger until the end of the simulation.

STL Importing and Consolidating facet and vertex

It is common for binary and ascii type STL files to have redundant definitions of vertices. This means that if all the vertices defined are used, then we will have duplicates defined. This is not a problem for most STL uses, since they are most commonly used as a static, unchanging definition on unchanging manifold geometry. When these redundant vertices exist representing the same points in space they act as different points when defined by each facet. So, as the facets regress, they push and pull their corresponding vertices. Facets defined as neighbors should share vertices. If neighbor facets are not actually sharing the same vertex, the regression will disconnect the geometry and destroy the manifold nature. A list of vertices should be created and reduced to eliminate duplicate definitions. The duplicate vertices eliminated should be replaced with the

reduced set to fix and define the facets. This list of vertices should contain no redundant vertices and will then work with the analytic code.

Boundary Condition Definition

Defining the geometry orientation is crucial. STL definition is dependent on cartesian coordinates in row vectors [x,y,z] for all vertices. The X and Y local zero are taken form the center of volume for the geometry. The position of the fuel grain geometry closest to the injector is locally defined as zero in the Z direction. This defines our axial direction of net flow in the Z+ direction (referred to as down the port).

Determining the boundary conditions is key for accurate results. If the outer edge facets are not constrained or ignored, the outer face geometry can regress along with the inner ones. The effect of this would mean that we have oxidizer flow between the case wall and the outer boundary of the fuel, this condition would usually correspond to case burning and port clogging. In general, for a simple case it can be assumed that the chamber ports containing the fuel are circular/cylindrical (most rocket and hybrid applications are). This would not necessarily be a good assumption for a slab burning test for hybrid applications.

The code is limited at this time to single port and with no bubbles or occlusions. This means the analysis code, at this time, would not be able to calculate multiple different port areas, which is a common design feature for flight level engines. The port area on this iteration of the code is calculated using the cross products of the vectors created by the intersection of the center plane of the slice and each facet. This means that you would have to define several local center lines to establish several cross-sectional

port areas. This could be done currently with many flow paths as long as the flow areas remain separate. The problem is deciding how the solution behaves when flow regimes meet or what to do about the velocity calculation. In addition, having to define or set up flow paths defeats the point of the automation this thesis work is trying to introduce. Calculating and detecting several flow paths is simply outside the scope of this current work. It may be possible determine a multi-port solution from surface normal to determine boundaries or centerlines. For general analysis this problem should be eventually overcome since most hybrids have multiple ports.

The time on simulation is taken from the results of the test geometry experiments [14] running for a 25 second duration in simulation time, at 0.1 seconds time increments indexed by the variable "*Tindex"* for time-index. There is a sensitivity analysis done for the time step increment in Appendix B. The mass flow of oxidizer remains a constant 0.133 kg/s for the entire duration of the burn. The initial pressures both in chamber and ambient are set to 14.7 psi. Locations along the center line have been selected to determine the exhaust velocity at the core to calculate the blowing coefficient. These positions are on the centerline an correspond to the center point of each slice.

For geometry the fuel grain is 574mm in length has an inner diameter of 25 mm and an outer diameter of ~133 mm (corresponding the inner diameter of the case [14]). There are also an ahead and aft chamber that need to be included in the analysis so pressure can be calculated. The ahead chamber is 65 mm long with an 80 mm diameter, the aft chamber is 65 mm long with a 70 mm diameter. A boundary cylinder of 65 mm radius has been set to exclude vertices outside this boundary from the simulation. The number of slices for the analysis was set arbitrarily to 100. There is a sensitivity analysis

to the number of slices seen in section IV. Placement of the injector is at [0,0,-60] mm so as to not produce a discontinuity in Reynolds number based off of axial distance. The nozzle is located at [0,0,740] mm. The area of the throat is 201 mm^2 with an expansion ratio of 2.44. The direction of net oxidizer flow is in the +Z. A start limit for the regression as a function of the fuel grain length was set a 5% of the total length of the fuel grain and an end limit for the regression was set at the 95% of the fuel grain length. These limits were set to exclude the ends of the fuel grain from the analysis. These are excluded because the end faces regress at a different rate and are functions of recirculation that have not been approximated in this analysis.

Ballistics Element approach

A ballistics element approach starts by stepping down the fuel grain at discrete distances. Each step is assumed to have similar operating conditions such as temperature, molecular weight, and species derived from the port pressure and oxidizer to fuel ratio. Figure 18

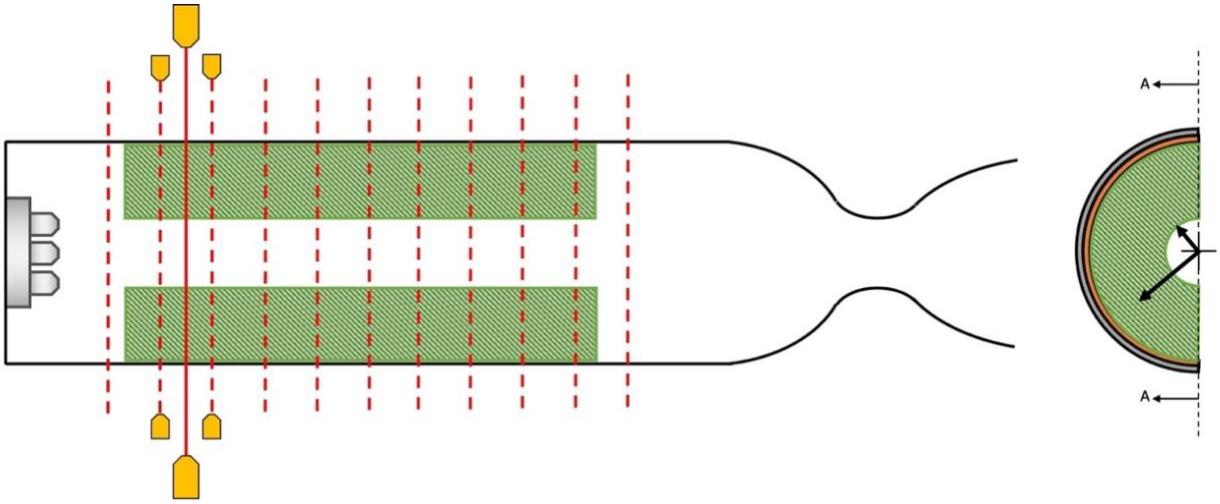

Figure 18 HRE fuel grain cut into slices

shows an example of the geometry being cut into several slices down the port axis. The fuel is sliced into "*SliceN"* slices where the slice is established by two planes oriented with their normal to the axial direction sub dividing the fuel grain in slices of height '*dSlice'*.

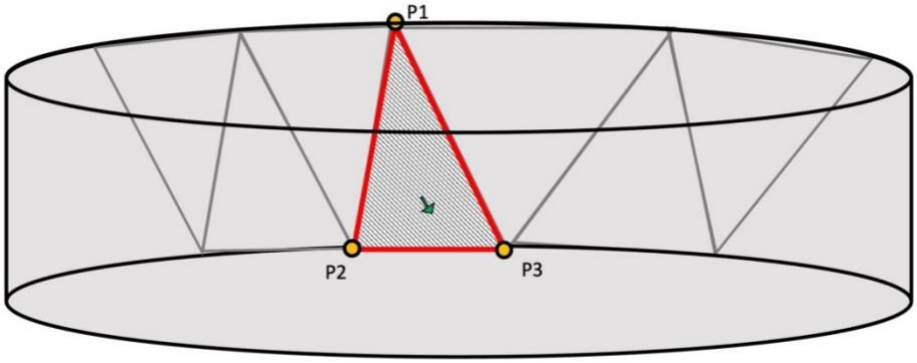

Figure 19 View if inner port surface made of triangualr facets

Figure 19 show a facet defined on the inner diameter of circular port. The burn area of a port slice is calculated by solving for the area intersected on each facet then summing the burn areas of the facets with intersection. Figure 20 and Figure 21 shows the facet being sliced by 2 cutting planes.

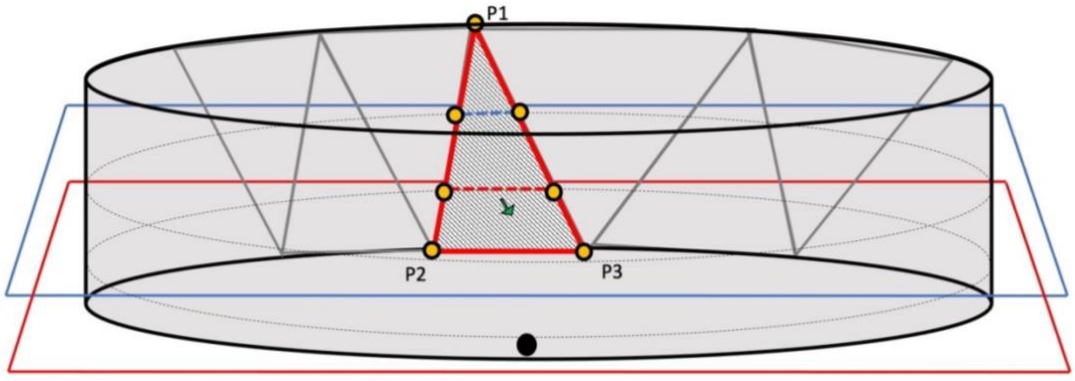

Figure 20 Facet on inner diameter of cylinder port cut by planes

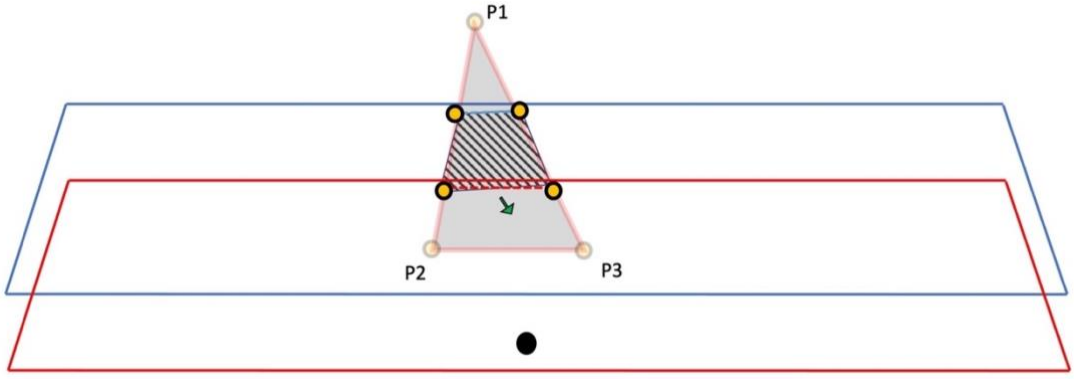

Figure 21 Facet cut by 2 planes

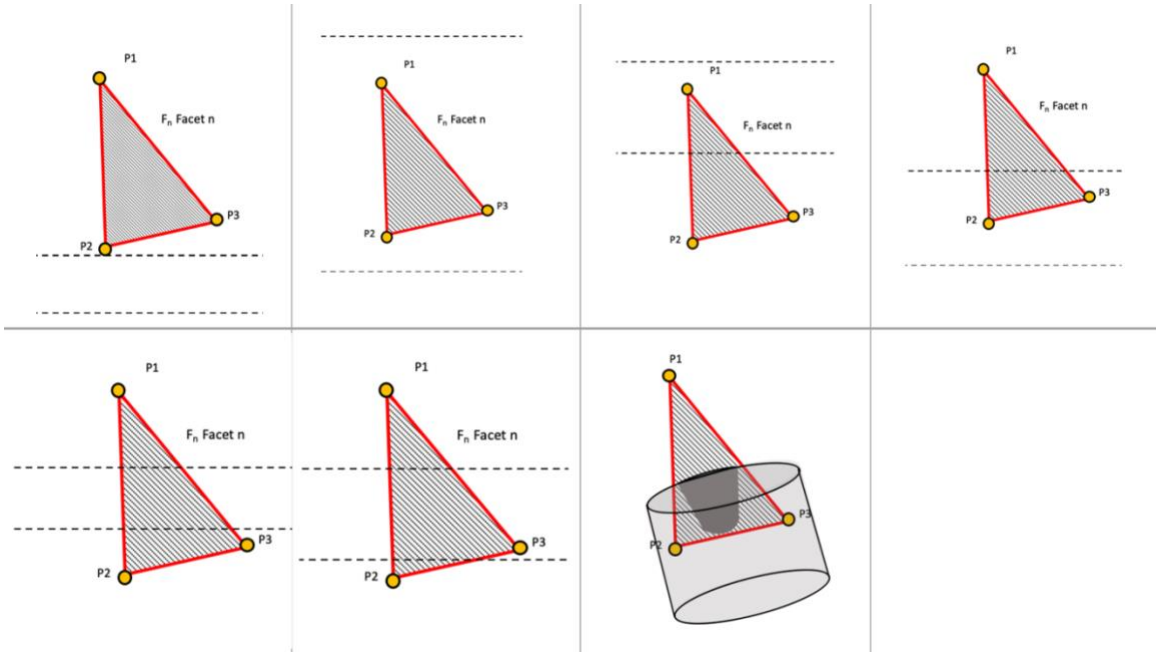

Figure 22 Possible intersection between cutting planes and facet geometry

The types of intersections created by slicing with ballistics element approach with STL facets are shown in Figure 22. Going from top left to right to the next row we have several definitions of how a facet can be intersected by slicing planes. Type 0 which has no intersection at all, and which requires no surface area calculation. Type 1 is where the facet is entirely engulfed in between the two slicing planes. For intersection types 2-5 we need to define temporary points in the locations where the slicing planes intersect the facet vectors. Type 2 and Type 3 are partial intersections including respectively either one or two of the vertices. Type 4 intersection the slicing planes intersect 2 vectors at 2 different points and produce a trapezoid shaped area. Type 5 intersections intersect all three vectors at least once and include a point creating a surface are the shape of a pentagon. Each require separate methods for calculating surface areas. The last intersection, Type 6 seen in the lower right-hand portion of Figure 22, is a complex

intersection mid-facet that has no intersection with any vectors or vertices defining the facets. A Type 6 intersection has been ignored for this work and might be considered to be ignored for further work as well. Type-6 intersections occur when unlike geometries meet, similar to the dilemma of a square peg and round hole. Where these would be critical would be when these intersections make up large portions of surface area and port area. Large area intersections like this would only occur when the facets are too coarse to represent the shape of the boundary definition. A good deal of work went into this developing this portion of code for the analysis, but it is an extended exercise in basic vector geometry to go into further detail in this document.

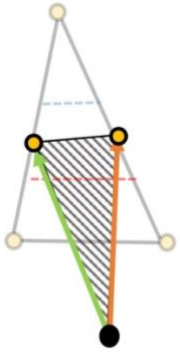

Figure 23 Example of port area contribution from a single facet

The area of the current port is calculated using a similar method taking the center point of the slice and creating another plane of intersection allowing the creation of vectors where this center plane intersects the facets included in the slice. Each vector from the center of the port is crossed and halved and then all summed together to get the port area of the slice.

Regression

The regression rate can be described in three separate phases based on mass flux of the oxidizer; radiation dominant regression, turbulent heat transfer dominant regression and gas-phase chemical kinetics driven regression. A graph describing these regimes can be seen in Figure 24.

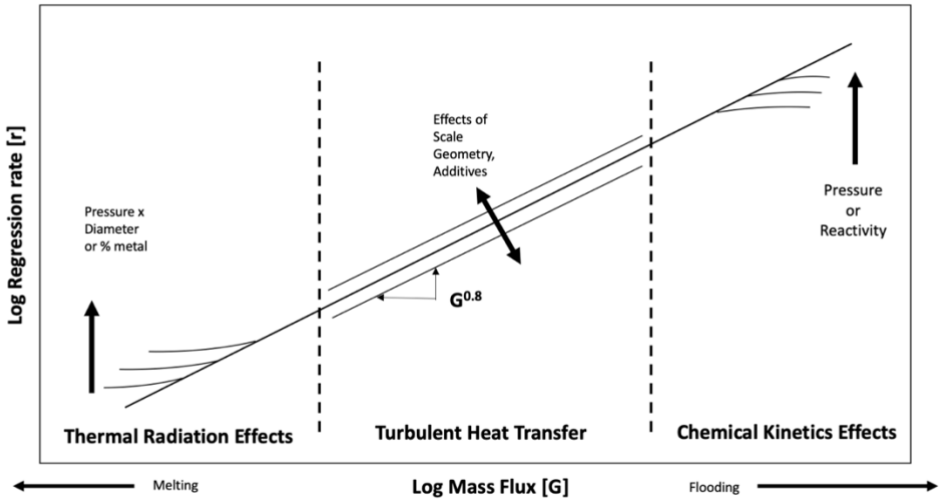

Figure 24 regression regimes related to mass flux

The radiation dominant heat-transfer regime of fuel regression is a function of flame temperature and the heat of vaporization of the fuel grain. This domain is difficult to maintain for larger systems since the flame temperature is often driven by the oxidizer-to-fuel ratio (O/F). The closer to stoichiometric ratios for the reactants, the hotter the flame and the larger the regression. This is particularly effective for smaller chambers since the surface area to port area ratio tends to produce more fuel rich mixtures. The distance from the flame to the fuel regression zone are smaller and so there is more

energy transferred from radiation as well. Larger combustion chambers trend towards oxidizer rich due to lower burn surface area to port area ratio. The turbulent heat transfer regime or intermediate regime is specifically dependent on the rate of oxidizer flow, and can be altered with scale, geometry, and additives. The direct driver of the regression rate here is the mass flux, composed of oxidizer and exhaust gases. This regime of fuel regression is of the most interest when using additives or fuel grain geometry to affect regression. The extreme end of the mass flux, where we are flooding the fuel port is where the fuel regression is a function of the fuel's reactivity and pressure. This work is focused on the turbulent heat transfer region where the regression rate is not a function of pressure or radiative heating effects.

The regression equation being used is critical to the validity of the analysis. Several regression equations have been established [4].

$$\dot{r} = aG^n \tag{5}$$

$$\dot{r} = 0.036 \frac{G^{0.8}}{\rho_f} \left[\frac{\mu}{x}\right]^{.2} \beta^{.23} \tag{12}$$

The fuel regression equation for simple port hybrid provided in Sutton [7] in Eq. 12 can only be used with English units due to the raised power of mass flux, viscosity, distance measured x and the leading constant which has English units [4].

Using a Reynolds number as a function of axial distance of the slice-center from the injector head (it's advisable to place the injector at some negative distance), the mass flux is calculated from mass flow and the current slice cross-sectional area.

$$Re_x = \frac{\rho_e \, v_e \, x}{\mu} = \frac{\dot{G}x}{\mu} = \frac{\dot{M}x}{\pi\left(\frac{D_h}{2}\right)^2 \mu} \tag{13}$$

$$D_h = \frac{4Ap}{Perimeter} \tag{21}$$

$$c = \sqrt{\gamma RT} \tag{22}$$

The blowing coefficient is calculated from Eq. 16 [11]. This is where we need to know the velocity at each center port. The velocity of the exhaust gas is used from the former time step to estimate the blowing coefficient. The velocity at the wall or flame velocity is set to be 1% of the local Mach velocity based off of the simulation boundary condition set in simulations by Majdalani [10] for high-speed flow effects in a hybrid rocket. An equation for Mach velocity can been seen in Eq. 22 it makes the assumption of an ideal gas and equilibrium flow. The enthalpy of the fuel and heat of pyrolysis/ vaporization are taken from the experiments used for geometric comparison [20]. The enthalpy of the exhaust gas is calculated from local conditions and solutions from the CEA surface.

$$\beta = \frac{Ve}{V_{fl}} * \left[\frac{\left(h_{fl} - h_w\right)}{\Delta \, H_{v,eff}}\right] \tag{16}$$

We use the substitutions for Reynolds number to prove the equations suggested by Sutton and Marxman are the same allowing the use of metric units. The equation suggested by Marxman, et al [11] is the regression Eq. 15 this analysis uses.

$$\dot{r} = 0.036 \frac{G}{\rho_f} Re_x^{-0.2} \beta^{0.23} \tag{15}$$

The mass flow into each slice is calculated from the sum of mass from the former slice. For initialization the first slice at each time step has only the injector mass flow seen in Eq. 24. The port area and burn area is calculated as described earlier in the ballistics elements section.

$$\dot{M}(1, Tindex) = \dot{M}_{oxinj} \tag{23}$$

$$\dot{M}(SliceN) = \dot{M}(SliceN - 1) + A_b(SliceN) r(SliceN) \rho_f \tag{24}$$

From this regression rate and geometric slicing there is now adequate information to calculate the fuel mass added to the flow. The O/F can also be calculated.

Implementing NASA Chemical Equilibrium, Analysis (CEA)

There are several parameters that change drastically based on varying combustion conditions. Due to their nature hybrids have a highly variable combustion environment. It is required to update several parameters that are important to this analysis. NASA's publicly accessible Chemical Equilibrium Analysis (CEA) is widely accepted as a reliable baseline that has widespread use for combustion analysis. Integrating a call to NASA CEA was deemed restrictive in run time and complexity for this analysis. Instead, it was decided to run a series of O/F and pressure conditions and create a local library to interpolate the local conditions based of inputs of O/F and pressure.

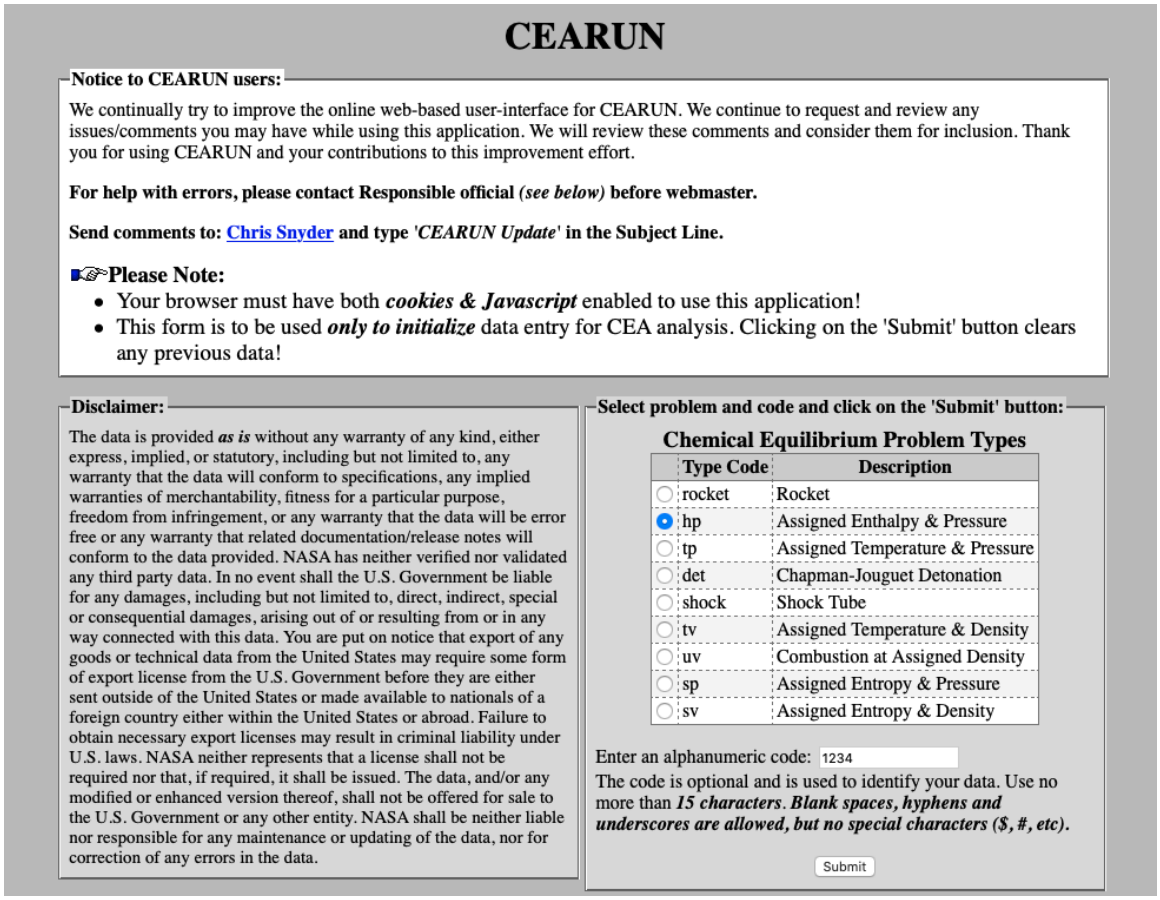

Figure 25 Landing page for NASA CEA Run https://cearun.grc.nasa.gov

For this analysis NASA CEA provides values of; ratio of specific heats (γ), temperature (K), molecular weight [amu] and viscosity [mPoise] as a function of O/F and pressures. Pressures are determined at the end of each time step. Using the Assigned Enthalpy and Pressure (HP type code) for the problem type turn on transport properties (for those unfamiliar, each run desires an arbitrary alphanumeric code).

Pressure values were used from 100 psia to 2,000 psia with an interval of 100psi.

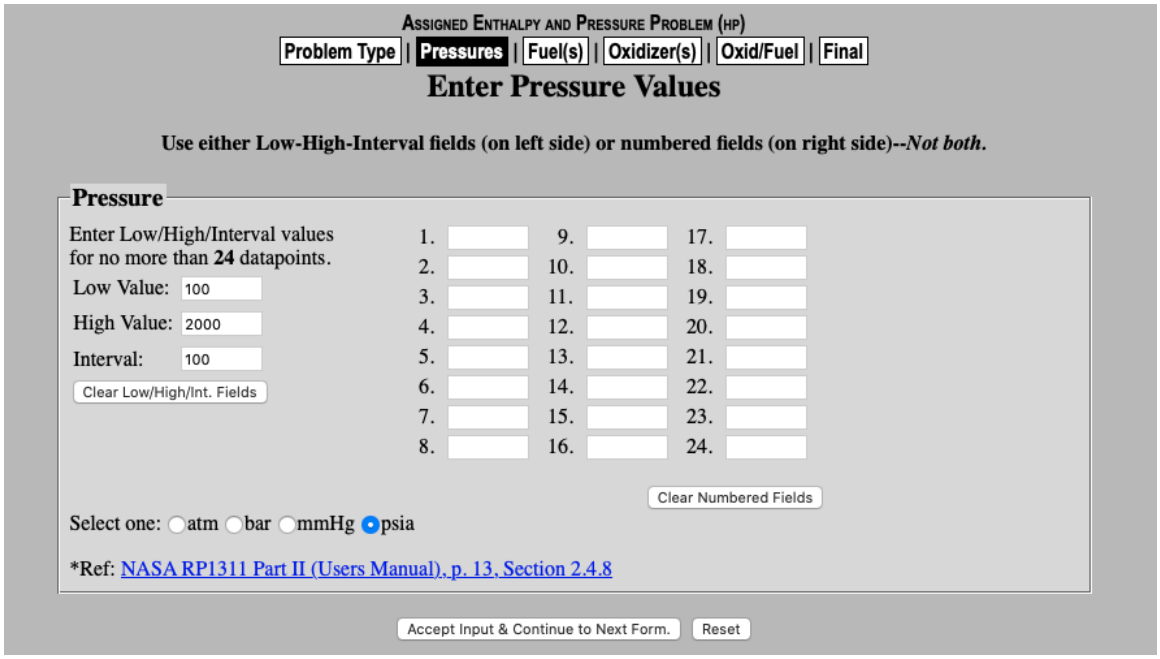

Figure 26 Pressure Selection for NASA CEA

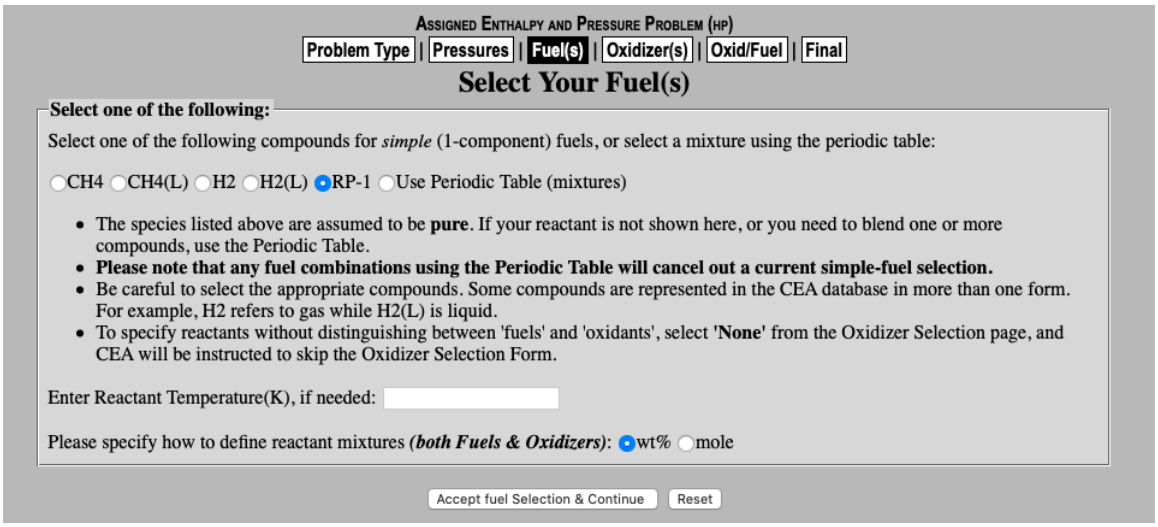

Figure 27 Fuel Selection for NASA CEA

RP-1 fuel is then selected for HTPB since the combustion has been historically noted to have similar characteristics to RP-1/LOX (Kerosene/LOX) [7] [2] and the O/F that we are tracking is going to be by weight so leave the radial button wt% selected.

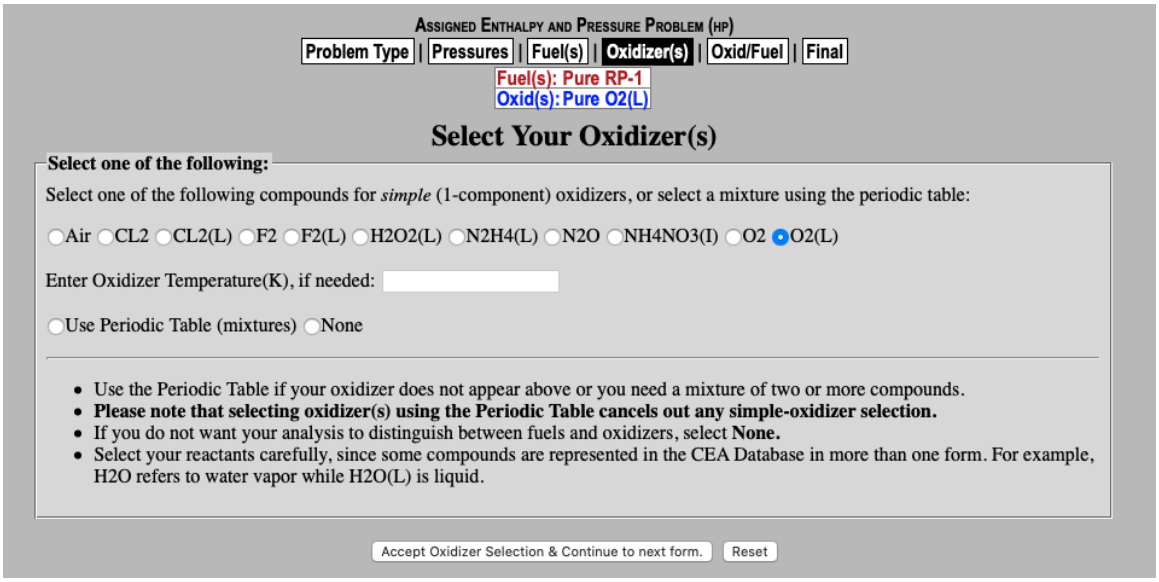

Figure 28 Oxidizer selection for NASA CEA

For Oxidizer selection pages seen in figure 28 select O_2(L). A starting temperature for the propellant can be entered if more precise combustion analysis is required but since the values are to create a sheet of properties, attempting to guess the starting temperature is not necessary.

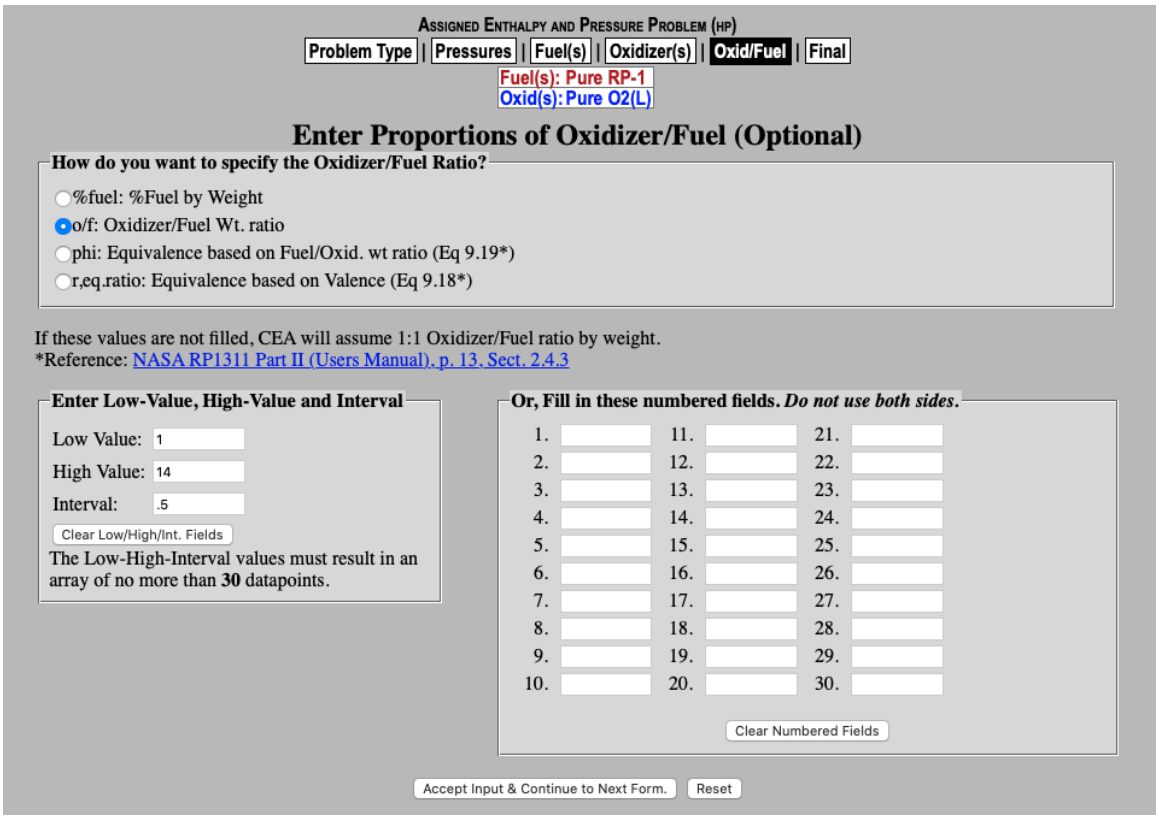

Figure 29 Mixture ration Selction fro NASA CEA

Values were entered for O/F ratios ranging from 1 to 32 with varying increments based off of variation of results and fit surfaces. In order to get an accurate fit for the critical regions of combustion, you will have to do several runs for the intervals of interest. There is a limit of 30 O/F data points. To achieve the surface in this analysis 59 O/F ratios were used and 20 Pressure levels.

In order to get the viscosity properties, it is required to select the "*Include transport properties?"* radial button. Run the CEA get the values in a table ready to import into Matlab. To create a fit surface, Excel was used to compile the results into a table. Create a table of the value you want. Each row is a different O/F and each column is a different pressure. Now using Matlab double click the .xlsx file and it will bring up an import interface. Change output type in output type dropdown to "Numeric matrix". Import the variables and change their names to Press and O_F. (by default imports the file name). This method has the first row and column as indexes so we can import them as variables 'Press' (CEA outputs in BAR I changed to psia) and O_F for oxidizer/Fuel ratio. Import the actual data by highlighting the columns and rows remaining as the variables. Run the code in Appendix A to get polynomial surface fit for algebraic values for a 5^{th} by 5^{th} order polynomial fit.

The fit function will output a polynomial equation with variables to plug in for the surface fit to solve for a solution corresponding O/F and pressure inputs to the properties surface for the code iterations. Due to large variability in results over the range of oxygen to fuel ratios, it was required to do several best fit surfaces with some conditionals for determining what was the best equation of best fit for the O/F regime. For this analysis 5 ranges of O/F were used to get good smooth matching data. Ranges of O/F were 1-2, 2-4, 4-12, 12-20, 20-28. Each data surface was created with overlapping values to get smooth continuity between data surfaces. There was less variation in the pressure, so there was

no need to sub divide the surfaces by the pressure ranges. The fits for 4 properties surface can be seen in Appendix A.

Flow Conditions

The burning rate of a hybrid is sensitive to the local flow field in the chamber and many assumptions like uniform burning as seen in SRMs are not adequate for characterizing the burning mechanics of a hybrid [10]. Pipe flow has also been seen as inadequate to describe the conditions at play given that the side walls exist as a source [10]. To fully characterize the turbulent flow condition and heat transfer of a hybrid rocket a computation fluid dynamic solution would need to be attained. The reality is that simulations required to accurately characterize the flow are not available one of the limiting factors is the ability to accurately simulate the chemical kinetics and the reaction rate for intermediate reactions. Often simulations are based on assumptions from SRM analysis with fixed concentrations or fixed geometry. In high Reynolds number flow conditions, SRM assumptions and simulations are used to reach an acceptable approximation for the flow fields in HRMs. The challenge is that the combustion products are not heterogenous in composition and change the entire length of the area-of-interest (the port). A broad assumption among hybrid flow field analysis is the no slip condition at the wall. This is not true at the fuel-oxidizer interface surface in an HRM or an SRM where the walls are ablating and producing gas at slower velocities than the core flow. In order to reduce the complexities, run time, and expertise required to create and run this analysis, a potential flow methodology was used to approximate the flow conditions within our port. There are many limitations to this solution, but the solution

seems adequate at this time to attain the flow-based parameters included in the blowing term of the regression equation. One limitation of this solution is if you probe a position outside the boundaries of the volume-of-interest the flow field exists and has arbitrary values that do not correspond to reality. Another problem with the potential flow solution

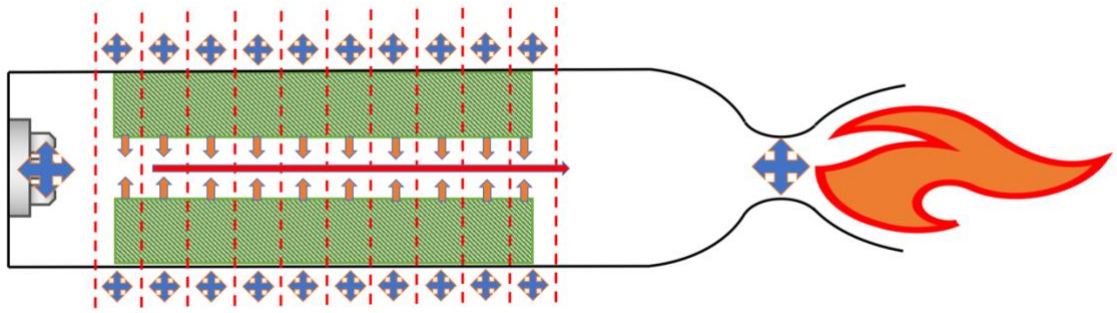

Figure 30 2-D representation of potential flow source placement

is that it cannot, by definition, account for recirculation, vortexes or turbulence. Many mass-flow source positions are known from the center points of the facets included in the boundary condition. Several potential sources are created on the boundary condition of our simulation to match or exceed the number of mass flow sources. Figure 30 presents a representation of a cross section of the 3-dimensional source locations relative to the flow area. The small orange areas are known mass flow and their surface normal vector. The blue 4 directional cross arrows represent the potential flow sources that will let us make an approximation of the overall flow conditions. Several known mass flows are included from the injector based on initial conditions, the nozzle based on the pressure solution for mass flow out, and the flows from the facet centers based on regression of each facet and surface area of the facets.

At each time instance the mass flow of fuel from the facets is know from the area of the facets A_{burn} [mm^2], regression rate r [mm/s], the surface normal ($\hat{n}$), fuel density [g/cm^3] by multiplying the density by 10^{-6} to convert [kg/mm^3] results with mass flow from each facet Mdot [kg/s]. Eq. 25 represents the mass flow at each facet.

$$\dot{\vec{M}} = (rA_{face})\rho_f \hat{n} \tag{25}$$

Then the influence coefficient matrix (ICM) is calculated. The ICM relates the position of known mass flow sources to the potential sources created in the boundary definition. Creating an ICM relates each mass flow facet center to the pre-defined potential source locations. The more facets there are, the more potential flow sources there are. So, increasing the facet count drastically increases the size of the ICM. With the ICM and known mass flows it is possible to ask MATLAB to solve a least-squares solution for the missing source strength vector relating the know mass flows to the proximity of potential flow sources. The trick is that this solution needs to represent a vector in three dimensions so that our general direction of velocity is not undefined. This requires separating our mass flow and our influence coefficient matrix in into x, y, z rows where every three-row set represents a direction vector.

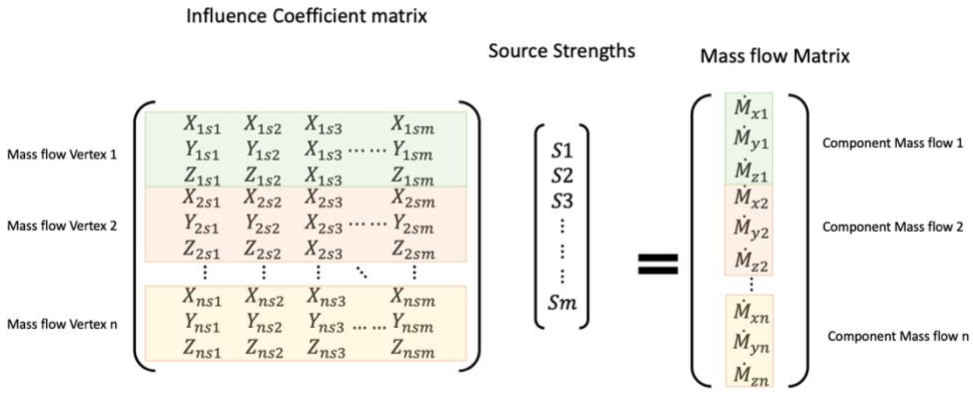

Figure 31 Influence Coefficient Matrix and source strength solution for mass flow

The influence coefficient matrix construction and the least min square flow solution are some of the longest running portions of the code. It becomes exponentially longer when there are more facets included in the solution. The ICM would be reduced if there was a filter to predetermine values if they are too far from the potential flow source. This solution represents a way to get the core velocity values needed but is not ideal for run time or high accuracy of a flow field. This solution is faster than more accurate methods and is sufficient at this stage of work.

Creating New Geometry

To regress the whole geometry, each facet is taken individually with all the slices and corresponding regression rates. A facet is regressed by the sum of these regression rates weighted by the percentage of the area of the facet present in each slice. Represented by Eq. 26.

$$r_{facet} = \frac{1}{A_{face}} \sum r_n A_{subfacet_n} \tag{26}$$

All facets' regressions are multiplied by the negative of their normal outward pointing vector. Every vertex is then checked to find what facets the vertices contribute in. Then all of the facet regression vectors a vertex contributes in are summed to determine the 3-dimensional direction to shift each vertex in. All vertices are moved given weight from every facet they are involved in and the geometry remains manifold and is regressed.

Performance Parameters

Parameters of interest in most propulsion analyses are c^*(c-star), F (thrust), and I_{sp}. In order to get these parameters, there are a few properties that need to be calculated for each time step. The first parameter needed is the characteristic velocity or c^*. For c^* two properties of the flow need to be known, Mach speed Eq. 22 with the ideal gas assumption and equilibrium assumption, and ratio of specific heats. These properties are derived from the CEA analysis.

$$c^* = \frac{c}{\gamma} \sqrt{\left(\frac{2}{\gamma + 1}\right)^{\left(\frac{\gamma+1}{(\gamma-1)}\right)}} \tag{27}$$

The chamber pressure needs to be calculated, not just for the thrust but also to update the chamber pressure at each time step. The first performance parameter to be calculated is c^* calculated in Eq. 27. An accounting of the mass remaining and the volume of the chamber is required for a pressure balance.

$$\dot{M}_{out} = \frac{P_c A_t}{c^*} dt \tag{28}$$

$$\dot{M}_{in} = \dot{M}_{inj} dt + \sum_{1}^{sliceN} \dot{M}_{fuel}(dt) \tag{29}$$

$$M_{net} = \dot{M}_{in} - \dot{M}_{out} \tag{30}$$

Mass out is calculated in Eq. 28 using the chamber pressure, throat area, and the c-star. Mass in is the summation of fuel input and the oxidizer flow at the time step. A representation of this is seen in Eq. 29. The net mass then is the difference of Eq. 29 and Eq. 28 as seen in Eq. 30. In addition to the changes we see in mass flow, there are changes in temperature and mixture ratio in the chamber volume that can be calculated by knowing the cavity volume at the start and volume based on the fuel mass over the solid fuel density this is seen in Eq. 31. Using the change in volume and the mass balance we can calculate the chamber density seen in Eq. 32. From chamber density the pressure can be calculated using Eq. 33. R and T are based off of molecular weight and temperature of the exhaust products form CEA.

$$V_{chamber} = V_{cavity} + \frac{\dot{\mathrm{M}}_{\mathrm{fuel}}}{\rho_f} \tag{31}$$

$$\rho_c = M_{net}/V_{chamber} \tag{32}$$

The new pressure is then calculated from the current chamber density based on the mass balance.

$$P = \rho_c RT \tag{33}$$

After we have the ratio of specific heats of the end port grain and the expansion ratio of the nozzle and nozzle size. We can iterate the pressure ratio at the exit to find thrust.

$$F = A_{throat}P_c\sqrt{\left(\frac{2\,\gamma^2}{(\gamma-1)}\right)\left(\frac{2}{\gamma+1}\right)^{\frac{\gamma+1}{\gamma-1}}\left(1-\left(\frac{P_{exit}}{P_c}\right)^{\frac{\gamma-1}{\gamma}}\right)} + (P_{exit} - P_{atm})A_{exit} \tag{34}$$

Calculating I_{SP} is the key performance parameter for comparing propulsion systems

$$I_{sp} = \frac{Fdt}{\dot{M}_{out}g} \tag{35}$$

Summary

The ballistics method involves treating the grain as series of sections and regressing the shape of the solid fuel based on the summation of regression rates and the direction of facet surface normal. This regression is based on an experimentally derived approximation for the regression values which is effective but does not account for smaller variation in port geometry.

IV. Analysis and Results

Chapter Overview

The code is effective at regressing geometry and updating regression based upon axial position. The regression rates are and pressure over time match well with experimentally derived results from the basis geometry. The trends of regression from literature are accurately represented, and the hybrid rocket engine analysis regression is effective at producing an automated iterative cycle of performance and regressing. The regression rates predicted here are predicted earlier in this model than the reference text. The close match on the results is surprising since the original Marxman regression equations were not modified and the values approximating the blowing term. This model is rudimentary but effective at visualizing and understanding the transient regression that occurs during a HRE burn duration.

Results of Simulation Scenarios

Figure 32-37 show regression at times that correspond to port hydraulic diameters of 25 mm, 32 mm, 35 mm, 42 mm, 49 mm and 60 mm. The data from this analysis is highlighted in circle markers. Mass flow regression for 42 mm diameter port are provided for reverence/comparison.

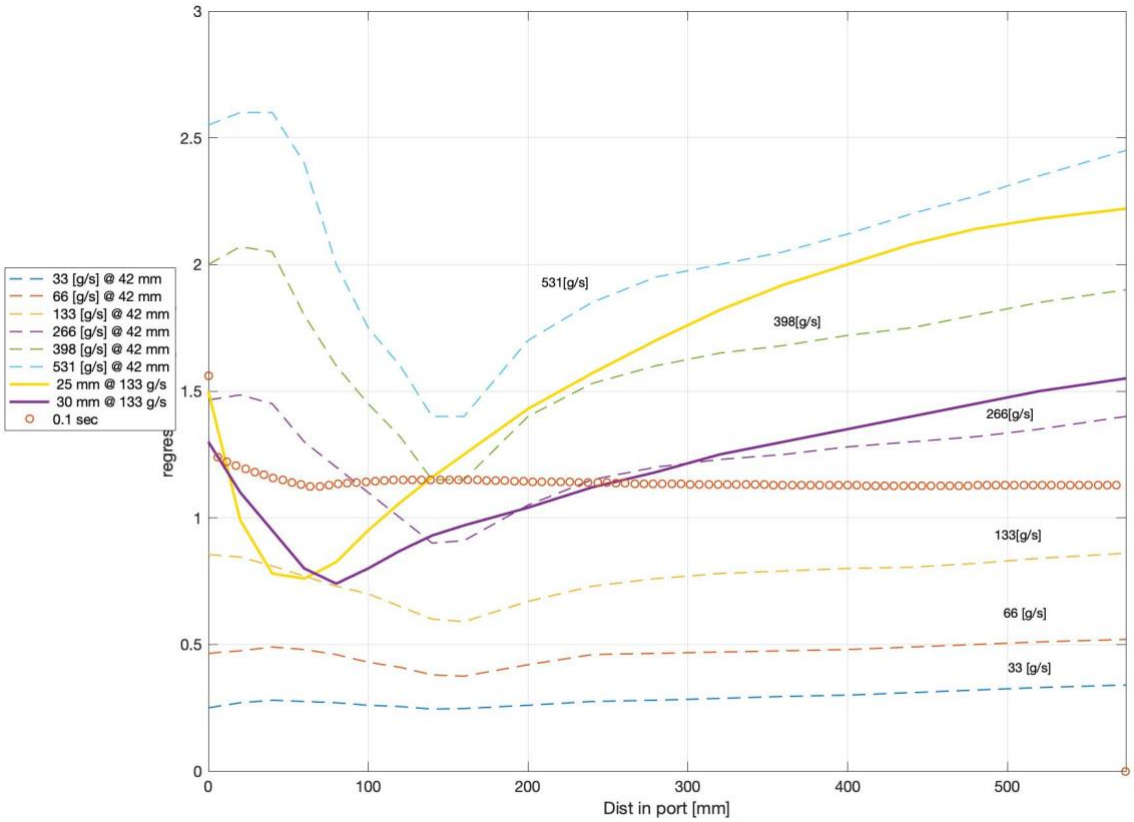

Figure 32 Regression Rates at Time Corresponding to Hydraulic Diameter 25mm

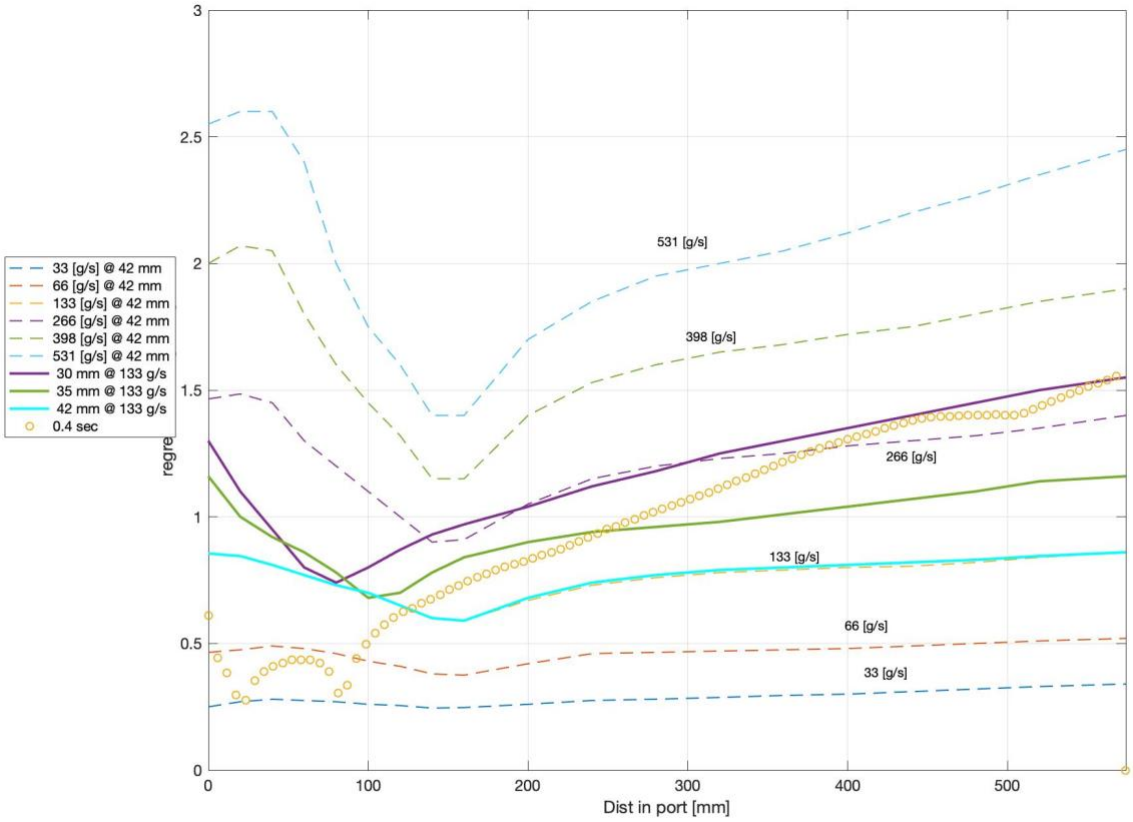

Figure 33 Regression Rates at Time Corresponding to Hydraulic Diameter 30mm

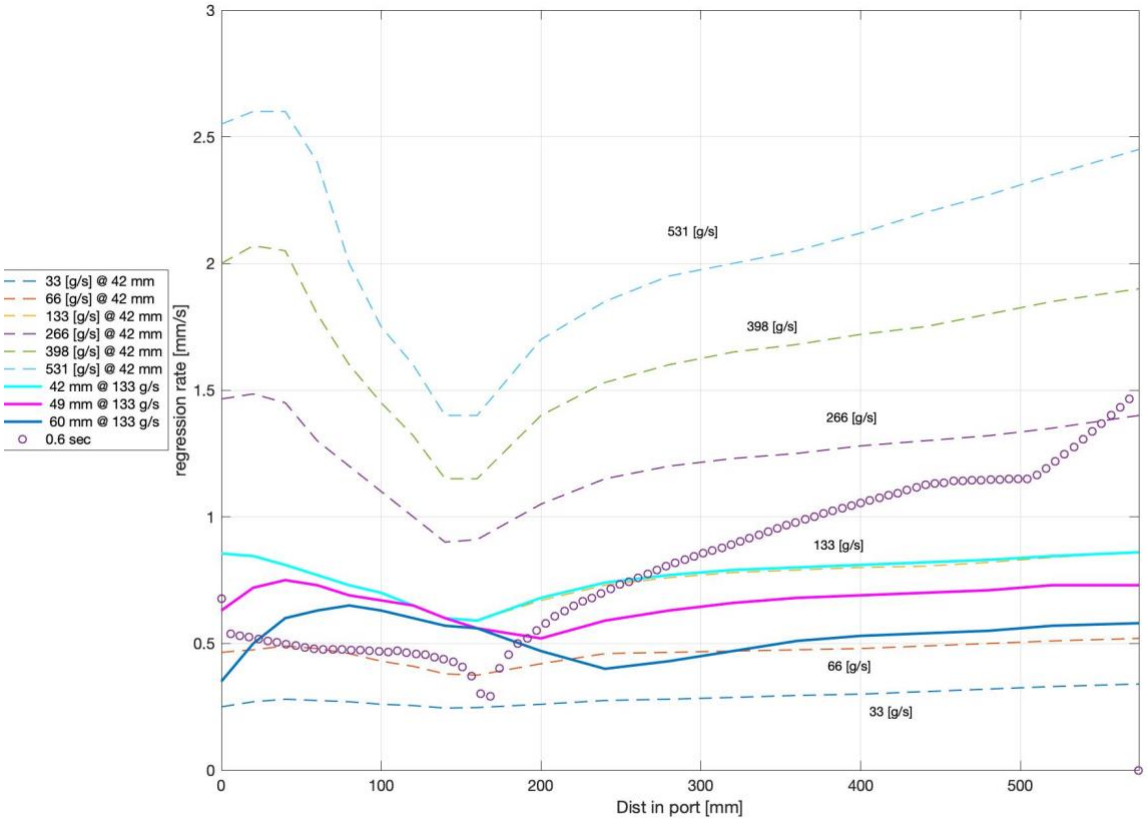

Figure 34 Regression Rates at Time Corresponding to Hydraulic Diameter 35mm

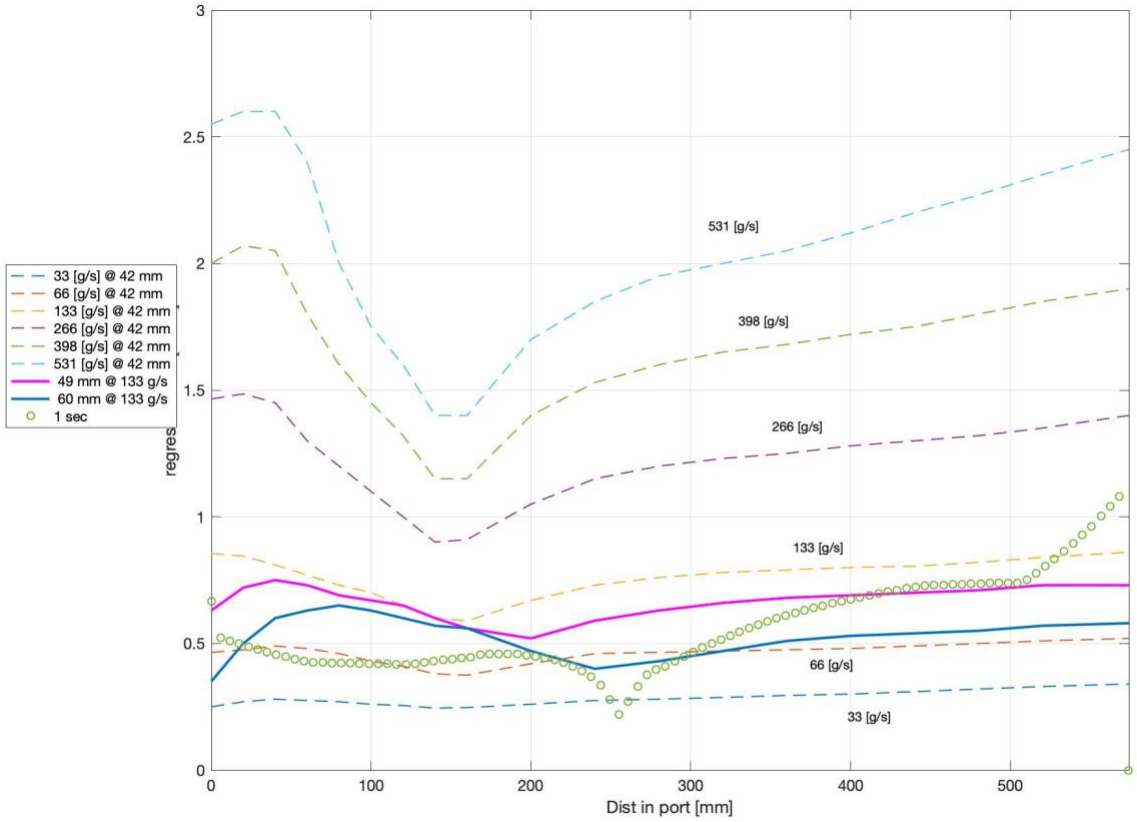

Figure 35 Regression Rates at Time Corresponding to Hydraulic Diameter 42mm

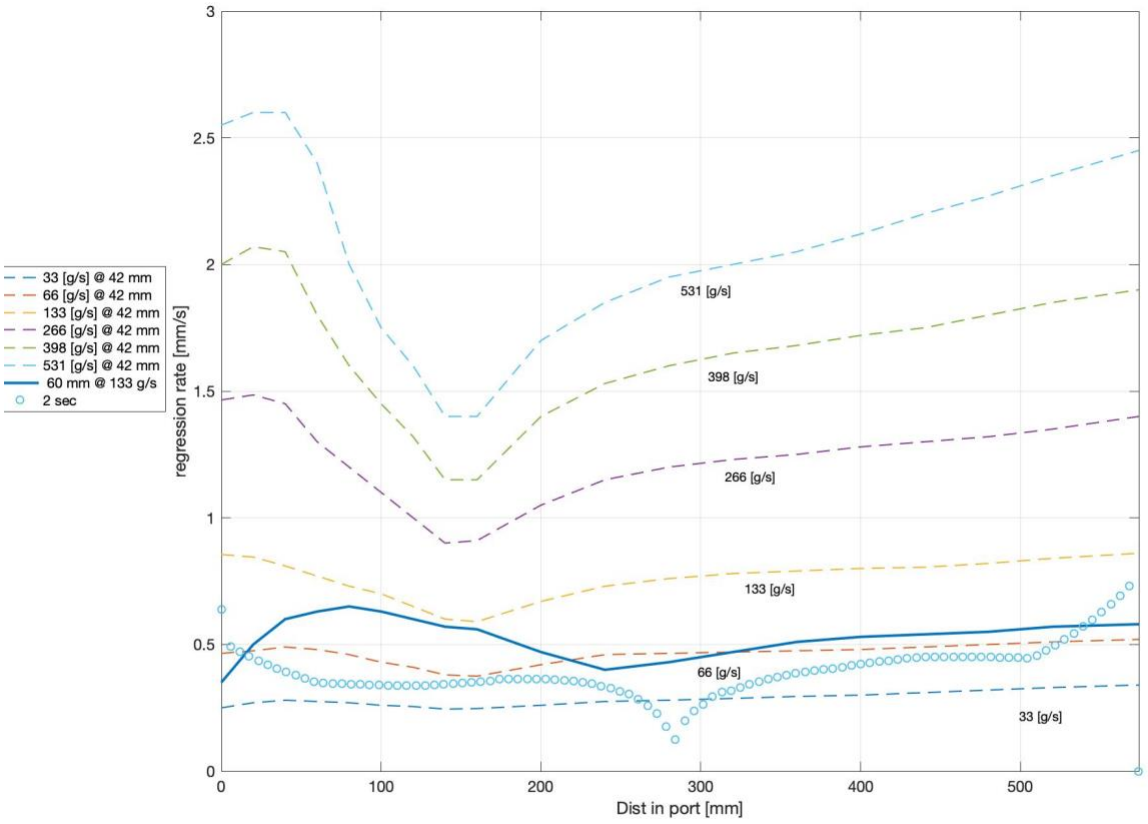

Figure 36 Regression Rates at Time Corresponding to Hydraulic Diameter 49mm

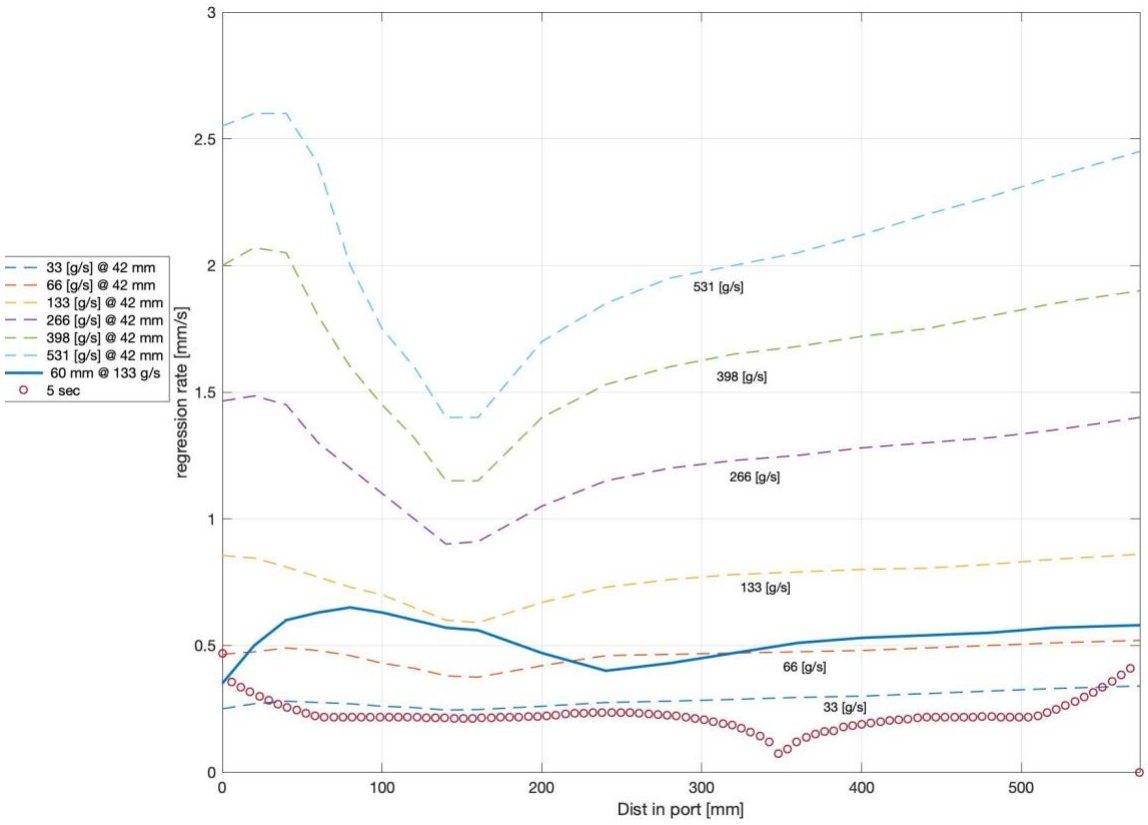

Figure 37 Regression Rates at Time Corresponding to Hydraulic Diameter 60mm

The area in regression plots where we see a reduced regression rate then a sudden increase, we will call the 'valley'. This valley seems to move down the port as the time and average hydraulic diameter increases. The various flow rates shown at 42 mm port diameter by Bianchi are shown provide a scale for reference. Bianchi's variation in flow rates show the effects of increasing flow rate suddenly. Based on the graphs it appears that the valley is located based on the hydraulic diameter.

Figure 32 through 37 show the reported results from the work the geometry and flow parameters are based on. The general trend and shape of the regression are accurate to experimental results. The simulation results of this work underestimate regression in comparison to Bianchi for most time instances. The regression rates at each space-

average port diameter do not match perfectly to the reported values in the Bianchi study [19]. The reason for this is the Bianchi data is based upon a regression based on a geometry that is always a fixed diameter for the entire port length. The results reported by Bianchi are also based off of CFD simulations assuming an ideal O/F ratio and not real experimental data. Actual data of regression as a function of the port would be difficult to get during burn time due to high temperatures and acoustics produced by turbulent combustion. The results show high regression at smaller diameter and low regression rates at larger diameters is expected and is the core problem with simple geometry HREs.

The regression rates at various space averaged port diameters doesn't correlate well with data from the reference text. There is significant variation of geometry along the length of the port as seen in Figure 38 so a space-averaged hydraulic diameter is not a good relationship to use. Also using a space-averaged mass flux would be a poor

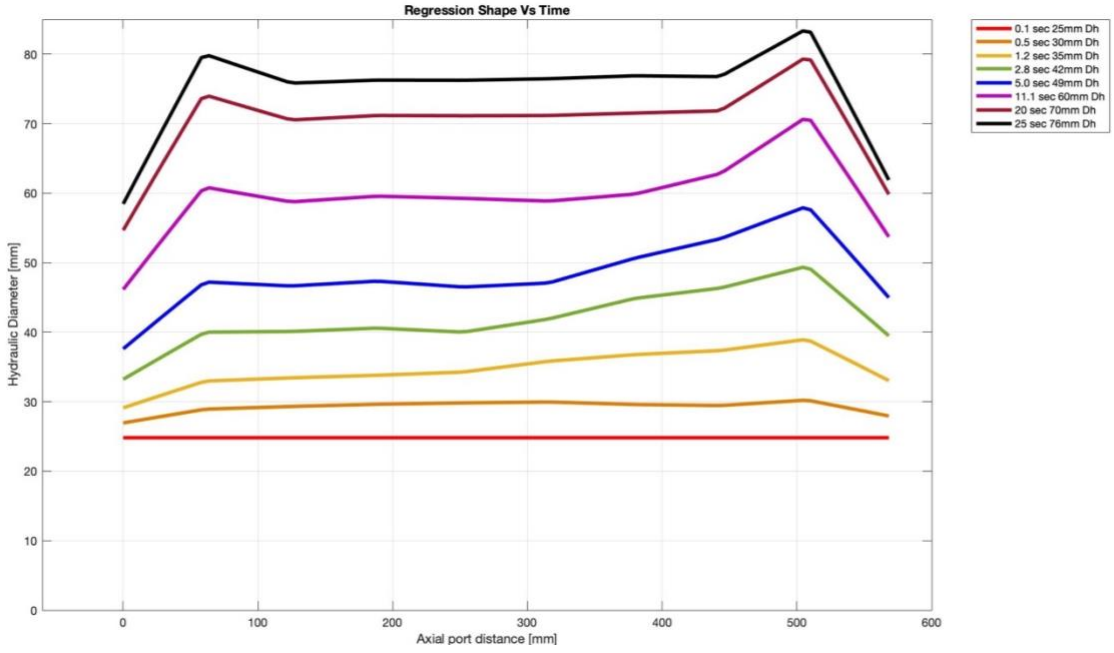

Figure 38 port shape a various times of critical space-averaged hydraulic diameters

correlation. The regression is largely a function of the geometry which changes locally. The geometry, seen in Figure 38 at the end of the burn time period is similar to what is expected for a basic cylindrical port. The diameter seen near the end of the burn appears far more uniform which would suggest a more even regression rate as a function of port

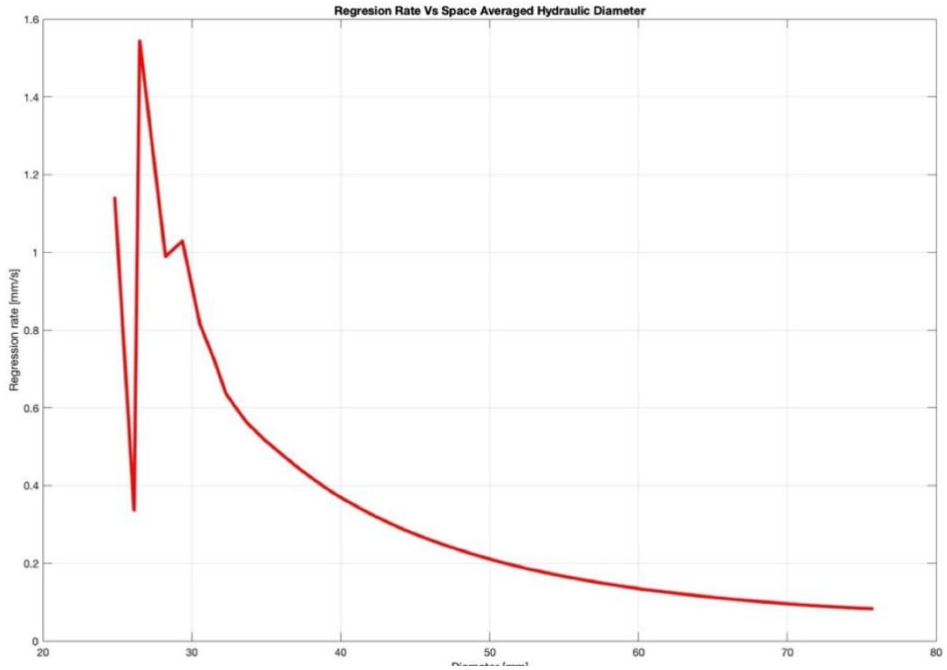

Figure 39 Regression rate vs the hydraulic diameter

length if all the data that you had was the beginning and the end. Most of the regression will occur in the port area with some around the entrance and exit causing coning. There will be some coning that should appear in on the end facets, but those facets were explicitly left out of this simulation. The coning is seen more on the aft end of the grain early in the time duration. The larger faster initial burn areas eventually slow down, and the slower areas catch up causing a more uniform looking burn as time continues. Figure 39 shows this simple expected inverse correlation of diameter to regression rate.

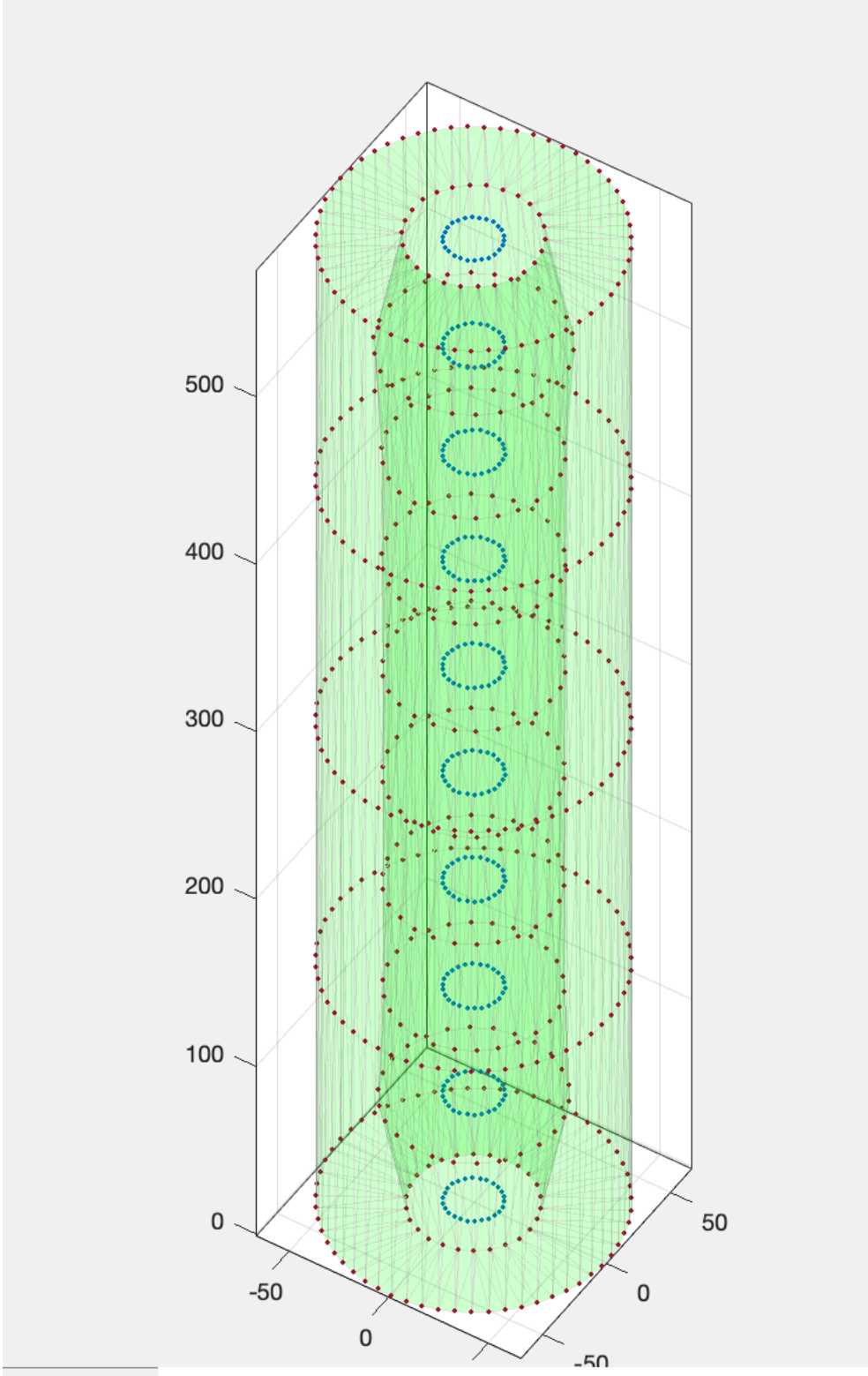

Figure 40 Final shape at the end of burn duration

The final shape exported by the analytic code is displayed in Figure 40. If the flow were dominated by the vortexes at the end grain, the simulation would look like Figure 41. If the port flow was dominant and had a strong correlation on axial length the results would look like Figure 42. If the regression showed a strong negative correlation to axial length, the regression geometry would look like Figure 43.

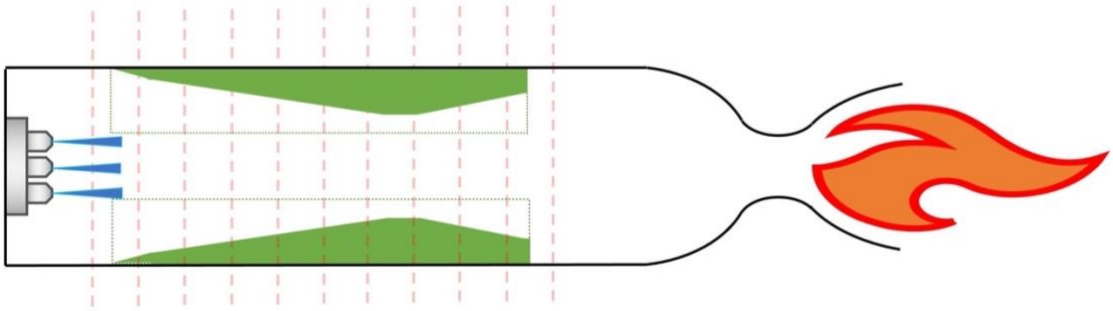

Figure 41 Large leading and training edge effects possible geometry

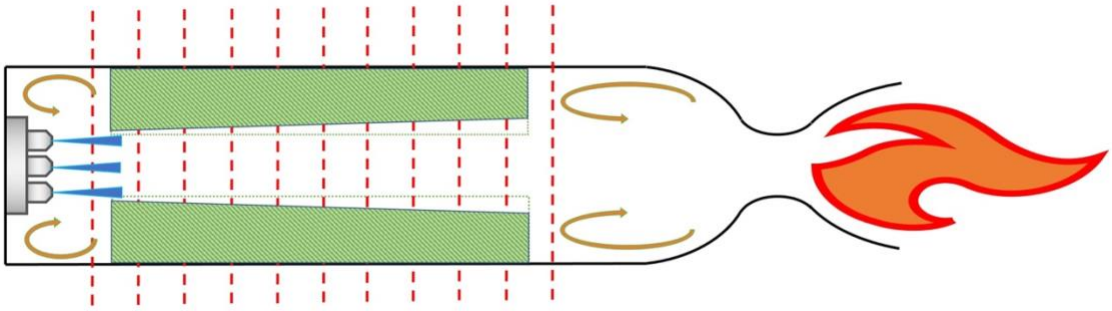

Figure 42 Regression rate with port length dependency

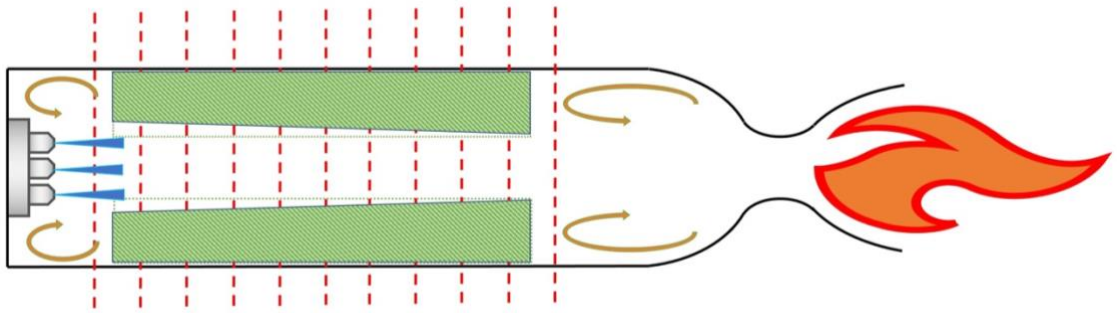

Figure 43 Regression rate with inverted port length dependency

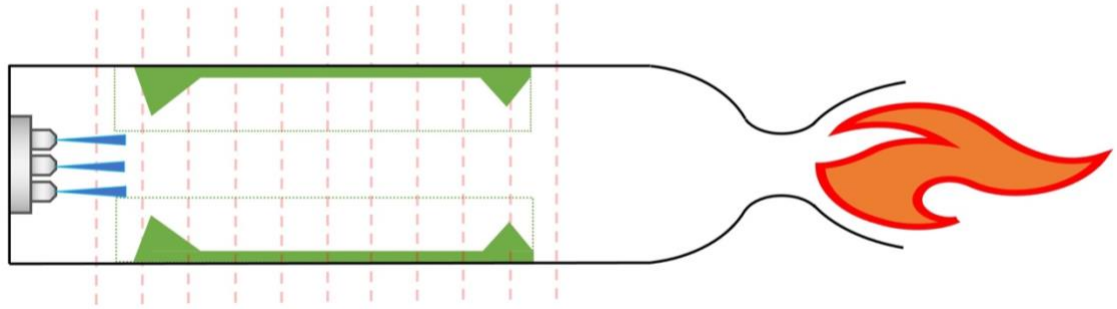

Figure 44 regression with normalizing effects down port and minimal end effects

The geometry on the end of the analysis shows that there is a dominant regression in the port and has a correlation that corresponds to axial length similar and there is some coning as in Figure 44. Initial iteration of the code showed coning and regression on the end cap. The current iteration of the code omits the end caps of the grains after identifying that the regression rate of the end grains was causing spikes in mass flow rate. Model resolution on the end caps is low, and that could be the cause of this behavior. At low resolution, large facets can cause large facet shape edge errors, as mentioned earlier. Small deviations on normal point accuracy can cause blips in regression of facets. Regression rates for the end caps is also identified as being different than the regression

rate for the port. Regression rate for the end caps is a function of vortex strength and this code does not allow for vortexes by definition, due to the potential flow model.

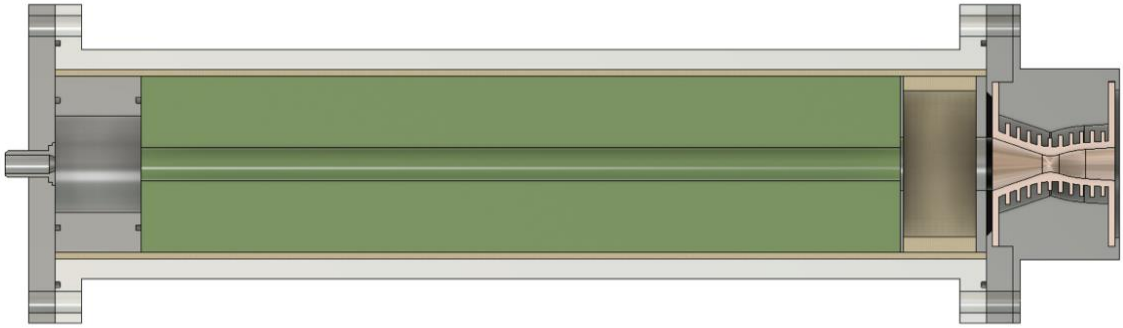

Figure 45 Initial fuel grain geometry

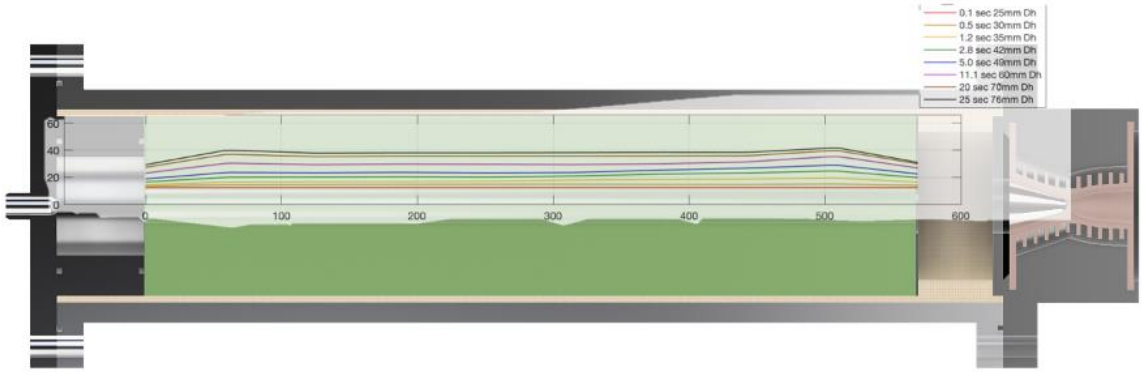

Figure 46 Fuel grain geometry at critical space-averaged hydraulic diameters

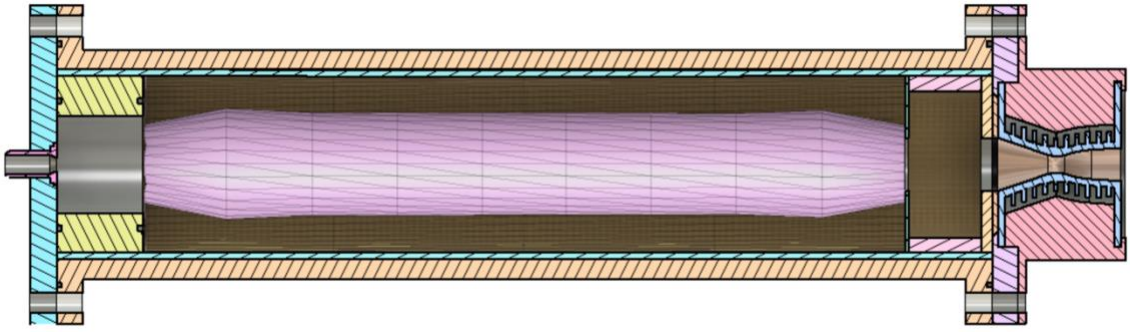

Figure 47 Fuel grain geometry at end of burn time

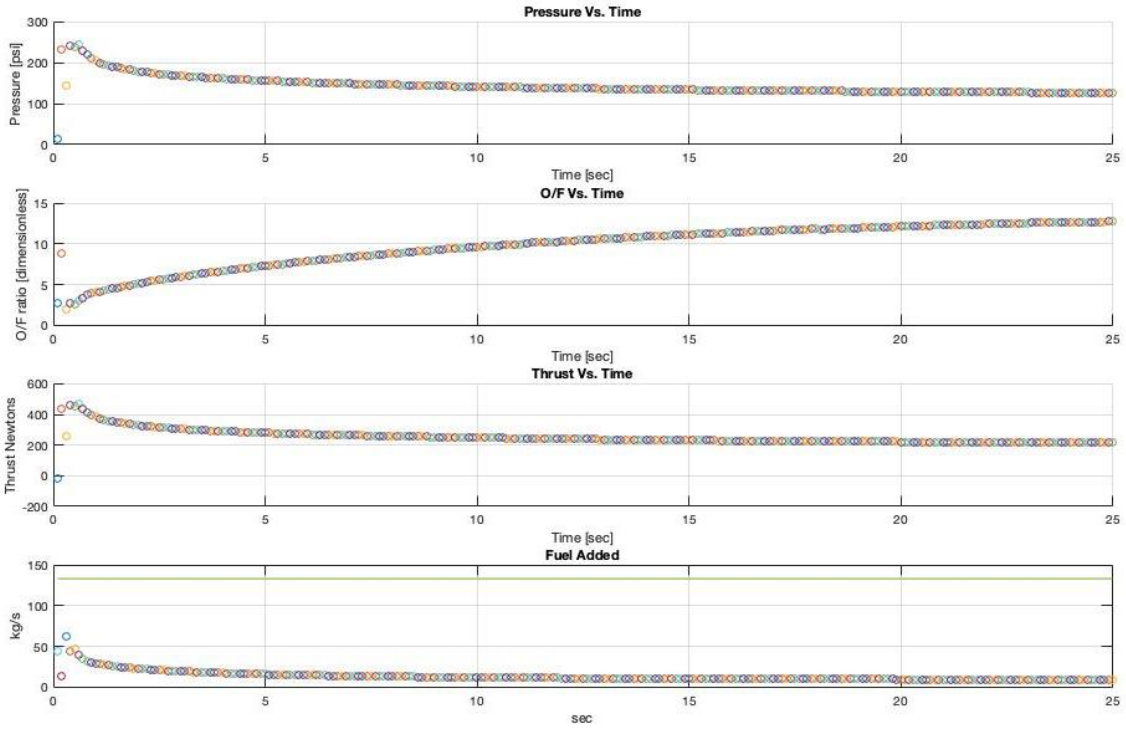

Figure 48 simulated performance parameters for burn duration

Figures 45 and 47 show before and after results for the grain in the test configuration described in the reference work. Figure 46 shows an overlay of the port radius over the fuel grain over time.

Performance is described in Figure 48. The original work this analysis is based upon [19] did not report performance parameters like thrust or I_{sp}. Temperatures were reported in a flow field in graphics produced by CFD. The temperature parameters from the reference and the results of this analysis seemed to corollate. Thrust and I_{sp} are reasonable and are in agreement with the limitations of I_{sp} . I_{sp} as a function of run time can been see in Figure 49. The results are under the theoretical max I_{sp}. The performance

from this analysis is hitting a maximum of around 250 sec in the initial instance then trailing off to 150 sec as the burn duration continues. The theoretical maximum of HTPB is about 320 and as O/F grows it approaches about 280 sec. The theoretical I_{sp} is based off thrust in vacuum and this can be seen in Figure 7. When we compare the I_{sp} to the

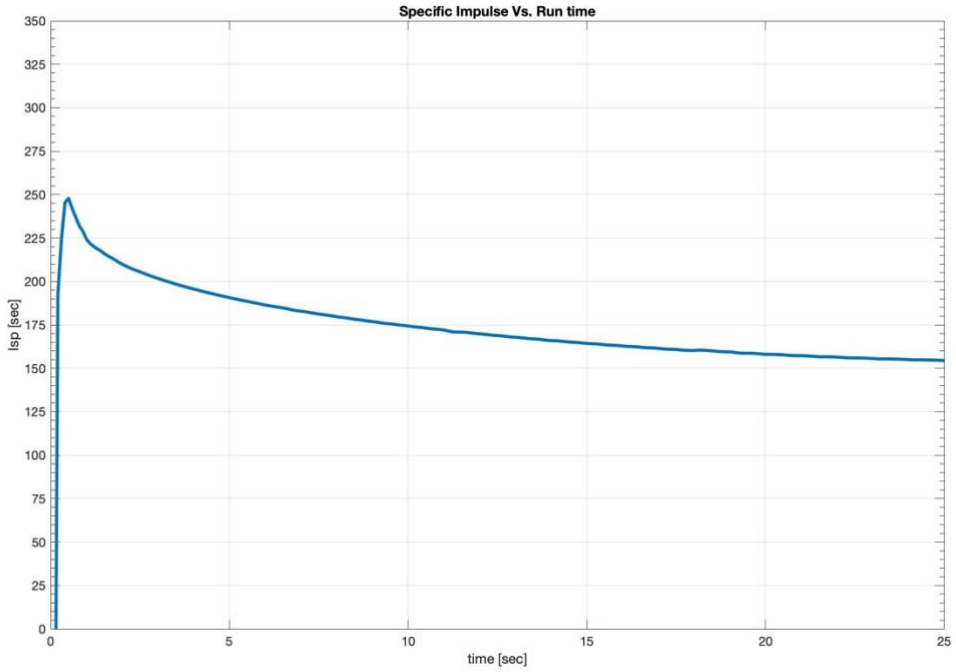

Figure 49 I_{sp} over burn duration

corresponding O/F of the system state as in Figure 50, it is still found that the general trend of the I_{sp} is appropriate.

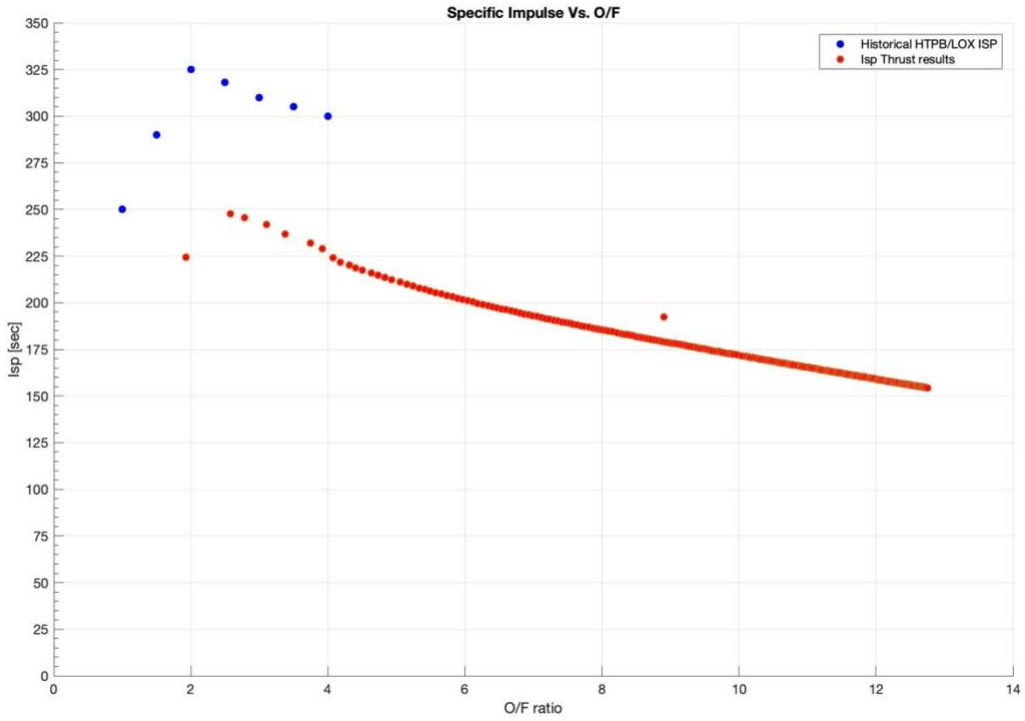

Figure 50 I_{sp} over range of opperating O/F compared to theory

The values recorded for impulse were within expected ranges. Typical specific impulse studies find HTPB LOX impulse, as reflected in Figure 7, are at theoretical maximum at vacuum conditions. Figure 50 compares the theoretical values from Figure 7 and the results for I_{sp} as a function of O/F operating conditions. A few of the operating conditions fall outside the trend; they are data from the start-up overshoot before the system gets to steady pressure.

Errors

There will be a general issue with modeling the end burning sections of the fuel grain. The problem with modeling this regression rate is that due to the geometry existing outside the port, the regression rate is a direct function of recirculation effects due to

injector design and placement and any flow mechanism aft of the fuel grain. Figure 48 shows a result of the regression code attempting to model the end burning of the fuel grain. The results of the ends are coarse and jagged. This is primarily due to large facet regression. There is characteristic chamfering that would be expected to be seen on the end grains but the geometry including the end grains does not supply normal trends expected due to these chaotic edges from large facets. This iteration of the code also saw that not omitting the end grains forced them to be the dominant mass contributors due to the facet sizes. End burning effects can lead to a mismeasurement in regression rate from multi-port hybrids [11]. If this code is to seek out solutions for multiport systems getting end grain regression and automated detection working is critical to simulating multiport HREs.

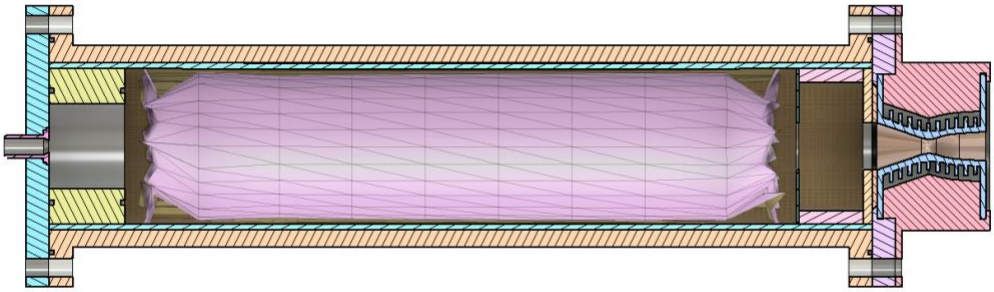

Figure 51 Jagged end-grain and large facet edge effects

Another possible error could arise from the method being used to update pressure. Pressure rise is tracked with each time iteration, so the pressure is a little slow to respond

unless extremely small timesteps are used. It is more ideal to include a feature for change in pressure based of the current pressure difference in those pressures that creates overshoots and would rise and oscillate more dynamically and would closer approximate to the pressure fluxuations caused by turbulence in combustion chamber of HRMs.

Some of the O/F conditions tracked within the port are not idea for combustion and would not burn, especially the forward section of the port. The analysis has the regression assuming a function of the combustion that is occurring somewhere in the port. The underlying question of the analysis is if the geometry or the defining geometry can be accurately compared to reality.

Slice Resolution Study

The correct slice height is heavily dependent on model resolution. It was initially believed that if the slice resolution was smaller than the facets, sub-dividing individual facets among more than one slice would provide sufficient resolution. The differences in slice layer regression would be averaged providing a smooth regression. The study increased the slices from 100 to 300 and the regression rates were identical to those seen in the 100-slice study. This is to be expected since the resolution of the slices was already sufficient to cover the 10 layers of triangles that compose the length of the simple port geometry. The simple cylindrical shape will tend to produce large facets from the CAD package because of the large mostly continuous surfaces that compose the length. A study of less than 10 slices for the length would lend to terrible results. Any number less than the corresponding layers would produce results with little difference as seen in Figure 52.

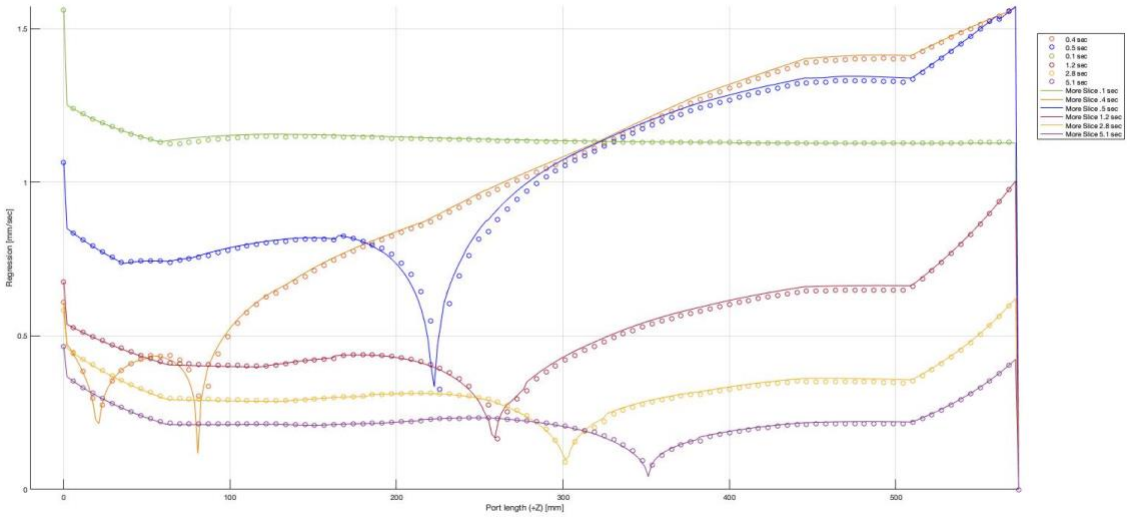

Figure 52 Compare normal slice resolution to 3 times as many slices

Facet resolution

In theory sufficient resolution for the STL file it can only be determined by experimental trials. For simple geometries as little as ~1,000 facets may be enough to lend good and quick results. Shapes of interest, like Figure 50 below, requires 63,802 facets to accurately express the geometry. A CAD package will often give the user some input on how fine the resolution of the exported STL file is. The model analyzed in this study would have been better served for accuracy if a ~3,000 facet or ~9,000 facet model had been used. The run time of a single time step for the ~3,000 instance is ~12 min for each 0.1 sec, and the run time of a single time instance of ~9,000 model was +20 min. For up to 250 time instances that would take about 3.5 days of constant running. The dimensional results for finer model are slightly different. The results can be seen in Appendix C. Figure 53 -Figure 59 show the default resolution this analysis was running a

moderate resolution composed of approximately 3 times as many facets and a high-resolution model with approximately 9 times as many facets as the default. The results of this analysis are shown with circle markers.

Figure 53 shows that all resolutions all show the same regression at the start (It is hard to seed the circle makers because they are all stacked on top of one another). This is not surprising since the values for blowing are hard coded since there is not data to update blowing term from yet. This does give us a baseline to determine that the results do not simply change from the number of facets being used.

Figure 54 shows a time instance of 0.4 seconds, that the default shape, corresponds to a diameter between 25 mm and 30 mm. A pattern appears here the more coarse the resolution of the geometry the larger the regression rate and the earlier the 'valley' is predicted to occur. Earlier valleys correspond to smaller diameters. This larger regression rate is possibly from slightly smaller port diameter based off of inaccuracies determining the inner port wall shape. These inaccuracies will grow smaller with increased resolution. With a coarse geometry under predicting volume and surface area makes sense. The three resolutions match extremely well with the reference paper Bianchi data for 35mm, 42mm, 49 mm with 133 g/s. There seems to be generally less regression at the start of the chamber which could be easily attributed to the no exitance of a pre-combustion chamber in this model. This data matches extremely well for regression rate and predicting the location of the regression 'valley'.

Figure 55 shows the 3 resolutions at 0.6 seconds corresponding to a diverse shape represented by a range of diameters around 30mm . Again we see good prediction of the 'valley' and regression rates seen at 42mm, 49mm, 60mm form Bianchi. These

regression rates occur earlier in this analysis than Bianchi's data. This indicates that there was a larger earlier regression that advanced the diameter early in the burn duration. Again, the default resolution seems to predict a larger regression rate than the refined models. Regression early in the port are again under the values presented in the reference data but now match much better.

Figure 56 shows the regression of the three resolutions at 1 second corresponding to diameters ranging from 32 mm to 38 mm. The regression rates from the refrence text no longer corresponds well for matching the location of the "valley" but match magnitude of the regression well for regression at uniform diameters of 49 mm and 60 mm. Larger diameter regression rates data as a function of the port length was not reported.

Figure 57 shows the regression of the three resolutions at 2 seconds corresponding to diameters ranging 38 mm to 49 mm. The regression rates here show the same pattern as before and are under the range predicted by Bianchi. Figure 58 shows the regression of the three resolutions at 5 seconds corresponding to diameters ranging 48 mm to 58 mm. Figure 59 8 shows the regression of the three resolutions at seconds corresponding to diameters ranging 48 mm to 62 mm. The regression rates all predict the same pattern of regression magnitude and order to predict occurrence of the regression 'valley'. The flow rates reported by Bianchi are all plotted here for reference and to see the effective mass flow through a 42 mm uniform port. At the start the burn time the regression rate predicted is more similar to the regression rate represented by mass flow of 266 g/s through a 42 mm uniform port. As the burn time continues the regression rate appears more like the regression from a mass flow below 33g/s through a uniform 42mm port.

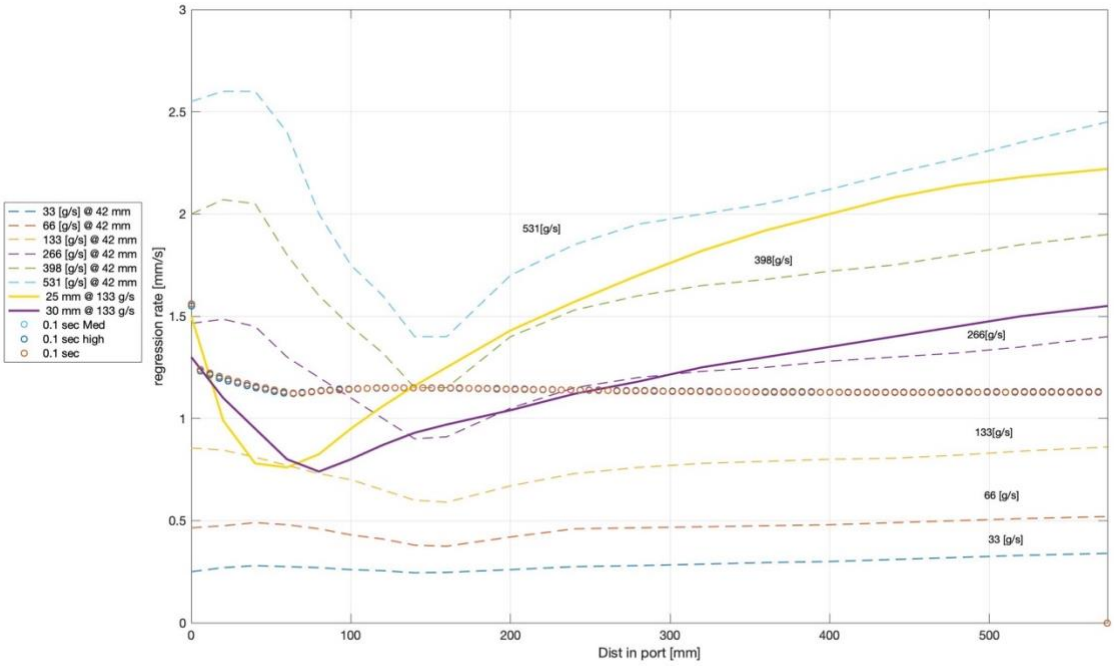

Figure 53 Various regressions based on resolution at time 0.1 sec

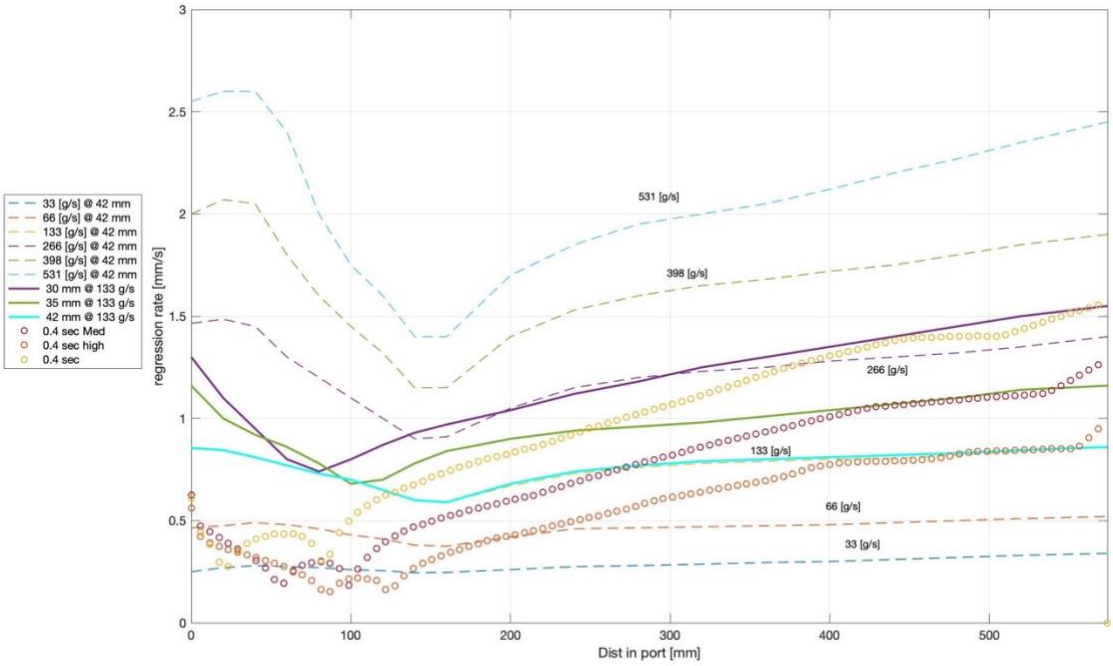

Figure 54 Various regressions based on resolution at time 0.4 sec

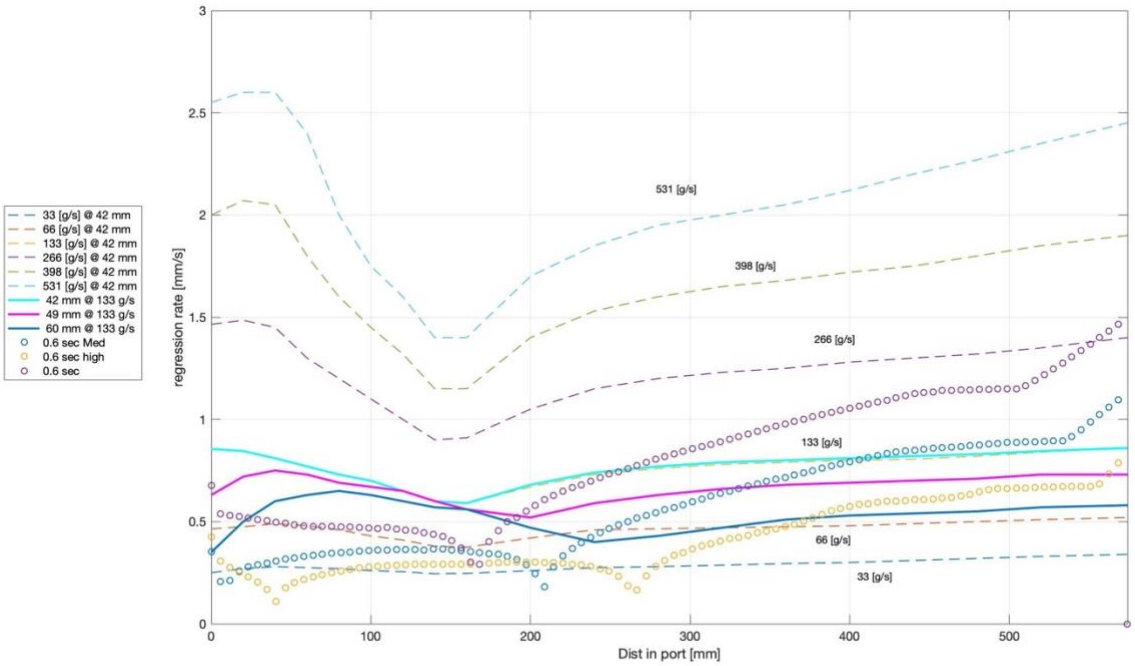

Figure 55 Various regressions based on resolution at time 0.6 sec

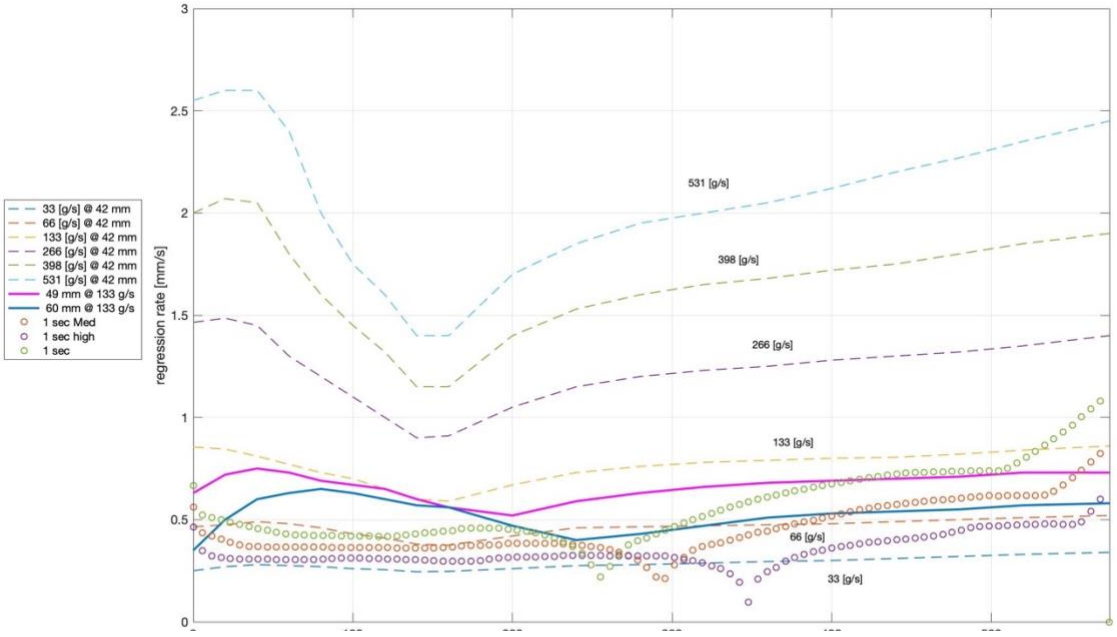

Figure 56 Various regressions based on resolution at time 1 sec

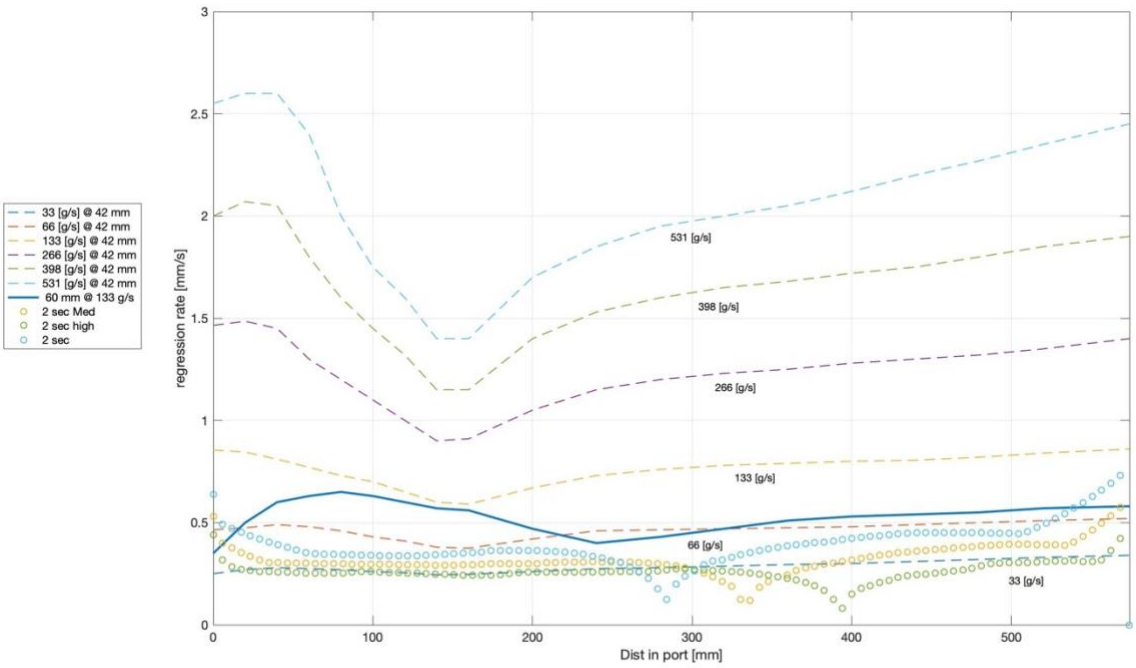

Figure 57 Various regressions based on resolution at time 2 sec

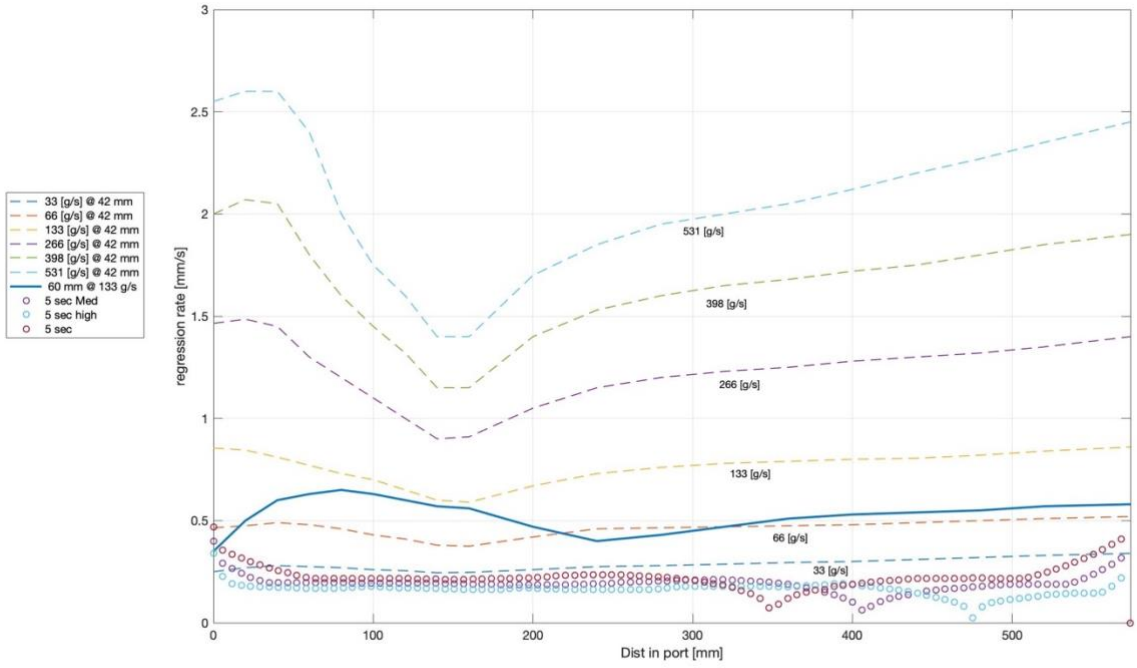

Figure 58 Various regressions based on resolution at time 5 sec

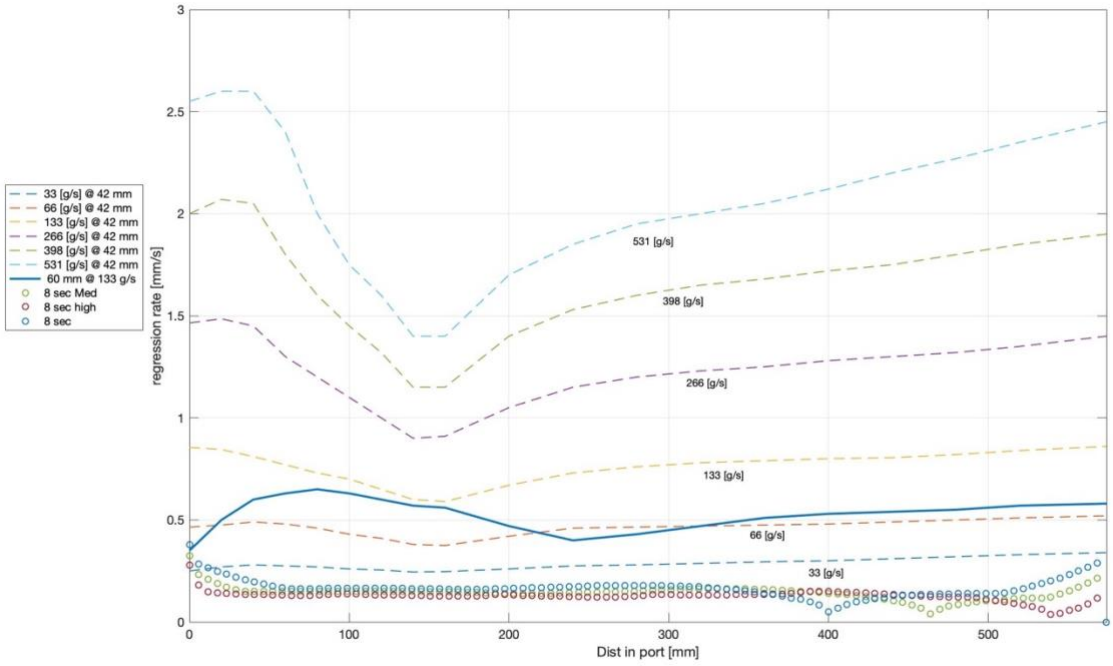

Figure 59 Various regressions based on resolution at time 8 sec

Investigative Questions Answered

It is possible to regress accurate geometry that updates regression rates. An STL file can be used as the basis for regression of an HRE analysis and for additive manufacturing. Using a common file for both analysis and manufacturing can help ensure accurate results. There are limitations to using an STL file as a base for geometric regression. The first being that the resolution of the initial file and method of tessellation will determine the accuracy of the geometric result. This will also have an effect on the number of slices required to get accurate results. There appears to be a correlation between the step resolution and the time resolution as well. When too large time steps are used on a small slice resolution there are ‘bumps’ in fuel addition and pressure/thrust. These likely occur due to a mismatch in time and slice solutions.

The inputs required to do a simple change in geometry are the boundary conditions (if they change) for end faces, number of slices, and starting volume of the fuel grain. If the flow rate of oxidizer changes but does not transition into the 1st or 3rd regression regime only the value for the flow rate needs to update. If the fuel material changes, there are significant changes required as inputs. A new regression equation could possibly be needed due to liquid entrainment or regression regime changing. Also, the property surfaces for gamma, temperature, viscosity, molecular weight that have been created as a shortcut for CEA results would be invalid. Solid fuel density will vary greatly even with a simple change, such as an additive. Finally, the heats of reactions (vaporization/pyrolysis) and heat capacity of solid fuel would need to be changed.

The performance analysis characteristics to compare designs against are thrust/pressure, O/F, I_{sp} vs time curve, and regression rates. The biggest one from comparing designs to other propulsion methods are sustained thrust/pressure. I_{sp} is a function of the overall combustion at an instance in time and the expansion ratio and the ambient pressures. O/F stability would be a good comparative parameter. How long the system maintains an optimal O/F ratio (in this case the optimal I_{sp} O/F is about 2). The regression rates are difficult to compare since they vary so much in space and time. When the geometry is changed, it would be easier to compare space-averaged regression rates.

The parameters that are sensitive to grid size analysis are regression/fuel addition. These in turn can affect the performance parameters. It appears that regression rates and mass addition occur at much higher rates at much larger time steps which is to be expected since large time gaps produce large error. This causes effects seen by geometry to occur earlier than would be expected. It also appears that the fuel mass addition is

sensitive to the number of facets. This is likely due to more accurate diameters or more facets that were incidentally excluded in more coarse iterations. Running the analysis on a higher resolution geometry is essentially running a different geometry.

Summary

It is possible to create a geometric regression algorithm based upon geometry defining in an STL format. The question is whether the model is accurate enough for the effects desired to be tested. The simple port is not the answer to the regression or scalability problem that hybrids have but it is the basis of comparison for more complex geometry analysis. The results for regression are surprisingly close to the reference data set for doing no modifications to the equations presented by Marxman. The main variation seen in regression rates are at the start of the port and that this model predicts regression rates earlier than the reference data.

V. Conclusions and Recommendations

Chapter Overview

Several lessons learned and limitations were found in the pursuit of a code that was capable of expressing regression rates and performance of a hybrid rocket fuel grain based on STL geometry. The geometry was capable of being used in an iterative process to determine regression rates and performance and to update geometry. The path forward has the regression model being capable of handling more materials, doing more complex geometries and improving automatic behavior.

Conclusions of Research

Stereolithography file geometry serves as a good basis for rapid prototyping approach to hybrid rocket propulsion. The methodology presented here can be refined to analyze complex geometry, possible only, with additive manufacturing. Regression rates for hybrid rocket motor configurations other than classical ones will need modification of not only the regression equations but possibly of the geometric constraints for defining subsets of the port. HTPB is a good candidate for regression analysis because of well documented historical data. Although HTPB is good for analysis it is not possible to additively manufacture since HTPB requires casting and is formed under a vacuum. However, most solid organic polymers burn at rates similar to the rates seen in HTPB. A recommended material is a 3D printable acrylic, but many other plastics are possible with printers. This analysis is a good starting point for understanding inner working and role of geometry in a hybrid rocket engine. The regression rates seen in this work were surprisingly accurate with no modification to the Marxman relations. This code can be refined to model more accurate results for more complex designs.

Significance of Research

The work started here is designed to improve the analysis methods used to design and test additively manufactured hybrid rocket grains. Hybrid rocket grains have not enjoyed the same successes that liquid rocket engines and solid rocket motors in space faring ventures have. Hybrid rockets have been seen to be far safer in manufacture, transport, testing, and operation. This is partly due to their inherent design, but also their reduced operational complexity. This reduction in complexity can also reduce costs to manufacture, store and operate. With possible higher safety, lower costs and comparable large-scale thrust performance, hybrids could be an answer for reducing risk and costs to space missions.

Recommendations for Action

The validity of this analysis needs to be backed up with lab tests and the regression code needs to be modified and iterated upon to account for alternative fuels, radiative heating, and turbulent effects of recirculating regions. The next steps for this work are, refinement of the analysis, and investigating families of geometries that show positive performance results. One such shape that has shown positive results in experiments is the Star-Swirl grain as seen in Figure 60. Various geometric families can be compared running the same

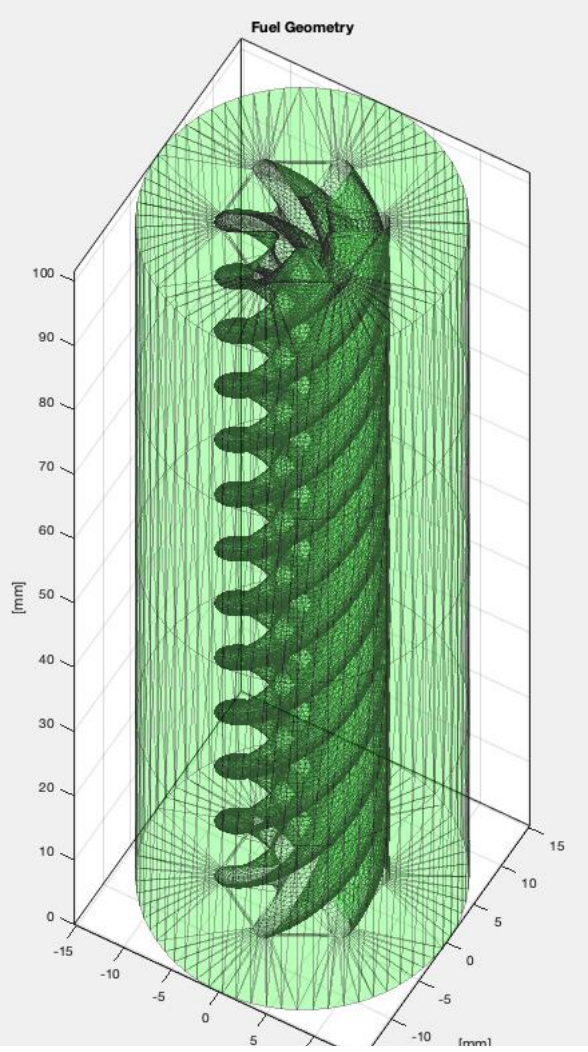

Figure 60 star-swirl fuel grain with 63,802 facets

conditions with the fuel geometry being the only free variable. This can allow for exploration of geometry families to overcome the geometric constants of hybrid rocket performance.

Recommendations for Future Research

- Expand the regression to be functional for more than one fuel material
- Determine if certain geometries are more effective for specific materials
- Analyze print test geometry using an acrylic printer with paraffin support.
- Validate regression relations to lab setups
- Develop a multi-port centerline/multiport capability for multiport hybrids
- Link analysis to CEA online or local batch-mode CEA
- Create iterative CFD simulation to pull out recirculation effects and blowing parameters and predict effective mass flux area
- Genetic algorithm to iterate on fuel geometry design to optimize for any given parameter
    - Thrust curve matching to mission profile
    - Optimization of thrust to burn time
    - Reduction of splinter conditions
    - Minimal O/F shift shapes (minimizes oxidizer requirements)
- Splinter/problematic shape detection. As resolution increases you have dimensional mismatch problem as facets exit the boundary conditions
- Sheet/neighbor tracking to reduce boundary condition stringency
- General fuel comparison with identical geometry and setup conditions

Summary

An algorithm has been created to regress geometry based on STL files representing hybrid rocket fuel. This regression code is effective at iterating a regression solution that is true to the trends seen in experimentation and in literature. It is capable of being adjusted and refined to attain more accurate predictions of hybrid rocket performance. The future of this work is working to analyze new complex geometries and more manufacturable materials. Further work on this is intended to make the benefits of HRE more accessible for larger thrust scale.

Appendix A – CEA surface Fit results

Gamma surface fit

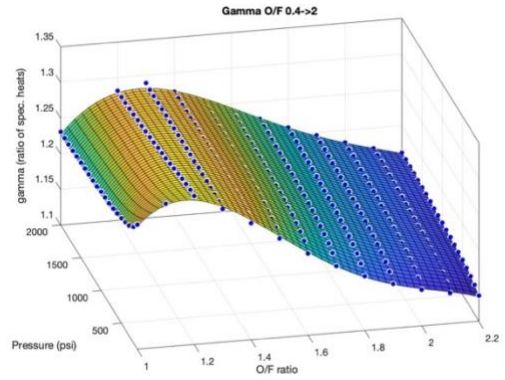

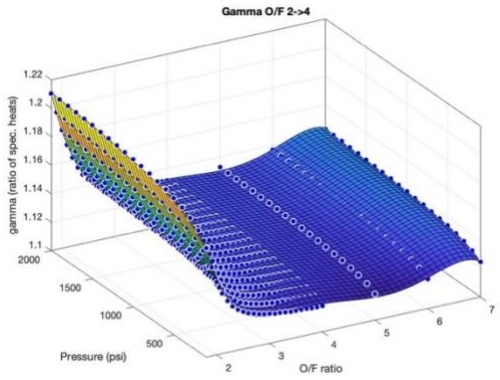

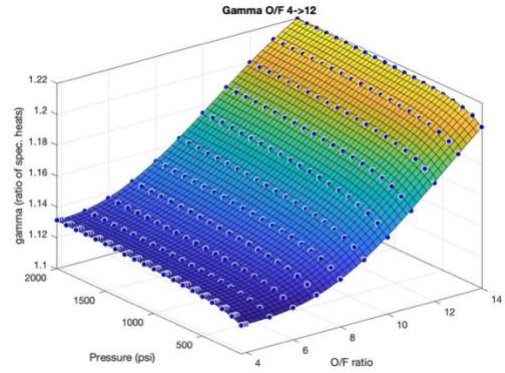

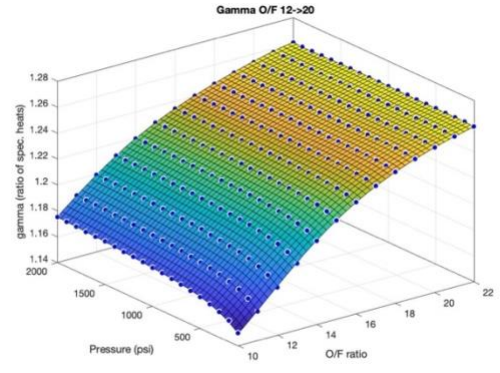

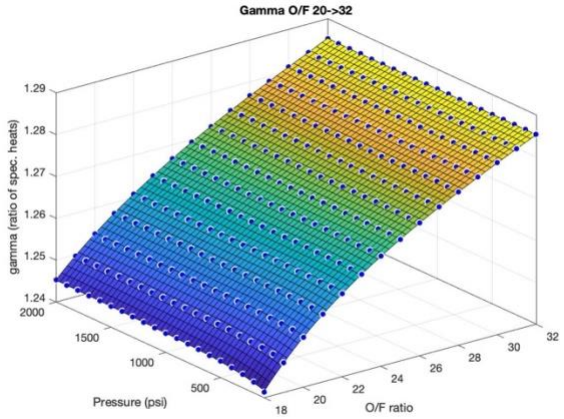

Molecular weight Surface Fit	
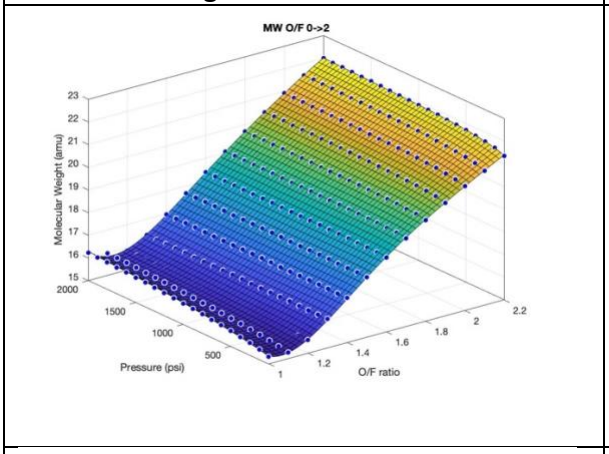	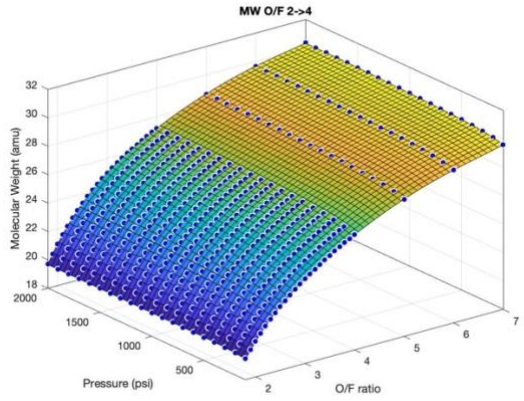
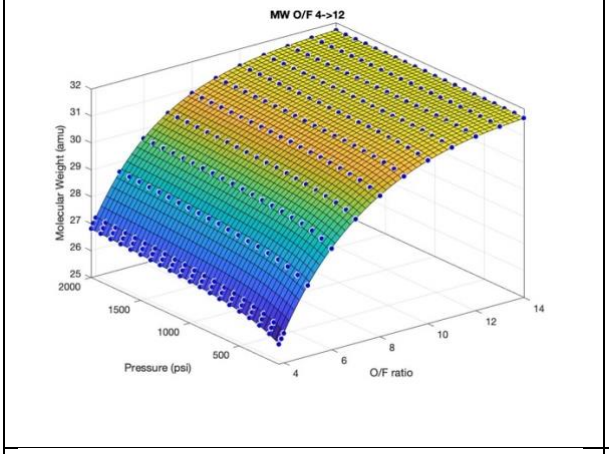	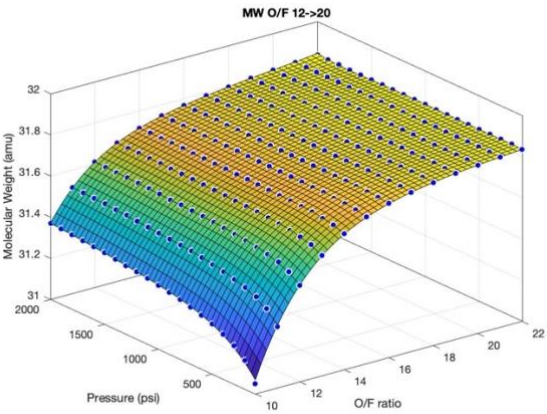
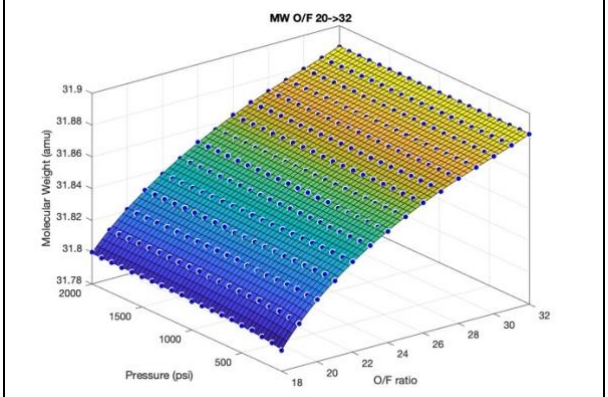	

Temperature Surface Fit	
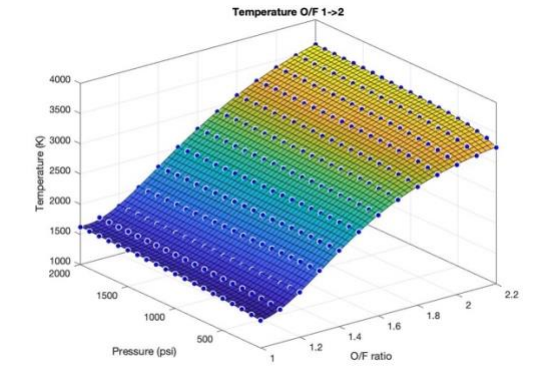	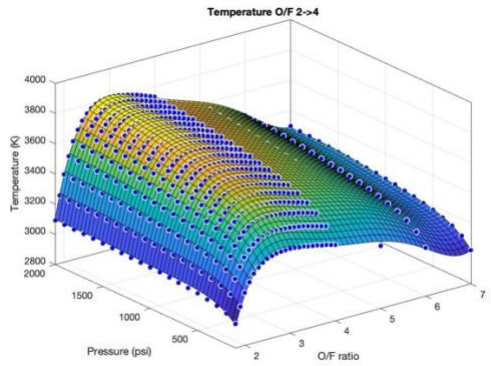
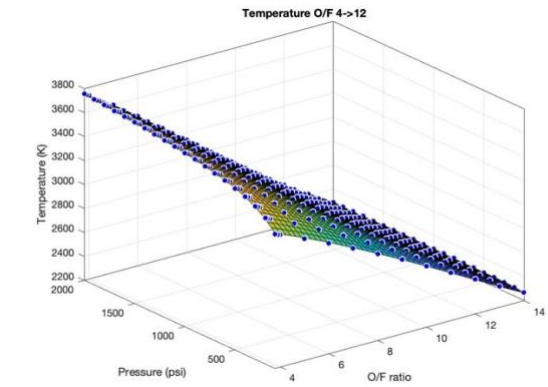	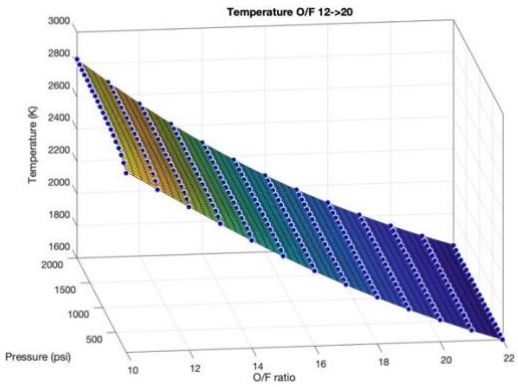
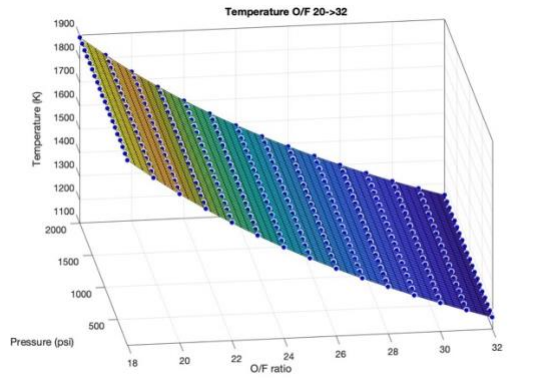	

Viscosity Surface fit	
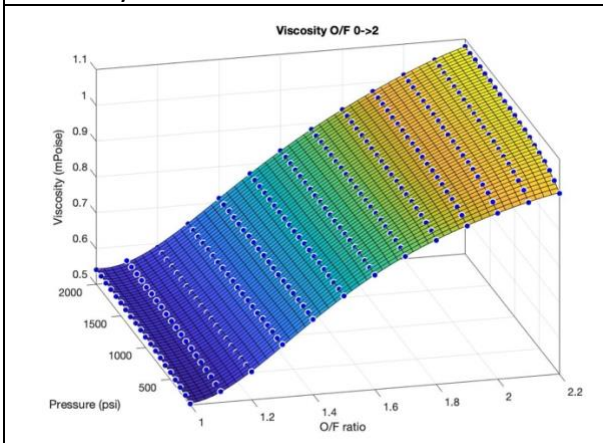	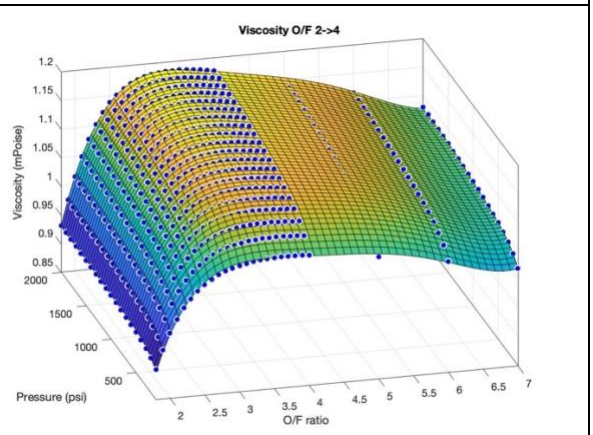
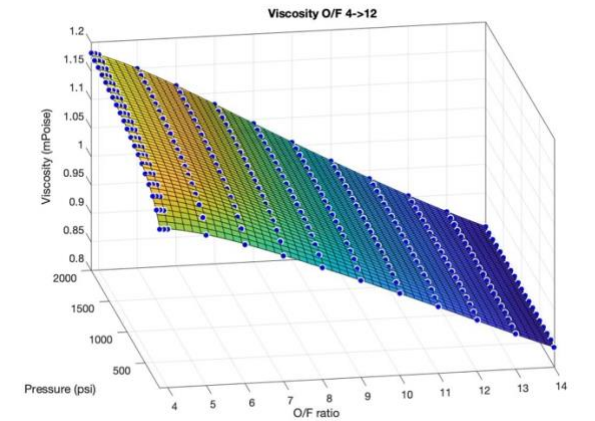	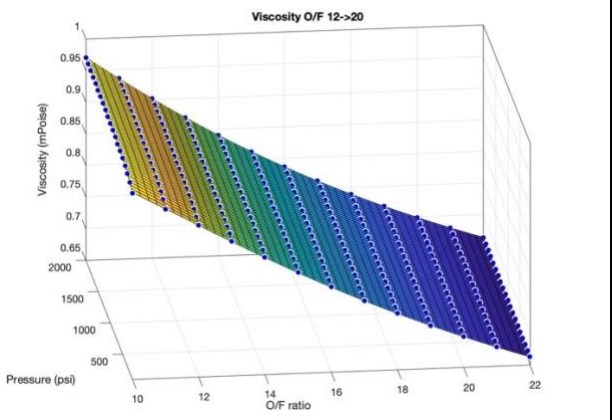
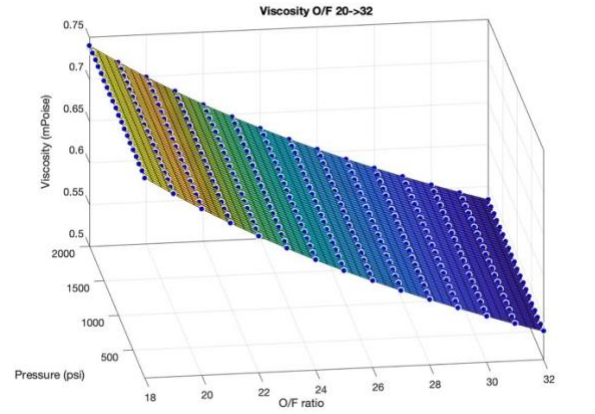	

Run the code below after importing the variables to get polynomial surface fit for algebraic values for a 5^{th} by 5^{th} order polynomial fit.

```
[GamX,GamY,GamZ]=prepareSurfaceData(O_F,Press,Gamma);
sf =fit([GamX,GamY],GamZ,'poly55')% 5th order by 5th order fit
plot(sf,[GamX,GamY],GamZ);
xlabel('O/F ratio');ylabel('Pressure (psi)');zlabel('gamma (ratio of
spec. heats)');
```

Appendix B -Time dependance study

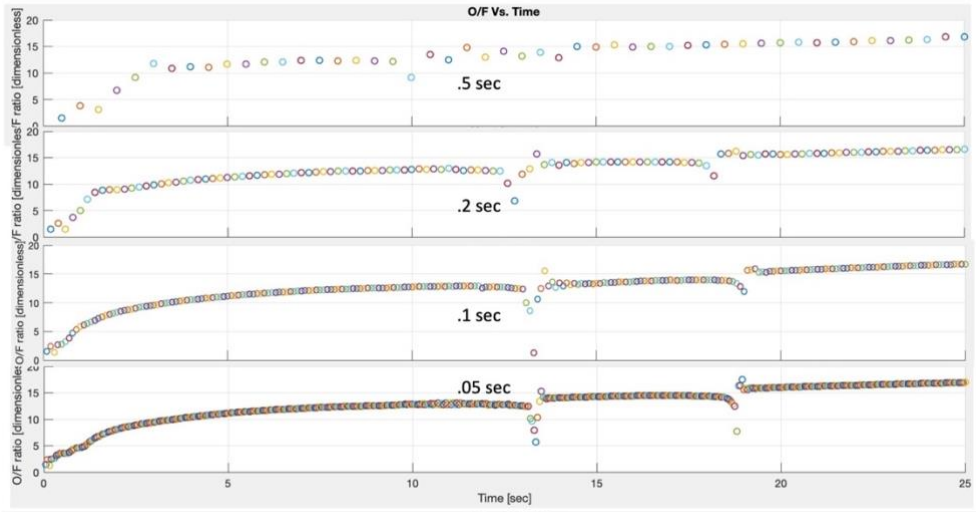

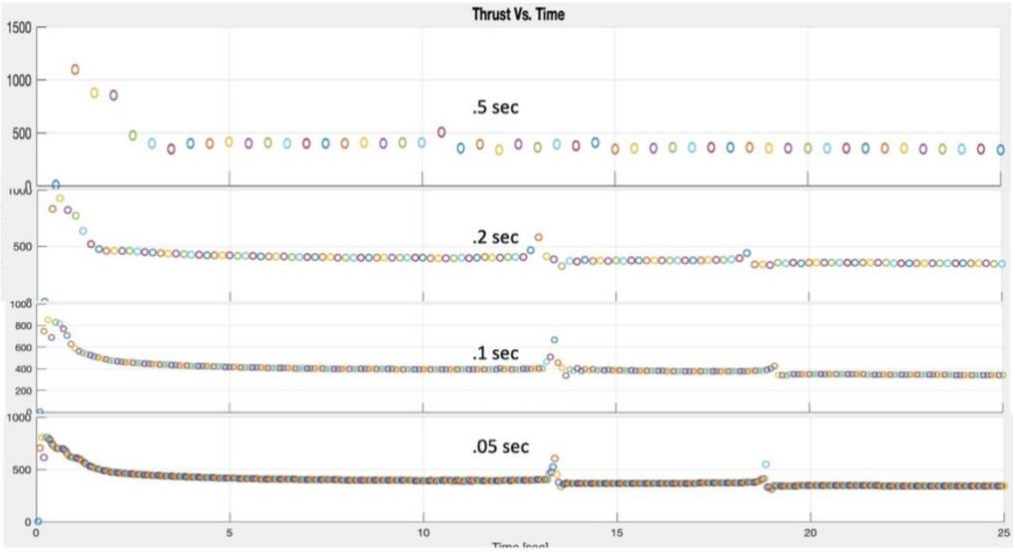

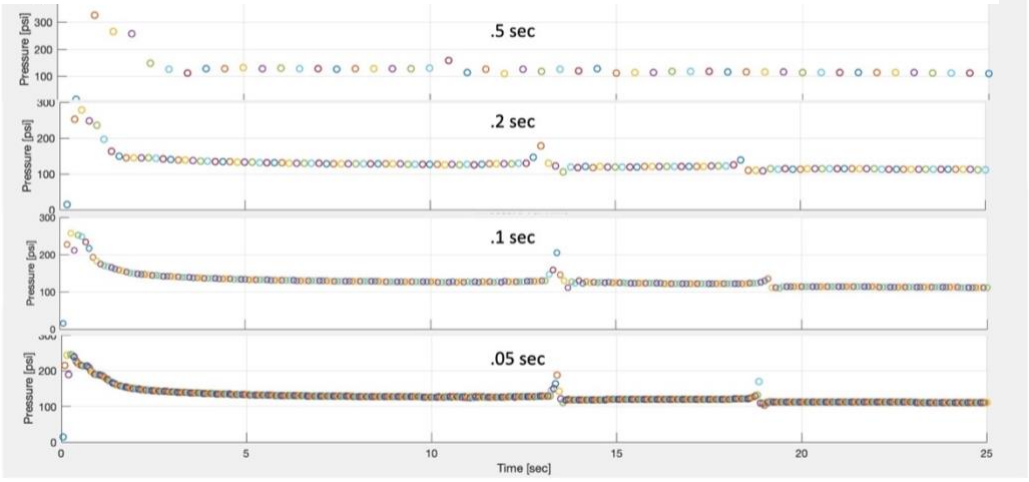

Appendix C - Facet Resolution dependance study

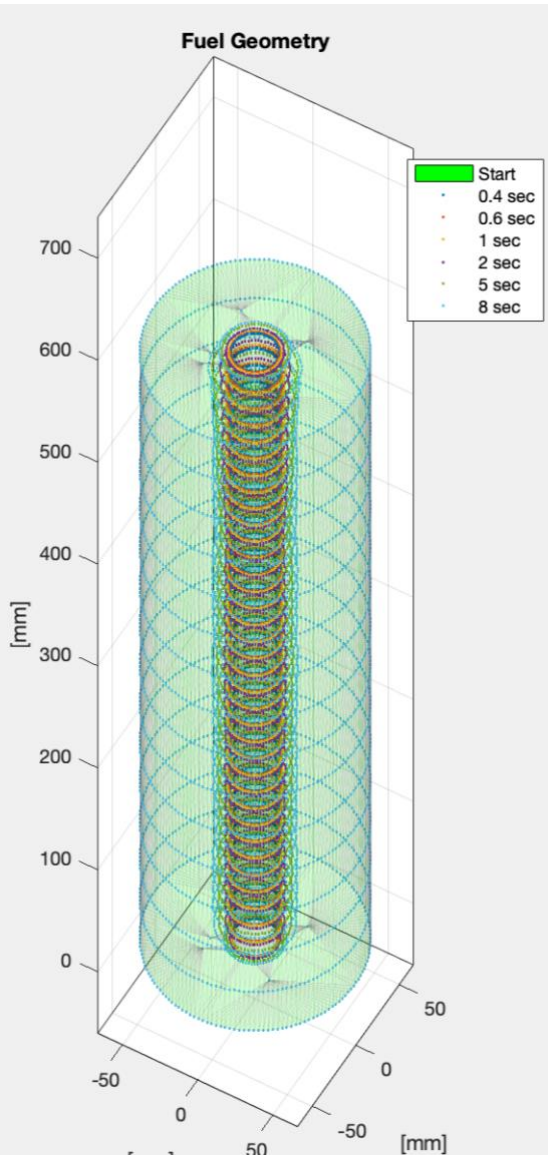

9604 facets

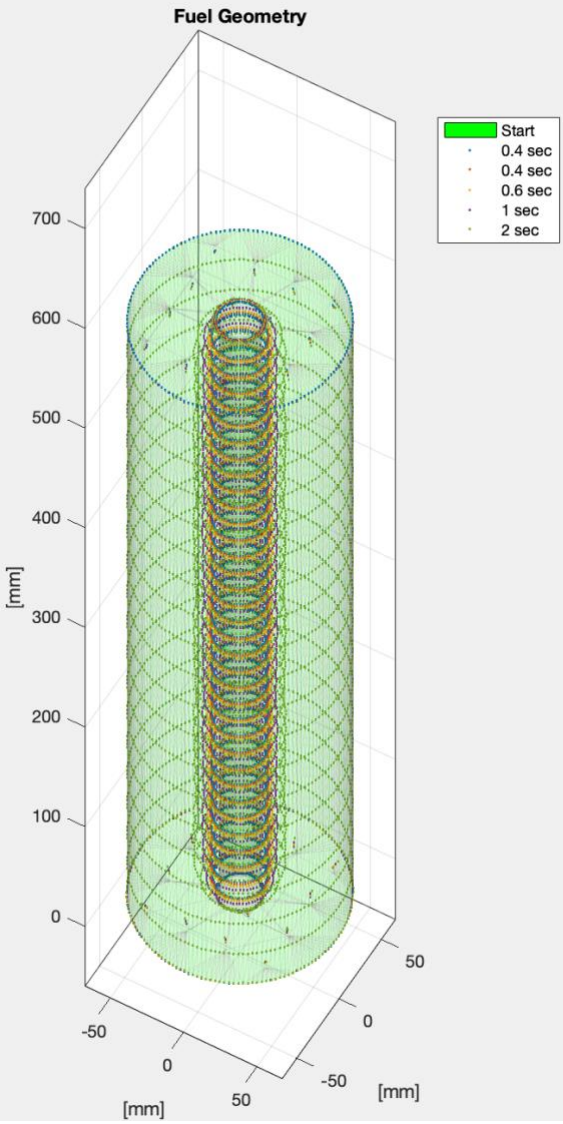

3244 facets

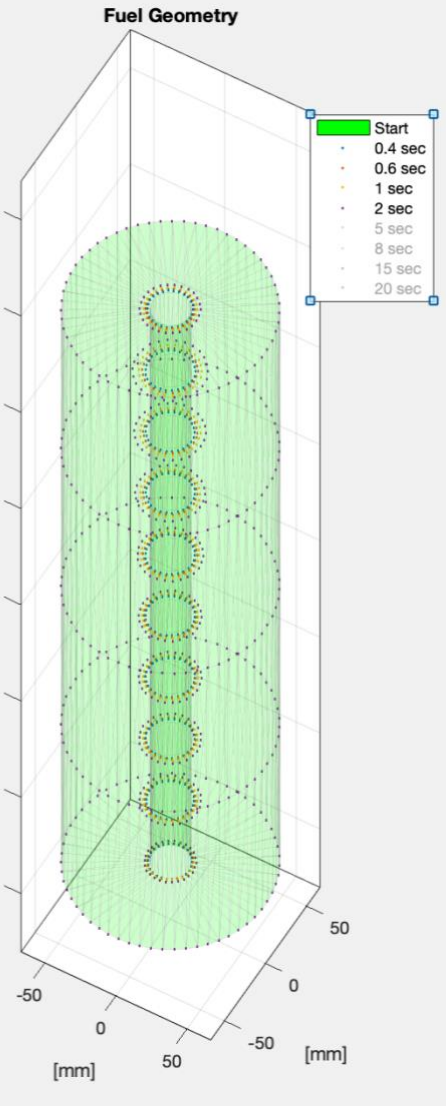

1110 facets

Appendix D -STL Example File

```
solid cube_corner
        facet normal 0.0 -1.0 0.0
          outer loop
            vertex 0.0 0.0 0.0
            vertex 1.0 0.0 0.0
            vertex 0.0 0.0 1.0
          endloop
        endfacet
        facet normal 0.0 0.0 -1.0
          outer loop
            vertex 0.0 0.0 0.0
            vertex 0.0 1.0 0.0
            vertex 1.0 0.0 0.0
          endloop
        endfacet
        facet normal -1.0 0.0 0.0
          outer loop
            vertex 0.0 0.0 0.0
            vertex 0.0 0.0 1.0
            vertex 0.0 1.0 0.0
          endloop
        endfacet
        facet normal 0.577 0.577 0.577
          outer loop
            vertex 1.0 0.0 0.0
            vertex 0.0 1.0 0.0
            vertex 0.0 0.0 1.0
          endloop
        endfacet
      endsolid
```

This example displays an example excerpt text for a corner to a simple tetrahedron in Stereolithographic (STL) ascii file format. Most STL files are binary and therefore are not ‘readable’ without a translator.

Bibliography

[1] A. MacMillen, "Hybrids Primer, Hybrids, Part 1," September 2002. [Online]. Available: https://hawkfeather.com/rockets/hybrids1.html. [Accessed 15 0 2020].

[2] M. J. Chiaverini and K. K. Kuo, Fundamentals of Hybrid Rocket Combustion and Propulsion, Reston, Virgina: AIAA, 2007.

[3] M. Calabro, "Overview ON Hybrid Propulsion," *EDP Sciences*, 2011.

[4] G. Story and J. Arves, "Flight Testing of Hybrid Vheicles," 1 January 2006. [Online]. Available: https://ntrs.nasa.gov/citations/20060048274.

[5] Holzman, Allen L. (United Technologies Corp.), "Hybrid Rocket Propulsion," in *NASA. Langley Research Center, Space Transportation Materials and Structures Technology Workshop. Volume 2: Proceedings*, San Jose, CA United States, Feb 1, 1993.

[6] R. S. Wolf and G. H. Henry, "Hybrid Rocket Education at the U.S Air Force Academy AIAA 92-3300," in *AIAA/SAE/ASME/ASEE 28th Joint Propulsion Confrence and Exhibit*, Nashville, TN, 1992.

[7] B. J. Cantwell, "Thin Film Stability fo Melting Solid Fuels with Application to Hybrid Propulsion," in *41st AIAA Fludi Dynamic Confrence and Exhibit* , Honolulu, Hawaii , 2011.

[8] G. P. Sutton and O. Biblarz, Rocket Propulsion Elements, Hoboken, New Jersey: Wiley & Sons Inc., 2010.

[9] S. Krishnan, "Hybrid Rocket Technology: An Overview," in *6th Asia pacific International Symposium on Combustion and Energy Utilization*, Kualalumpur, Malaysia, 2002.

[10] G. Risha, B. J. Evans, E. Boyer and K. K. Hup, "Metals, Energetic Aditivesm and Special Binders Used in Solid Fuels for Hybrid Rocekts," in *Fundamentals oF*

Hybrid Rocekt Combustion and Propulsion, Reston, Va, AIAA, 2007, pp. 413-456.

[11] J. Majdalani, "Vortex Injection Hybrid Rockets," in *Fdndamentals of Hybrid Rocket Combustion and Propulsion*, Reston, VA, American Institute of Aeronautics and Astronautics (AIAA), 2007, pp. 247-276.

[12] M. Chiaverini, "Review of Solid-Fuel Regression Rate Behaviors in Classical and Nonclassical Hybrid Rocket Motors," in *Fundamentals of Hybrid Rocket Combustion and Propulsion*, Reston, VA, Americal Institute of Aeronautics an Astronautics (AIAA), 2007, pp. 37-125.

[13] S. Kim, J. Lee, H. Moon, J. Kim, H. Sung and O. C. Kwon, "Regression Characteristics of the Cylindrical Multiport Grain in Hybrid Rockets," *JOURNAL OF PROPULSION AND POWER*, vol. 29, no. 3, pp. 573-581, 2013.

[14] W. C. S. H. P.L Schoonover, "Application of Genetic Algorithms to the Optimization of Hybrid Rockets," in *34th AIAA/ASME/SAE/ASEE Joint Propulsion Confrence & Exibit*, Cleveland, OH , 1998.

[15] D. Vonderwell, I. F. Murray and S. D. Heister, "Optimization of Hybrid Rocket Booster Fuel Grain Design," in *30th AIAA/ASME/SAE/ASEE Joint Propulsion Confrence*, Indianapolis, IN, 1994.

[16] D. Arnold, E. J. Boyer, K. K. Kuo, J. D. DeSain, T. J. Curtiss and J. K. Fuller, "Test of Hyrbid Rocket Fuel Grains with Swirl Patterns Fabricate usign Rapid Prototyping Technology," in *49th AIAA/ASME/SAE/ASEE Joint Propulsion Confrence*, San Jose, CA, 2013.

[17] S. Zhang, F. Hu and W. Zhang, "Numerical investigation on the regression rate of hybrid rocket motor with star swirl fule grain," *Acta Astronautica*, vol. 127, pp. 384-393, 2016.

[18] J. (. K. Fuller , D. A. Ehrlich, P. C. Lu, R. P. Jansen and J. D. Hoffman, "Advantages of Rapid Prototyping for Hybrid Rocket Motor Fuel Grain Fabrication," in *47th AIAA/ASME/SAE/ASEE Joint Propulsion Confrences & Exhibit*, San Diego, CA, 2011.

[19] Aerospace Corp., "3D PRINTED ROCKET MOTOR IS FUEL EFFICIENT," Aerospace corp., 16 4 2018. [Online]. Available:

https://aerospace.org/article/3d-printed-rocket-motor-fuel-efficient. [Accessed 16 4 2018].

[20] D. Bianchi, B. Betti, F. Nasuti, C. Carmicino and A. R. Sorge, "Numerical Modeling of GOX/HTPB Hybrid Rocket Flowfields and Comparison with Experiments," in *AIAA Propulsion and Energy Forum*, Cleveland, OH, 2014.

[21] P. Bourke, "STL format," October 1999. [Online]. Available: http://paulbourke.net/dataformats/stl/. [Accessed 5 October 2020].

[22] Library of Congress, "STL (STereoLithography) File Format, ASCII," 1988. [Online]. Available: https://www.loc.gov/preservation/digital/formats/fdd/fdd000506.shtml. [Accessed 5 10 2020].

[23] 3D Systems Inc. , "Stereolithography Interface Specification," 3D Systems Inc. , 10 July 2014. [Online]. Available: https://people.sc.fsu.edu/~jburkardt/data/stla/stla.html. [Accessed 20 November 2019].

[24] X. Sun, T. Hui, L. Yuelong and C. Guobiao, "Regression rate behaviors of HTPB-based propellant combinations for hybrid rocket motor," *Acta Astronautica,* vol. 2015, no. 119, pp. 137-146, 22 January 2015.

[25] T.-V. Chelaru and F. Mingireanu, "Hybrid rocket engine, theoretical model and experiment," *Acta Astronatutica,* vol. 2011, no. 68, pp. 1891-1902, 7 January 2011.

[26] G. Cai, Y. Zhang, H. Tian, P. Wang and N. Yu , "Effect of grain port length–diameter ratio on combustion performance in hybrid rocket motors," *Acta Astronautica,* vol. 2016, no. 128, pp. 83-90, 8 July 2016.

[27] F. Barato, N. Bellomo and D. Pavarin , "Integrated approach for hybrid rocket technology development," *Acta Astronautica,* vol. 2016, no. 128, p. 257–261, 16 July 2016.

[28] D. Altman and A. Holzman, "Overview and History of Hybrid Rocket Propulsion," in *Fundamentals of Hybrid Rocket Compustion and Propulsion* , Reston, Virgina, AIAA, 2007, pp. 1-36.

[29] G. J. Jacobs, "Jacobs Rocketry," Jacob's Rocketry, [Online]. Available: https://jacobsrocketry.com/rocketry_overview.htm. [Accessed 17 September 2020].

[30] J. M. Seizman, "AE6450 Rocket Propulsion Hybrid rockets," Georgia Tech College of Engineering, 2019. [Online]. Available: http://seitzman.gatech.edu/classes/ae6450/hybrids.pdf. [Accessed 21 September 2020].

[31] G. Lengelle, "Solid-Fuel Pyrolysis Phenomena Part 1: Mechanics," in *Fundamentals of Hybrid Rocket Combustion and Propulsion*, Reston, VA, American Institute of Aeronautics and Astronautics, 2007, pp. 127-165.

REPORT DOCUMENTATION PAGE

Form Approved
OMB No. 074-0188

1. REPORT DATE *(DD-MM-YYYY)*	2. REPORT TYPE	3. DATES COVERED *(From – To)*
09-11-2020	Master's Thesis	March 2016 – Dec 2020

TITLE AND SUBTITLE
Analysis for hybrid rocket fuel regression using stereolithographic geometry

5a. CONTRACT NUMBER

5b. GRANT NUMBER

5c. PROGRAM ELEMENT NUMBER

6. AUTHOR(S)
King, Michael, P, Mr, CIV GG-12

5d. PROJECT NUMBER

5e. TASK NUMBER

5f. WORK UNIT NUMBER

7. PERFORMING ORGANIZATION NAMES(S) AND ADDRESS(S)
Air Force Institute of Technology
Graduate School of Engineering and Management (AFIT/ENY)
2950 Hobson Way, Building 640
WPAFB OH 45433-8865

8. PERFORMING ORGANIZATION REPORT NUMBER
AFIT-ENY-MS-20-D-062

9. SPONSORING/MONITORING AGENCY NAME(S) AND ADDRESS(ES)
AGENCY Intentionally left blank
ADDRESS Intentionally left blank
PHONE and EMAIL Intentionally left blank
ATTN: POC Intentionally left blank

10. SPONSOR/MONITOR'S ACRONYM(S)
Intentionally left blank

11. SPONSOR/MONITOR'S REPORT NUMBER(S) Intentionally left blank

12. DISTRIBUTION/AVAILABILITY STATEMENT
DISTRUBTION STATEMENT A. APPROVED FOR PUBLIC RELEASE; DISTRIBUTION UNLIMITED.

13. SUPPLEMENTARY NOTES
This material is declared a work of the U.S. Government and is not subject to copyright protection in the United States.

14. ABSTRACT
Hybrid Rocket Engines have characteristically low fuel regression that limits their performance. Additive manufacturing and rapid prototyping can possibly solve some of the problems with Hybrid propulsion regression by creating geometry not possible with conventional manufacturing. This work is attempting to make geometric regression simulation of Hybrid Rocket Engines easier by using STereoLithography (STL files) as the geometry. The STL file is generated by most CAD software. This analysis sets flow conditions, boundary conditions, propellant selection, and allows for fuel geometry to be altered to simulate geometry's effects on regression rate and propellant performance. This will allow for more complicated geometry to be analyzed. This work demonstrates a rudimentary analytical model that is can be refined to predict and compare regression rates of fuel and performance. This model can be used for more advanced geometric analysis to improve and predict performance of hybrid rocket engines.

15. SUBJECT TERMS
Hybrid propulsion, Rocket propulsion, Additive manufacturing, 3D Printing

16. SECURITY CLASSIFICATION OF:			17. LIMITATION OF ABSTRACT	18. NUMBER OF PAGES	19a. NAME OF RESPONSIBLE PERSON
a. REPORT	b. ABSTRACT	c. THIS PAGE			Hartsfield, Carl R CIV AFIT/ENY
U	U	U	UU	110	19b. TELEPHONE NUMBER *(Include area code)* (937) 255-6565, ext 4667 (carl.hartsfield@afit.edu)

Standard Form 298 (Rev. 8-98)
Prescribed by ANSI Std. Z39-18